

# Searching for missing heritability: Designing rare variant association studies

Or Zuk<sup>a,b,1</sup>, Stephen F. Schaffner<sup>a</sup>, Kaitlin Samocha<sup>a,c,d</sup>, Ron Do<sup>a,e</sup>, Eliana Hechter<sup>a</sup>, Sekar Kathiresan<sup>a,e,f,g</sup>, Mark J. Daly<sup>a,c</sup>, Benjamin M. Neale<sup>a,c</sup>, Shamil R. Sunyaev<sup>a,h</sup>, and Eric S. Lander<sup>a,i,j,2</sup>

<sup>a</sup>Broad Institute of Harvard and MIT, Cambridge, MA 02142; <sup>b</sup>Toyota Technological Institute at Chicago, Chicago, IL 60637; <sup>c</sup>Analytic and Translational Genetics Unit, Department of Medicine, Massachusetts General Hospital and Harvard Medical School, Boston, MA 02114; <sup>d</sup>Program in Genetics and Genomics, Biological and Biomedical Sciences, Harvard Medical School, Boston, MA 02114; <sup>e</sup>Center for Human Genetic Research, Massachusetts General Hospital, Boston, MA 02114; <sup>f</sup>Cardiovascular Research Center, Massachusetts General Hospital, Boston, MA 02114; <sup>g</sup>Department of Medicine, Harvard Medical School, Boston, MA 02115; <sup>h</sup>Division of Genetics, Brigham and Women's Hospital, Harvard Medical School, Boston, MA 02115; <sup>i</sup>Department of Biology, Massachusetts Institute of Technology, Cambridge, MA 02139; and <sup>j</sup>Department of Systems Biology, Harvard Medical School, Boston, MA 02115

Contributed by Eric S. Lander, December 10, 2013 (sent for review September 23, 2013)

Genetic studies have revealed thousands of loci predisposing to hundreds of human diseases and traits, revealing important biological pathways and defining novel therapeutic hypotheses. However, the genes discovered to date typically explain less than half of the apparent heritability. Because efforts have largely focused on common genetic variants, one hypothesis is that much of the missing heritability is due to rare genetic variants. Studies of common variants are typically referred to as genome-wide association studies, whereas studies of rare variants are often simply called sequencing studies. Because they are actually closely related, we use the terms common variant association study (CVAS) and rare variant association study (RVAS). In this paper, we outline the similarities and differences between RVAS and CVAS and describe a conceptual framework for the design of RVAS. We apply the framework to address key questions about the sample sizes needed to detect association, the relative merits of testing disruptive alleles vs. missense alleles, frequency thresholds for filtering alleles, the value of predictors of the functional impact of missense alleles, the potential utility of isolated populations, the value of gene-set analysis, and the utility of *de novo* mutations. The optimal design depends critically on the selection coefficient against deleterious alleles and thus varies across genes. The analysis shows that common variant and rare variant studies require similarly large sample collections. In particular, a well-powered RVAS should involve discovery sets with at least 25,000 cases, together with a substantial replication set.

mapping disease genes | power analysis | statistical genetics

Genomic studies over the last half decade have shed light on the genetic basis of common polygenic human diseases and traits, identifying thousands of loci and revealing key biological pathways. Nonetheless, the genetic variants identified thus far appear to explain less than half of the estimated heritability in most diseases and traits. The sources of the so-called missing heritability remain unclear (1). This article is our second paper exploring the mystery of missing heritability.

In our first paper (2), we explored a methodological issue. We showed that genetic interactions, if present, could account for substantial missing heritability. Still, this is likely to be only a partial explanation. In this paper, we turn to the search for additional genetic variants underlying common human diseases, focusing on rare genetic variants.

The discovery of genes underlying common diseases depends on association studies (except in special cases where Mendelian subtypes of common diseases show clear segregation in large families). Association studies involve testing whether the frequency of a set of one or more alleles differs between cases and a control population, indicating that the set of alleles is associated with the disease. Association studies to date have largely focused on studying individual common variants, because they could be more readily assayed with initial genomic technologies. However, association studies are increasingly being applied to sets of rare variants as well.

Association studies of individual common variants are often referred to as genome-wide association studies (GWAS), whereas association studies of sets of rare variants in coding regions are often described as exome-sequencing studies. This nomenclature is unfortunate because it conflates statistical methodology (association testing) and laboratory methodology (DNA sequencing). To highlight the parallelism, we will use the terms common variant association study (CVAS) and rare variant association study (RVAS). Ideally, the term GWAS should encompass both types of association studies.

**CVAS.** By common variants, we mean those that occur often enough that it is practical to test each variant individually by estimating its frequency in cases and controls. Given the feasibility of collecting many thousands of cases, common variants will be operationally defined as those with frequency  $\geq 0.5\%$  (one carrier per 100 people).

The theory and practice of CVAS is well advanced. Catalogs of common variants in human populations are nearing completion, and tens of thousands (and in some cases, hundreds of thousands) of cases and controls have been genotyped for many traits and diseases. Studies to date have largely used genotyping arrays and linkage disequilibrium patterns, but will increasingly use inexpensive massively parallel sequencing.

## Significance

Discovering the genetic basis of common diseases, such as diabetes, heart disease, and schizophrenia, is a key goal in biomedicine. Genomic studies have revealed thousands of common genetic variants underlying disease, but these variants explain only a portion of the heritability. Rare variants are also likely to play an important role, but few examples are known thus far, and initial discovery efforts with small sample sizes have had only limited success. In this paper, we describe an analytical framework for the design of rare variant association studies of disease. It provides guidance with respect to sample size, as well as the roles of selection, disruptive and missense alleles, gene-specific allele frequency thresholds, isolated populations, gene sets, and coding vs. noncoding regions.

Author contributions: O.Z., E.H., M.J.D., B.M.N., S.R.S., and E.S.L. designed research; O.Z., S.F.S., K.S., R.D., E.H., B.M.N., S.R.S., and E.S.L. performed research; K.S., R.D., and S.K. contributed new reagents/analytic tools; O.Z., S.F.S., K.S., E.H., M.J.D., B.M.N., S.R.S., and E.S.L. analyzed data; and O.Z., M.J.D., B.M.N., S.R.S., and E.S.L. wrote the paper.

The authors declare no conflict of interest.

Freely available online through the PNAS open access option.

<sup>1</sup>Present address: Department of Statistics, The Hebrew University of Jerusalem, Mt. Scopus, Jerusalem 91905, Israel.

<sup>2</sup>To whom correspondence should be addressed. E-mail: [lander@broadinstitute.org](mailto:lander@broadinstitute.org).

This article contains supporting information online at [www.pnas.org/lookup/suppl/doi:10.1073/pnas.1322563111/-DCSupplemental](http://www.pnas.org/lookup/suppl/doi:10.1073/pnas.1322563111/-DCSupplemental).

Some missing heritability is clearly due to additional common variants that remain to be discovered. First, CVAS to date has used genotyping arrays with good coverage of variants with frequency 5–50% but poorer coverage of the range 0.5–5%. [The potential importance of these low-frequency common variants, sometimes called “Goldilocks” alleles (3), is demonstrated by nonsense mutations of *PCSK9*, which have led to new therapeutics for decreasing LDL cholesterol (4, 5).] Second, CVAS has been limited by sample size; studies with larger sample sizes continue to reveal many new loci (6–8). Third, indirect statistical methods indicate that association with common variants can explain at least 30% (and likely more) of the heritability for a number of diseases and traits (9–11).

**RVAS.** Rare variants may also make a major contribution to missing heritability, although much less is known at present. The theoretical case for an important role of rare variants is that alleles that strongly predispose to disease are likely to be deleterious and thus kept at low frequencies by purifying selection (12–14). Moreover, rare variants with strong effects are valuable, because they may enable clinical studies in individual patients and reveal protective null alleles that define targets for pharmaceutical intervention.

RVAS differs from CVAS in two key respects. First, rare variants are too numerous to catalog comprehensively and so must be directly enumerated in every sample by DNA sequencing rather than by genotyping known variants. The importance of this distinction is fading, however: with the plummeting cost of DNA sequencing, both CVAS and RVAS will increasingly use direct DNA sequencing. Second and more fundamentally, rare variants occur too infrequently to allow association tests of individual variants. RVAS thus require aggregating rare variants into sets and comparing the aggregate frequency distribution in cases vs. controls (15).

The need to aggregate variants poses a challenge: which variants to aggregate? Ideally, one would aggregate only damaging alleles and ignore benign alleles. Unfortunately, one cannot perfectly distinguish the former from the latter. To enrich for harmful alleles, RVAS typically focuses on (i) nonsynonymous variants in protein-coding regions, ignoring the rest of the genome; and (ii) variants with frequency below a specified threshold  $T$ . Even with these limitations, the resulting variants remain a mixture of damaging and benign alleles.

The practice of RVAS is still in its infancy. In pioneering studies of the genetics of obesity, O’Rahilly and colleagues studied unrelated cases with a common disease to look for rare variants in candidate genes related to the disease (16). Hobbs and Cohen subsequently applied this approach to well-established candidate genes for lipid-related phenotypes, showing, for example, that *PCSK9*, in which gain-of-function alleles caused a Mendelian hypercholesterolemia syndrome, also harbored rare loss-of-function alleles that lowered LDL cholesterol (4).

The challenge, however, has been to move beyond handfuls of candidate gene studies to unbiased gene discovery. Some early efforts organized by the US National Institutes of Health were premised on the notion that rare variants underlying common diseases could be reliably identified in small collections of 50–100 cases. However, results have made clear that RVAS, like CVAS, requires much larger samples.

The few discoveries from RVAS to date have largely emerged from candidate gene studies rather than unbiased surveys and, in some cases, have reached only nominal rather than genomewide significance (17–24). However, exomewide studies of large samples are now underway for several diseases.

Given the early stage of the field, the analytical methodology for RVAS remains in flux. Many authors have proposed a rich collection of possible statistics (reviewed in refs. 25 and 26 and tests compared in ref. 27; [SI Appendix, Section 3.4](#)). Our goal here is neither to evaluate their relative merits nor to propose alternatives.

Rather, the goal of this paper is to offer a simple conceptual framework that provides insight into the design of RVAS and to apply it to address some fundamental questions:

- i. Choice of variants. What are the relative merits of disruptive alleles (stop, frameshift, and splice-site mutations, which severely disrupt protein structure) vs. missense alleles?
- ii. Frequency threshold. What is the optimal threshold  $T$  for filtering alleles? Is it constant or does it vary with the properties of each gene?
- iii. Sample sizes. How many cases are needed to detect association by RVAS? How does the answer depend on the properties of the gene, the relative risk of harmful alleles, and the strategic choices above?
- iv. Other strategies. What approaches might be used to increase power, such as studying special populations, specific gene sets, or de novo mutations?
- v. Whole genome analysis. Can RVAS be extended from the exome to include the noncoding portion of the genome?

To gain intuition, we focus on a simple situation. We consider a binary trait (e.g., a disease, such as schizophrenia, or the tail of a quantitative phenotype, such as LDL cholesterol above 200 mg/dL) analyzed with *burden tests* (which compare the number, or ‘burden’, of variants in cases and controls), where the variants studied are those with frequency below a fixed threshold. We assume a ‘two-class model’, wherein all alleles are either null (abolishing gene function) or neutral (having no effect on gene function). Although the model is simple, it can provide clear insight into the many alternative methods for RVAS.

Below, we show how the answers depend crucially on the selection coefficient of each gene; more modestly on the proportion of missense mutations that are null; and in some cases on population history. Results are summarized in the main text and supported by mathematical formulas, proofs, simulations, graphs and tables in the extensive Supplementary Information.

## Results

**Designing an Association Study.** A burden test for association with a disease examines whether a class  $C$  of alleles in a gene  $G$  is enriched or depleted in cases vs. random controls from the general population, with individuals assumed to be unrelated so that events are independent. (Although we consider random population controls, one can alternatively compare cases with disease-free controls.) The class of alleles may be selected in many ways. It could, for example, consist of a single allele (as in CVAS), all nonsense alleles, all missense variants with frequency  $<1\%$ , or all variants at evolutionarily conserved nucleotides in a given gene.

The power of an association study depends on two key quantities: (i)  $f_C$ , the combined allele frequency (CAF) of class  $C$ , meaning the expected number of alleles present in a haploid genome in the population; and (ii)  $\lambda_C$ , the excess relative risk of disease conferred by alleles in the class, meaning that a heterozygous carrier has a  $(1 + \lambda_C)$ -fold higher risk of disease than a random member of the population.<sup>†</sup> By Bayes’ theorem,  $(1 + \lambda_C)$ -fold is also the expected enrichment of such alleles in cases vs. the overall population [[SI Appendix: Eq. 3.1](#)]. Consequently,  $\lambda_C$  can be directly estimated from the excess enrichment in cases ([SI Appendix, Section 3.1](#)). Enrichment of alleles in cases can be tested with likelihood ratio tests (LRTs) ([SI Appendix, Section 3.2](#)).

<sup>†</sup>We focus on risk to heterozygous carriers. Our calculations implicitly assume that the risk to individuals carrying two null alleles ( $\lambda_C^*$ ) is the same as the risk to heterozygous carriers ( $\lambda_C$ ). Although such individuals may well have higher risk, they are much rarer than heterozygous carriers (because  $f_C$  is small) and thus their impact on RVAS is typically negligible. [The effective relative risk is increased by  $f_C(\lambda_C^*/\lambda_C)$ , which is  $\ll 1$  unless  $\lambda_C^*/\lambda_C$  is huge; this case would essentially be a monogenic recessive trait.]

The number of cases<sup>‡</sup> needed to detect an association using an LRT is given by a formula (*SI Appendix*, Eq. 3.6) that is well approximated, when  $f_C$  is small, by

$$n_{a,b} \approx \frac{\nu_{a,b}}{4f_C g(\lambda_C)} \quad [1]$$

Here,  $g(\lambda)$  is a simple function<sup>§</sup> and  $\nu_{a,b}$  is a constant that controls the false-positive rate  $a$  and false-negative rate  $b$ . For 90% power ( $b = 10\%$ ),  $\nu_{a,b} = 10.5$  when testing a single hypothesis ( $a = 0.05$ ) and  $\nu_{a,b} = 35.9$  when correcting for multiple hypothesis testing of 20,000 genes ( $a = 2.5 \times 10^{-6}$ ). The values for 50% power are  $\nu_{a,b} = 3.8$  and 22.2, respectively. Calculations below assume multiple hypothesis correction.

Although discussions of RVAS often contemplate alleles that increase disease risk, the formulas apply equally well to alleles that decrease disease risk—that is, protective alleles. In this case,  $\lambda_C$  is a negative number between  $-1$  and  $0$ . (For example, protective alleles that decrease risk by fourfold have  $\lambda_C = -0.75$ .)

To maximize the power of an association study, we want  $f_C$ , the combined allele frequency, and  $|\lambda_C|$ , the absolute value of the excess relative risk, to be as large as possible. Unfortunately, these goals sometimes pull in opposite directions. For example, expanding the alleles under study increases  $f_C$  but dilutes  $\lambda_C$ .

Below, we explore six strategies for RVAS. To lay the foundation, we start by considering several issues related to alleles and their frequencies.

**Mutation Rates for Observable Classes.** First, we need to understand the rate at which various types of mutations are born. For protein-coding regions, three classes of mutations can be directly observed: silent (S), missense (M), and disruptive (D, defined as nonsense, splice site, and frameshift changes, which severely disrupt protein structure). For any human gene, we can obtain good estimates of the mutation rates for these observable classes ( $\mu_S$ ,  $\mu_M$ ,  $\mu_D$ ) based on (i) the length and sequence composition of the gene and (ii) the rate and mutational spectrum for point mutations in the local region. (The latter quantities can be estimated from comparative genomics, medical genetics or large-scale human parent-offspring trio sequencing studies.) (*SI Appendix*, Section 2.6). Below, we will focus on a typical human gene with the median mutation rate and a coding region of 1,500 bp. (One could readily incorporate gene-specific rates, if desired.) For this typical gene, the mutation rates for silent, missense, and disruptive mutations are  $5.6 \times 10^{-6}$ ,  $12.8 \times 10^{-6}$ , and  $1.7 \times 10^{-6}$  per gene copy per generation, respectively (Table 1).

**Two-Class Model for Impact of Mutations.** Second, we need to consider the impact of mutations on gene function. We will adopt a simple two-class model in which mutations in protein-coding regions are either (i) neutral, having no effect on function, or (ii) null, abolishing gene function. Null alleles cause excess relative risk  $\lambda = \lambda_{\text{null}} \geq 0$  and have selection coefficient  $s = s_{\text{null}} \geq 0$ , which is assumed to have been constant.

We will assume that (i) all silent mutations are neutral, (ii) all disruptive mutations are null (which is reasonable, at least if one

excludes disruptive mutations occurring late in a coding region), and (iii) missense mutations are a mixture of null and neutral alleles, with proportion  $\alpha$  being null and  $1 - \alpha$  being neutral.

Our model is clearly a simplification, because we ignore the possibility of alleles with intermediate effects. Evolutionary studies and analysis of mutations responsible for Mendelian diseases suggest that ~25% of missense mutations are strongly deleterious (essentially equivalent to disruptive mutations, with selection coefficients in the range of  $10^{-2}$  and below); ~50% are weakly deleterious (hypomorphic alleles, with selection coefficients in the range  $10^{-3}$ – $10^{-4}$ ); and ~25% are truly neutral (13, 28–30). [Some studies have suggested slightly different proportions for strongly deleterious mutations (31–33).] In our two-class model, we will ignore the hypomorphic mutations, treating them as being effectively neutral. We also ignore the possibility of countervailing alleles; e.g., protective alleles if null alleles are deleterious or vice versa (4, 5). *Discussion* elaborates on the reasons for and limitations of the model.

Our analyses below will primarily use the value  $\alpha = 25\%$ , because it is the average value reported for human genes. Of course, the actual proportion  $\alpha$  varies across genes. For example, the depletion of missense alleles relative to silent alleles suggests values  $\alpha \approx 5\%$  for *BRCA2* but 50% for *CHD8* (*SI Appendix*, Section 2.1).

To illustrate the impact of varying proportions of null missense alleles, we sometimes compare results for four values:  $\alpha = 10\%$ , 25%, 33%, or 60%. For these values, Table 1 shows that (i) the mutation rates for all null alleles (disruptive plus missense) are 3.0, 5.0, 6.0, and  $9.4 \times 10^{-6}$ ; (ii) the ratio of all null alleles to disruptive alleles is 1.8-, 2.8-, 3.5-, and 5.5-fold; and (iii) disruptive alleles comprise 57%, 34%, 29%, and 18% of all null alleles.

**CAF.** Third, we need to understand the properties of the CAF. For this purpose, we focus on classes where all alleles have the same selection coefficient  $s$ .

The ancestral human population that existed ~1,000 generations ago is typically modeled as being at equilibrium with a constant effective population size  $N_{eq}$  of ~10,000 (34). For a population at equilibrium, classical population genetics (35–37) provides a precise formula for the expected CAF (*SI Appendix*, Proposition 2), which is well approximated by

$$f_C \approx \begin{cases} \mu_C/s & \text{for } 4N_{eq}s \gg 1 \text{ (significant selection)} \\ 4\mu_C N_{eq} & \text{for } 4N_{eq}s \ll 1 \text{ (nearly neutral)} \end{cases} \quad [2]$$

where  $\mu_C$  is the rate per chromosome per generation of new mutations in class  $C$ .

Modern human populations have undergone massive expansions, interrupted in some cases by bottlenecks. Although no simple formulas are available, the value of  $f$  can be found by

**Table 1. Mutation rates per gamete**

Mutation type	Absolute mutation rate ( $\times 10^{-6}$ )			
	$\alpha = 10\%$	25%	33%	60%
Silent	5.6	5.6	5.6	5.6
Missense	12.8	12.8	12.8	12.8
Null	1.3	3.2	4.2	7.7
Neutral	11.5	9.6	8.6	5.1
Disruptive	1.7	1.7	1.7	1.7
Nonsense, splice	0.9	0.9	0.9	0.9
Frameshift	0.8	0.8	0.8	0.8
All null	3.0	5.0	6.0	9.4
Disruptives: All nulls				
Ratio	1: 1.8	1: 2.8	1: 3.5	1: 5.5
Percentage	57%	34%	29%	18%

For a typical gene as defined in the text, with  $\alpha$  being the proportion of newborn missense alleles that are null.

<sup>‡</sup>We focus on the number  $n$  of cases needed when the frequency  $f_C$  in the population is known perfectly based on an (infinitely) large population survey. We make this assumption in the belief that very large datasets will become available in the coming years and that shared population controls can be used across studies. In the meanwhile, one can estimate  $f_C$  within a study based on the frequency in either unaffected or random individuals. If a study involves cases and unaffecteds in proportion  $r$  and  $1 - r$ , one requires approximately  $n/(1 - r)$  cases and  $n/r$  controls to detect association, where  $n$  is the number of cases given in Eq. 1 (*SI Appendix*, Section 3.3). For a balanced design, this corresponds to  $2n$  cases and  $2n$  controls.

<sup>§</sup> $g(\lambda) = [(\lambda + 1)\ln(1 + \lambda) - \lambda]$ , which is approximately  $\lambda^2/2$  for small  $\lambda$  ( $0 \leq \lambda < 1$ ) and  $c\lambda\ln(\lambda)$  for larger  $\lambda$  (with  $c$  in the range 0.7–0.8 for  $2 < \lambda < 100$ ).



simulation. We analyzed various population histories (*SI Appendix, Section 1.3*), including two models of uninterrupted expansions (denoted expansions 1 and 2) and models meant to represent Europe (bottleneck of 1,550 chromosomes occurring 1,250 generations ago), Finland (100 chromosomes, 100 generations), and Iceland (1,000 chromosomes, 50 generations).

Importantly, the expected value of the CAF is essentially unaffected by the vast changes in the size or structure of human populations over the last ~1,000 generations [Fig. 14]. The reason is intuitively clear: (i) for alleles under significant selection, the expected CAF is held at  $\mu_C/s$  by mutation-selection balance (38), whereas (ii) for nearly neutral alleles, a simple back-of-the-envelope argument shows that the expected CAF increases from the equilibrium value of  $4\mu_C N_{eq}$  at an extremely slow rate.<sup>†</sup> Eq. 2 thus provides a good approximation for the expected CAF in modern human populations. (Note: although the expected CAF is constant, the variance across genes varies across populations; see RVAS strategy 4 below.)

The CAF depends strongly on the selection coefficient, with the expected value falling precipitously as selection increases:  $f_C \sim 40,000\mu_C$ ,  $13,000\mu_C$ ,  $1,000\mu_C$ ,  $100\mu_C$ , and  $10\mu_C$  for  $s = 0$ ,  $10^{-4}$ ,  $10^{-3}$ ,  $10^{-2}$ , and  $10^{-1}$ , respectively (see Eq. 2 and *SI Appendix, Proposition 2* for exact formula). If their birth rates were identical, neutral alleles would thus outnumber deleterious alleles by 400-fold if  $s = 10^{-2}$  and by 4,000-fold if  $s = 10^{-1}$ .

Using the mutation rate for disruptive alleles in our typical gene ( $1.7 \times 10^{-6}$ ) and the approximation in Eq. 2, the expected frequency for disruptive alleles is 0.17%, 0.017%, and 0.0017% for  $s = 10^{-3}$ ,  $10^{-2}$ , and  $10^{-1}$ , respectively; that is, approximately one heterozygote per 300, 3,000, and 30,000 individuals. For our typical gene with  $\alpha = 25\%$ , the expected frequency of all null alleles (disruptive plus missense) is ~2.8-fold higher (Table 1).

**Individual Allele Frequencies.** Fourth, we need to understand the individual allele frequency (IAF) distribution,  $\Psi_C(x)$ , for a class  $C$  of alleles, defined as the probability that an individual allele in  $C$  sampled from a random chromosome<sup>‡</sup> has population frequency  $\leq x$ . The IAF distribution may be calculated from closed-form formulas for populations at equilibrium (35, 36) and from simulations for other models (*SI Appendix, Sections 1.2 and 1.3*).

The IAF distribution (i) shows when selection is strong enough that the allelic spectrum will consist primarily of rare variants and, (ii) by providing the frequency of null and neutral missense alleles, allows one to calculate the proportion  $p_C(T)$  of missense alleles with frequency  $\leq T$  that are null.

Unlike the CAF, the IAF distribution may be significantly shaped by population history. We calculated the IAF distribution for each population model (equilibrium and European model in Fig. 1 *B* and *C*; remaining populations in *SI Appendix, Section 2.3*).

For the ancestral human population, the frequency distribution of null alleles in a gene (sampled from a randomly chosen chromosome) should be roughly equally balanced between common and rare frequencies if  $s \sim 10^{-2.5}$ . If selection is stronger, null alleles will be mostly rare, comprising  $\geq 90\%$  of alleles on randomly chosen chromosomes for  $s \geq 10^{-2}$ . If selection is weaker, null alleles will be mostly common.

The dramatic expansion of the human population has important effects on allele frequencies. Even if the population were to

stabilize at current levels, the large modern population size would eventually drive all nonneutral alleles toward extremely low allele frequencies. However, the speed of approach to this new equilibrium varies substantially depending on  $s$  (39). Population expansion over the last  $\sim 10^3$  generations has a dramatic effect for alleles with  $s \gg 10^{-3}$ , but little effect when  $s \ll 10^{-3}$ . In the former case, the ancestral alleles are largely eliminated and replaced by new alleles, which are born at a much lower frequency as a result of population expansion. In the latter case, the ancestral alleles continue to dominate and the median remains relatively high (although there is a small excess of rare variants that provides valuable information about population history) (40, 41).

The greater impact of population expansion on alleles under strong selection can be seen by comparing the ancestral population vs. European model: the median allele frequencies are 1.7% vs. 0.6% if  $s = 10^{-3}$ ; 0.18% vs. 0.005% if  $s = 10^{-2}$ ; and 0.02% vs. 0.00005% if  $s = 10^{-1}$  (*SI Appendix, Table S3*). The selection intensity  $s$  at which common and rare variants are equally frequent is slightly weaker in Europe than in the ancestral population ( $10^{-3}$  vs.  $10^{-2.5}$ ).

#### Impact of Population Expansion on the Genetic Architecture of Disease.

Various authors have speculated that the dramatic increase in the number of new alleles caused by population expansion has altered the genetic architecture of disease and the explanation for missing heritability (42–44). Specifically, it has been suggested that expansion may have dramatically increased (i) the total frequency of genetic disease by raising mutational load; (ii) the relative importance of new alleles in disease risk; or (iii) the role of rare variants in disease risk.

- i. Disease frequency. In fact, population expansion does not increase disease frequency. The increase in the number of distinct alleles caused by population expansion does not translate into a meaningful increase in the combined frequency of alleles, because the vast majority of the newly added alleles are so rare. Although the number of alleles is relevant for studies of population history, disease frequency depends on the CAF, which, as noted above, is largely unaffected by recent human population expansion.
- ii. Role of new alleles. Similarly, population expansion does not substantially increase the proportion of disease due to new alleles. For alleles under significant selection, simulations show that the age distribution of a randomly chosen allele is essentially unaltered by population expansion (*SI Appendix, Section 2.4*).
- iii. Role of rare alleles. Population expansion does increase the role of rare variants, although the effect is limited. Expansion shifts the allelic spectrum from predominantly common to predominantly rare only for  $s$  in a relatively narrow range ( $10^{-3} \leq s \leq 10^{-2.5}$  for Europe). Outside this range, the allelic spectrum remains either predominantly common or predominantly rare.

**Relevant Range of Selection Coefficients.** The analysis above shows that RVAS is important when  $s > 10^{-3}$  and essential when  $s > 10^{-2.5}$  (with  $\geq 90\%$  of variants being rare). We focus below on  $s$  in the range of  $10^{-3}$ – $10^{-1}$ .

To understand how this range of selection might relate to common diseases, it is useful to consider the situation of direct selection—where the reduction in fitness caused by a null allele is proportional to the extent to which it increases risk for the disease under study. In this case,  $s = (\lambda\pi)s_D$ , where  $\pi$  is the disease prevalence in the general population and  $s_D$  is the decreased reproductive fitness of individuals manifesting the disease. Schizophrenia (prevalence ~1%) has a severe fitness cost, which has been estimated at  $s_D = 50\%$  (45). An allele conferring relative risk of 10-fold ( $\lambda = 9$ ) would have  $s = 0.045$  ( $\sim 10^{-1.3}$ ), whereas one with 3-fold risk ( $\lambda = 2$ ) would have  $s = 0.01$  ( $\sim 10^{-2}$ ). Type 2 diabetes has a higher prevalence of ~10%, but likely has

<sup>†</sup>The expected CAF for new neutral alleles born in a given generation is  $\mu_C$  and thus the increase in the expected CAF over  $k$  generations cannot exceed  $k\mu_C$  (and will be lower because many newborn alleles are lost). It follows that the collection of neutral alleles born since the onset of human population cannot increase the CAF of neutral alleles by more than 5% ( $= k\mu_C/4\mu_C N_{eq}$ , where  $k=1,000$  and  $N_{eq}=10,000$ ). The actual increase is typically much smaller due to loss of newborn alleles.

<sup>‡</sup>The relevant sampling frame for disease studies involves randomly selecting a chromosome and inspecting it for alleles. Alleles are thus sampled according to their frequency, yielding a frequency-weighted frequency distribution.

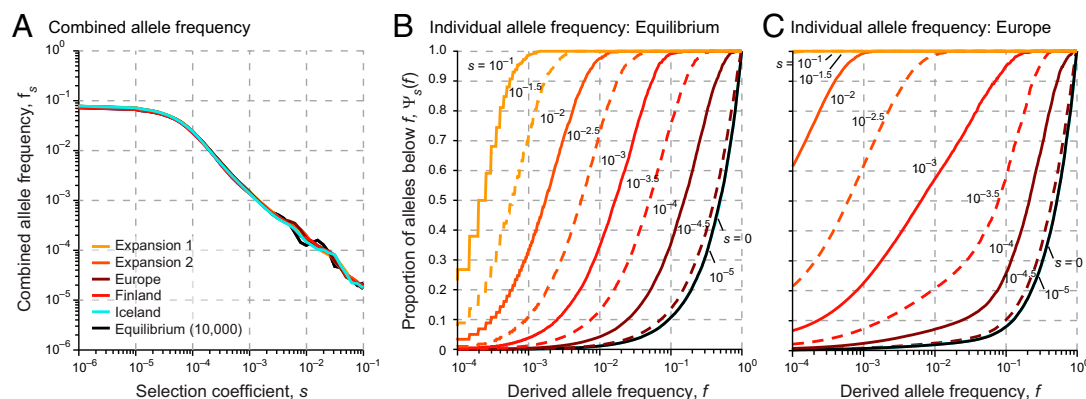


**Fig. 1.** Allele frequencies from simulations for various demographic models. (A) CAF (average 50,000 simulations) as a function of selection coefficient  $s$ . CAF is not sensitive to demographic history, as noted in the text. (B) Cumulative distribution of IAF as a function of  $s$ , for the ancestral population at equilibrium. (C) Cumulative distribution of IAF as a function of  $s$ , for the European population. Compared with the ancestral population, the IAF distribution is skewed toward rare alleles for intermediate to strong selection  $s$  (SI Appendix, Sections 2.2–2.3).

more modest effect on fitness—perhaps  $s_D = 1\%$ . Alleles conferring 10-fold and 3-fold risk would have  $s = 10^{-2.0}$  and  $s = 10^{-2.7}$ , respectively. For very late-onset diseases such as Alzheimer's, the disease itself likely has little impact on reproductive fitness. Direct selection would be weak ( $s \ll 10^{-3}$ ) and CVAS would likely be the better strategy. Of course, these illustrations assume direct selection. Genes may be under pleiotropic selection for their effect on multiple phenotypes.

**Knowledge of Key Parameters.** Below we typically assume that the values of  $\mu$ ,  $f_D$ ,  $s$ , and  $\alpha$  for each gene are known. In reality, they must be inferred from data.

- Mutation rate  $\mu$ . From local mutation rates, one can estimate the mutation rate  $\mu$  for observable classes (S, M, D).
- Frequency  $f_D$ . The allele frequency  $f_D$  for the class D of disruptive alleles can be estimated simply by counting alleles in a large sample, with the precision increasing with sample size. For a coefficient of variation of 20%, about 25 events must be seen (corresponding to 6,250, 62,500, and 625,000 people for  $s = 10^{-3}$ ,  $10^{-2}$ , and  $10^{-1}$ , respectively).
- Selection coefficient  $s$ . The selection coefficient for each gene can be obtained from  $f_D = \mu_D/s$  (Eq. 2), by using the estimated values of  $f_D$  and  $\mu_D$  and solving for  $s$ . The estimate's precision is inherently limited by the fact that the realized value of  $f_D$  in any given population fluctuates around the expected value due to the stochastic nature of population history; this variation cannot be reduced by increasing the sample size. When selection is strong,  $s$  can be estimated to within roughly half an order of magnitude (SI Appendix, Section 12.1). The precision might be improved by combining results across unrelated populations.
- Proportion of nulls,  $\alpha$ . The fraction  $\alpha$  of newborn missense mutations that are null can be estimated from the deficit of missense alleles seen in a population or evolutionary comparisons. However, there are issues with the precision and accuracy of these estimates (SI Appendix, Section 12.2). The best solution may be to use a range of values of  $\alpha$  in RVAS analysis.

With these foundations, we now turn to the design of RVAS.

**RVAS Strategy 1: Studying Disruptive Alleles Only.** One simple strategy is to study only disruptive (D) variants in each gene: they are all null alleles and confer the same excess relative risk  $\lambda_D (= \lambda_{\text{null}})$ . Disruptive alleles can thus be lumped into a single meta-allele, whose frequency can be measured in cases and the overall population, with the ratio providing an estimate of  $(1 + \lambda_{\text{null}})$ .

For disease-predisposing alleles, Fig. 2A shows the number of cases needed to detect association with 90% power. (To achieve 50% power, one needs  $\sim 62\%$  as many cases.) The expected values are largely independent of population history.

- For the weakest selection in our range ( $s = 10^{-3}$ , where common and rare variants occur with equal frequency), we need 260, 770, 2,700, 8,400, and 28,000 cases where the relative risk  $(1 + \lambda)$  is 20-, 10-, 5-, 3-, and 2-fold, respectively. Current case-control collections used for CVAS for many diseases already have the required sizes for RVAS.
- For stronger selection ( $s = 10^{-2}$ ), the sample size is 10-fold larger: 2,600–280,000 cases. Current collections should suffice to detect strong effects ( $1 + \lambda > 5$ ).
- For the strongest selection in our range ( $s = 10^{-1}$ ), the sample size grows another order of magnitude: 26,000–2.8 million. Achieving such numbers is challenging, but should eventually be feasible by aggregating clinical information, with patient consent, across populations.

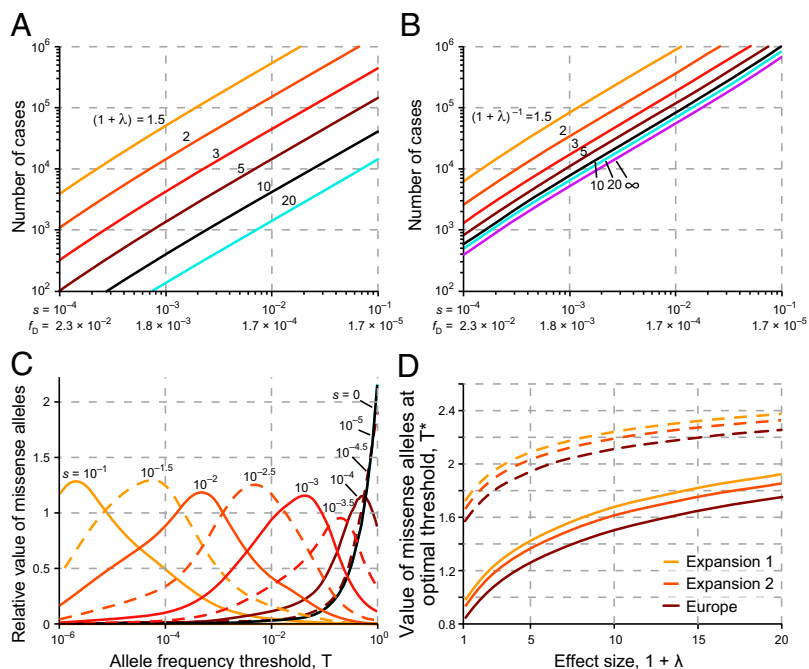
The corresponding sample sizes for detecting protective alleles are shown in Fig. 2B. More samples are needed to detect protective alleles than harmful alleles, because it is harder to detect a deficit (rather than an excess) of null alleles in cases against the already low background in the population. In the extreme case of a completely protective allele ( $\lambda = -1$ ), the required sample size is the same as for detecting harmful alleles that increase disease risk by a factor of  $e \approx 2.718$ .

**Bottom line.** Contrary to some initial expectations, the number of cases needed for a well-powered RVAS is large and similar to that needed for CVAS. To obtain enough cases to detect association, RVAS for disease should thus focus primarily, for the foreseeable future, on sequencing case-control collections rather than cohorts randomly selected from the population.

**RVAS Strategy 2: Adding Missense Alleles Filtered by Frequency.** One obvious idea for increasing power is to include null missense alleles in the association study. If we could perfectly recognize the null missense alleles, we could simply count them alongside the disruptive alleles. For a typical gene with  $\alpha = 25\%$ , the number of events would increase by 2.8-fold (Table 1) and the required sample size would decrease by 2.8-fold.

Given that we lack perfect knowledge, the question is as follows: how close can we come to this best possible case of 2.8-fold reduction in sample size? The inability to distinguish between null and neutral missense alleles creates a serious problem because neutral alleles are much more abundant. The usual solu-

**Fig. 2.** Power to detect association for a typical gene. (A) Number of cases needed to detect association based on excess of disruptive disease-predisposing variants in cases vs. general population, as a function of selection coefficient  $s$  (or frequency  $f_D$  of disruptive alleles). Curves represent various effect sizes  $1 + \lambda$ . (Values for 90% power and 5% false-positive rate after Bonferroni correction for testing 20,000 genes.) (SI Appendix, Sections 3.2 and 4). (B) Number of cases to detect association based on deficit of disruptive protective variants. Curves represent various values of  $(1 + \lambda)^{-1}$ . The curve for  $(1 + \lambda)^{-1} = 2$  corresponds to twofold protection (50% lower disease risk), whereas the curve for  $(1 + \lambda)^{-1} = \infty$  corresponds to complete protection. (C) Relative contribution of missense vs. disruptive variants for European model. Curves for various selection coefficients show ratio of expected LOD scores for testing an excess of rare missense variants with frequency below threshold  $T$  divided by expected LOD score for disruptive variants. Values are calculated for effect size for null alleles of  $1 + \lambda = 4$ . For each  $s$ , there is an optimal threshold  $T^*$  at which missense alleles provide maximal relative contribution (typically  $\sim 1.0$ - to  $1.3$ -fold) (SI Appendix, Section 5). (D) Relative contribution of missense (vs. disruptive) variants at optimal threshold  $T^*$  as a function of  $1 + \lambda$  for various populations. Solid lines show values when filtering missense alleles by frequency threshold  $T^*$ . Dashed lines show values when also filtering to include only missense alleles predicted to be deleterious (by a high-quality predictor with false-positive and false-negative rates of 20%). The functional predictor increases the contribution of missense alleles—e.g., from 1.5-fold to 2.1-fold for genes  $1 + \lambda = 10$  in the European population (SI Appendix, Sections 5 and 6).



tion is to impose a frequency threshold  $T$ —that is, to study only missense alleles with frequency  $\leq T$ —with the aim of eliminating the vast majority of neutral alleles (which tend to have higher frequencies) while retaining most null alleles.

Even with this approach, missense alleles may be less useful than disruptive alleles because the null alleles are always diluted by neutral alleles: the proportion  $\rho(T)$  of nulls among missense alleles with frequency  $\leq T$  is always lower than the proportion  $\alpha$  among newborn alleles (for example,  $\alpha = 25\%$  for our typical gene). As a consequence, the observed enrichment of missense alleles in cases will always underestimate the true excess enrichment for null alleles: specifically,  $\lambda_{M(T)} = \rho(T)\lambda_{\text{null}}$ . It is thus essential that missense variants and disruptive variants be analyzed separately.

The threshold  $T$  is often chosen in an ad hoc manner (e.g., 1%, 0.5%, or 0.1%), but it should ideally be chosen to maximize power (SI Appendix, Section 5). In general, the optimal threshold  $T^*$  turns out to be roughly the frequency where (i)  $\sim 75\%$  of null alleles are retained and (ii)  $\sim 16\%$  of retained missense alleles are null, meaning that the apparent value of  $\lambda$  will underestimate the true value by  $\sim 6.5$ -fold (SI Appendix, Tables S4–S9). Importantly, the optimal threshold  $T^*$  depends strongly on the selection coefficient and thus differs across genes.

Using the optimal values of  $T^*$  for Europe, missense alleles together contribute 0.6- to 1.3-fold as much information as the disruptive alleles, with the value rising as  $\lambda_{\text{null}}$  increases from 0 to 10 (Fig. 2 C and D). When disruptive and missense alleles are combined, the sample size thus falls by 1.6- to 2.3-fold.

Achieving this reduction requires using the optimal threshold  $T^*$ . If the threshold is too high or too low by 10-fold, the contribution of missense alleles can fall by approximately twofold (Fig. 2C). Moreover, using too high a threshold will underestimate the apparent relative risk (possibly dramatically), owing to dilution by neutral alleles.

**Bottom line.** Disruptive alleles provide the most robust information and require no knowledge of  $s$  and  $\alpha$ . Missense alleles should be analyzed as well, but require care in selecting the correct frequency cutoff for each gene (based on its selection coefficient). For typical genes with  $\alpha = 25\%$ , incorporating missense alleles may decrease sample size by approximately twofold. [The po-

tential improvement in sample size is only  $\sim 1.4$ -fold for genes where only a small proportion ( $\alpha = 10\%$ ) of missense alleles are null and could be as high as 3-fold for genes where the proportion is unusually high ( $\alpha = 60\%$ ).]

**RVAS Strategy 3: Filtering Missense Alleles by Severity.** It may be possible to glean information about whether missense alleles are null or neutral—either from biochemical experiments (24) (where in vitro assays are available) or computational programs, such as PolyPhen-2, SIFT, or MutationTaster (reviewed in ref. 46)—that offer computational predictions of whether a mutation is likely to be damaging. Given the quality of the predictions (proportions,  $\gamma_{\text{null}}$  and  $\gamma_{\text{neutral}}$ , of true null and neutral variants declared to be damaging), one can calculate the optimal threshold  $T^*$  and the corresponding sample size.

If we use a predictor with  $\gamma_{\text{null}} = 80\%$  and  $\gamma_{\text{neutral}} = 20\%$  [close to the values reported for PolyPhen-2 (47)] and filter with the optimal threshold  $T^*$ , missense alleles contribute 1.2- to 2.0-fold as much information as the disruptive alleles (SI Appendix, Section 6) and thus decrease total sample size by 2.2- to 3.0-fold. **Bottom line.** For typical genes with  $\alpha = 25\%$ , using a high-quality predictor of the mutational impact of missense alleles can yield a decrease of  $\sim 2.5$ -fold in sample size (vs. twofold when filtering by frequency alone).

**Example: LDL Receptor in Early-Onset Myocardial Infarction.** The points above are nicely illustrated by a recent analysis of the association between rare variants in the LDL receptor (LDLR) and early-onset myocardial infarction (MI) (SI Appendix, Section 7.1). The study found that *LDLR* harbors (i) disruptive variants in 20/2,743 cases and 1/2,465 controls corresponding to a relative risk of 18.1 (or  $\lambda_D = 17.1$ ), and (ii) missense variants with frequency  $\leq 1\%$  in 172 cases and 102 controls, for a dramatically lower relative risk of 1.5 (excess relative risk of  $\lambda_{M(1\%)} = 0.5$ ).

What accounts for the striking difference in the apparent relative risk between disruptive and rare missense alleles? Our framework provides a simple quantitative explanation. The selection coefficient for null alleles can be estimated as  $s \sim 10^{-1.7}$  [from the equation  $s = \mu_D/f_D$ , using  $f_D = 1/(2 \times 2,465)$  and the



mutation rate for *LDLR* ( $\mu_D = 3.8 \times 10^{-6}$ ; *SI Appendix, Section 2.6*). Given such strong selection, the frequency threshold of 1% used by the authors is expected to result in only a small proportion of missense alleles being null:  $\rho(0.01) = 0.02$ . Given this low proportion, the expected excess relative risk is only  $\lambda_{M(1\%)} = (0.02)\lambda_{\text{null}} = 0.35$ , which is in good agreement with the observed value of 0.5. In fact, the optimal threshold  $T^*$  given such strong selection is not 0.01 but  $\sim 0.0001$ . At this much lower threshold, we expect  $\sim 17\%$  of missense alleles to be null and to observe an excess relative risk of  $1 + \lambda_{M(0.01\%)} = 3.8$ .

We note that there is a practical problem with using such low thresholds. We assumed above that the frequency  $f_D$  is known precisely for every allele based on large population surveys. Based on a limited number of samples, we cannot tell precisely which alleles have frequency  $\leq 0.0001$ . The best solution is to focus only on singleton alleles (*SI Appendix, Section 7*). Given the sample size, the expected relative risk for singleton alleles is  $1 + \lambda = 3.7$  compared with 3.8, when the frequencies are known precisely. It is successful because the sample has  $\sim 10,000$  chromosomes, and thus singleton alleles are likely to have a true frequency that is not much greater than 0.0001. If the sample size was much smaller, the apparent effect size ( $1 + \lambda$ ) for singletons would be much lower: 2.1 and 1.4 for 1,000 and 100 chromosomes, respectively.\*\*

**Bottom line.** The strong effect of null *LDLR* alleles on early-onset myocardial infarction is evident from the enrichment of disruptive alleles. [Interestingly, the relative risk is similar to that inferred in the classic study of familial hypercholesterolemia (48).] The true effect is much harder to discern from the missense variants, because the apparently strong selection on *LDLR* causes missense variants to be swamped by neutral alleles even when one imposes a frequency threshold of 1%.

**RVAS Strategy 4: Hitting the Jackpot with Isolated Populations.** Another approach to reducing sample size is to hope to be lucky. Although the expected value of the CAF is essentially identical across populations (see above), the variance of the CAF differs substantially. Accordingly, we might select a population in which the CAF for some genes associated with a disease happens, by chance, to be much larger than the expected value of  $\mu/s$ . If we are lucky enough that the CAF is 10-fold higher than expected, we will be able to detect the gene with a sample size that is 10-fold lower than expected.

Using simulations, we find that the CAF has a tight coefficient of variation for expansion models and Europe but has a fat right tail for isolated populations with recent bottlenecks (Fig. 3 and *SI Appendix, Section 8*). If the expected CAF is small relative to the reciprocal of the bottleneck size, we expect either 0 or 1 ancestral allele to pass through the bottleneck. In the latter case, the CAF suddenly jumps to a much higher frequency (e.g., 1% for Finland, with a bottleneck of 100 chromosomes) and declines only slowly back to the expected level. This phenomenon explains the high prevalence of dozens of so-called “Finnish diseases” (monogenic disorders found at much higher frequencies than in the rest of Europe). It also explains genetic features in the Ashkenazi Jewish population, including the high prevalence of certain disorders and the simpler allelic spectrum for certain diseases [such as *BRCA1* and *BRCA2*, in which three founder alleles together account for the majority of early-onset breast cancer among Ashkenazi Jewish women (49)].

\*\*One can also perform an analysis considering only those missense alleles with frequency  $\leq 1\%$  that are predicted to be probably damaging by PolyPhen-2 (that is, RVAS strategy 3). One observes 89 such missense alleles in cases vs. 32 in controls, which corresponds to an apparent excess relative risk  $\lambda_{M(1\%), \text{PolyPhen2}} = 2.5$ . This result agrees closely with the expectation of  $\lambda_{M(1\%), \text{PolyPhen2}} = 2.3$ , given the inferred value of  $s$  and the frequency threshold of 1%. For this type of analysis (assuming  $\gamma_{\text{null}} = 80\%$  and  $\gamma_{\text{neutral}} = 20\%$ ), the optimal threshold turns out to be  $T^* = 0.15\%$ , which would yield a much higher apparent effect size of  $\lambda_{M(T^*), \text{PolyPhen2}} = 8.2$ .

For Finland’s tight bottleneck, the “sweet spot” occurs when  $s \sim 10^{-2.5} - 10^{-3}$ . For  $s = 10^{-3}$ , the CAF for null alleles in Finland will be 5-, 10-, and 20-fold higher than expected for about 6%, 3.5%, and 1% of genes, respectively. For Iceland’s wider bottleneck, the sweet spot occurs for somewhat stronger selection ( $s \sim 10^{-1.5} - 10^{-2}$ ). For  $s = 10^{-2}$ , the CAF for null alleles in Iceland will be 5-, 10-, and 20-fold higher for about 5%, 2%, and 0.5% of genes, respectively. The distributions depend on the bottleneck size, number of generations since expansion, mutation rate of the allelic class, and selection coefficient (*SI Appendix, Section 8*).

**Bottom line.** Tight bottlenecks scatter the relative contributions of genes. Studying recently bottlenecked populations should thus make it much easier to discover some disease-associated genes, although it will be harder to detect other genes (whose ancestral alleles failed to pass through the bottleneck). Although incomplete, such early discoveries may prove especially valuable by providing initial insights into disease pathogenesis. Studying multiple bottlenecked populations may be a powerful strategy.

**RVAS Strategy 5: Studying Gene Sets.** Another potentially powerful idea is to focus not just on single genes but on gene sets. Given a gene set  $G$  with  $m$  genes, the simplest approach is to compare the total number of events (e.g., disruptive alleles) across all genes seen in cases and controls. The analysis is straightforward if each gene in  $G$  has the same background frequency  $f_D$ : the sample size to achieve a given nominal significance level is smaller (relative to detecting a single gene with excess relative risk  $\lambda$ ) by a factor of  $m g(\lambda_{\text{avg}})/g(\lambda)$ , where  $\lambda_{\text{avg}}$  is the average excess relative risk across the set (*SI Appendix, Section 9*). If 50 genes each confer the same high relative risk, we thus need 50-fold fewer samples to achieve the same nominal significance level for the set as for any individual genes alone. If 20 of 100 genes confer a relative risk of  $1 + \lambda = 11$  and the rest have no effect, the sample size required to detect the set is smaller by a factor of  $\sim 8$  ( $= 100 g(2)/g(10)$ ) than the size required to detect one of the risk-increasing genes alone.

The analysis is trickier if the background frequency differs across genes. Genes with larger  $f_D$  will disproportionately affect the variance. On average, these genes will be under weaker selection (because  $f \approx \mu/s$ ) and thus likely to have smaller effect size  $\lambda$ . More sophisticated LRT methods can be used to improve power. Methods such as overdispersion tests can also allow for both deleterious and protective alleles (50, 51).

The challenge is to select a set likely to be enriched for genes associated with the disease or trait. An obvious set is the genes implicated by CVAS, as genes related to a disease are likely to harbor both common and rare variants. [For example, many genes related to lipid levels harbor both types of variants (7).] CVAS may provide a valuable foundation for RVAS.

**Bottom line.** Studying gene sets, especially those identified by CVAS, is likely to be a powerful strategy. Discovering association with a gene set does not reveal precisely which genes are connected with the disease, but the findings can suggest targeted population-based follow-up and laboratory investigation.

**RVAS Strategy 6: Studying De Novo Mutations.** An extreme example of a frequency threshold is studying only de novo mutations. The framework above applies directly, with the allele frequency  $f_{D, \text{denovo}}$  being the mutation rate  $\mu_D$ . Focusing only on de novo mutations would seem to be very inefficient, because they are so rare ( $\mu_D \sim 2 \times 10^{-6}$  for our typical gene). By Eq. 1, detecting a gene in which disruptive alleles increase risk by 20-fold would require  $\sim 100,000$  cases.

However, RVAS with de novo mutations can be effective for genes with very large effect sizes. For example, *CHD8* was associated with autism with mental retardation (prevalence  $< 1/300$ ) (52) based on the observation of de novo disruptive mutations in 3 of 1,078 cases (53, 54). Given the mutation rate of *CHD8* ( $\mu_D \sim 5 \times 10^{-6}$ ), this observation is highly improbable ( $P \sim 1.7 \times 10^{-6}$ ),

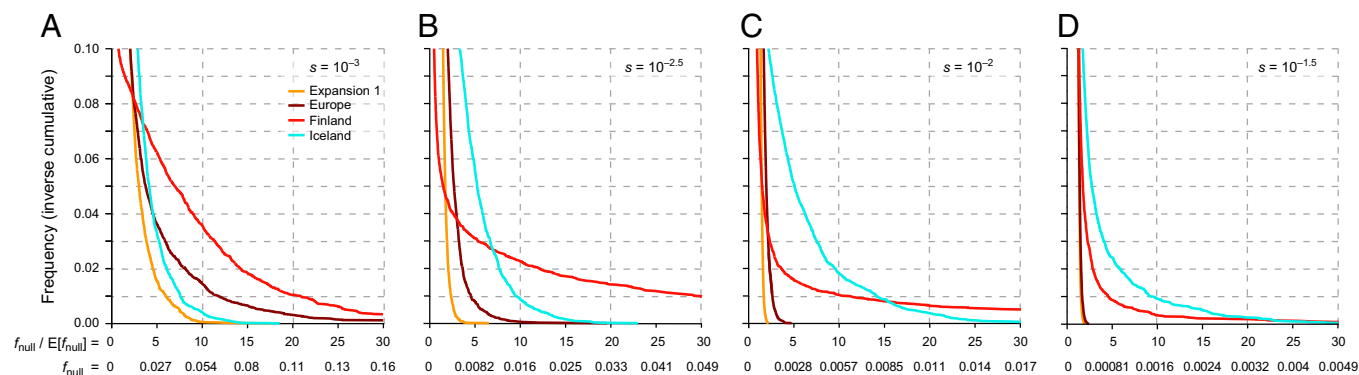


**Fig. 3.** Chances of being lucky. Figures show the right tail of the CAF ( $f_{\text{null}}$ ) distribution for four selection coefficients ( $s = 10^{-3}$ ,  $10^{-2.5}$ ,  $10^{-2}$ ,  $10^{-1.5}$ ) and four demographic models. Curves show probability that the realized value of the CAF ( $f_{\text{null}}$ ) for all null alleles, (in absolute terms and normalized to the expected value given the selection coefficient) exceeds the value on the x-axis, with results obtained from 50,000 simulations of gene histories for each value of  $s$  and demography. Finland and Iceland show heavy right tails (genes with CAF much larger than the expected value), because population bottlenecks scatter allele frequencies. For  $s = 10^{-3}$  in Finland, 3.5% of genes have CAF that is 10-fold higher than expected—making it possible to discover the genes with a 10-fold lower example size than expected. The distributions depend on bottleneck size, number of generations since expansion, mutation rate and selection coefficient (SI Appendix, Section 8). Tighter bottlenecks, as in Finland vs. Iceland, allow fewer alleles to pass, but result in greater proportional increase in allele frequency. (Calculations assume  $\mu_{\text{null}} = 5 \times 10^{-6}$ , corresponding to  $\alpha = 25\%$ .)

and the effect size appears to be huge ( $\sim 300$ -fold before correcting for the “winner’s curse”), corresponding to nearly complete penetrance (SI Appendix, Section 2.6 and 10).

The example highlights a subtle advantage of de novo mutations vs. standing variation in the general population. We assumed above that background allele frequencies are known precisely, but they must actually be inferred from data. The observation for *CHD8* (three de novo events in cases) is only significant because the extremely low frequency  $f_{D,\text{denovo}} = \mu_D$  can be estimated with high precision without the need for population studies, based on the ability to infer mutation rates with high precision. A study of *CHD8* based on standing variation could be similarly effective given a precise estimate of  $f_D$ ; however, this could require a survey of more than half a million people in the case of strong selection (e.g.,  $s = 0.1$ ).

The comparative advantage for de novo mutations is thus greatest for genes with the largest selection coefficient. The proportion of null alleles that are de novo mutations is largest for such genes. Indeed, under mutation selection balance, the expected proportion of null alleles that are de novo is precisely  $s$ .

The gene set approach discussed above can be applied to de novo mutations, with the nice feature that the genes contribute more evenly because the frequency  $f_{D,\text{denovo}}$  does not depend on the selection coefficient. For example, the set of all 20,000 protein-coding genes shows an excess of de novo variants for autism, indicating that many genes likely contribute (53, 54).

**Bottom line.** RVAS with de novo mutations can be valuable for genes with huge effects and large values of  $s$ . However, the design is not well suited for finding genes that increase risk by merely 20-fold or selection coefficients of merely 1%. Notably, the approach does not require prior knowledge of population frequencies, which can be a significant advantage.

**Prospects for RVAS in Noncoding Regions.** Whereas the methodology for CVAS applies identically to both coding and noncoding regions, extending RVAS to noncoding regions poses major new challenges. The problem is that RVAS requires selecting the genomic regions across which to aggregate variants. The choice is problematic.

- i. If one focuses on a single regulatory element, such as a promoter or enhancer, the target size is so small that the CAF is tiny and the required sample size is huge. For example, focusing on a 50-base regulatory element (vs. a 1,500-base coding region) necessitates a 30-fold larger sample.

- ii. On the other hand, if one combines all variants across a large intergenic region, most sites will be functionally unimportant; this dilutes the apparent value of  $\lambda$  and thereby inflates the sample size. If  $\sim 5\%$  of intergenic DNA is functional, the signal will be diluted by 20-fold and the sample size will be inflated by 20- to 400-fold (depending on the value of  $\lambda$ ).
- iii. Outside of coding regions, there are no classes analogous to disruptive variants, which can provide a pure signal largely undiluted by neutral mutations, or silent mutations, which can be discarded as benign.

In addition, scanning the entire genome requires imposing a more stringent threshold for statistical significance, which increases the sample size by  $\sim 50\%$  (55) (SI Appendix, Section 11.1).

Finally, it is unclear whether noncoding regions will harbor many signals to be found by RVAS. Although common variants with moderate effects found by CVAS occur predominantly in noncoding regions, there is reason to think that most rare variants of large effect may lie in coding regions. This expectation is based on the fact that single-base changes may have dramatic effects in coding regions but rarely obliterate the function of noncoding elements. Consistent with this, the inferred selection coefficient in coding regions is about 10-fold higher than in evolutionarily conserved noncoding sequences (56, 57).

Despite these challenges, it is appropriate to explore whole-genome RVAS in certain well-chosen situations. A recent paper (58) reported whole-genome sequence from 962 individuals and searched for an association of HDL cholesterol levels with both common and rare variants. The rare variant analysis involved studying alleles with frequency  $\leq 1\%$  in sliding windows of 4 kb across the genome. A handful of peaks with low  $P$  values was identified, although none reach statistical significance.<sup>††</sup>

**Bottom line.** To perform RVAS with reasonable sensitivity in noncoding regions, it will be important to have fairly precise knowledge of the functionally important regulatory sequences related to each human gene to aggregate them together. Without

<sup>††</sup>The paper reports that the best nominal  $P$  value observed across the genome is  $2.7 \times 10^{-8}$  but does not address whether the value is significant. To correct for scanning the entire genome, one can apply extreme value theory for Ornstein-Uhlenbeck diffusions (SI Appendix, Section 11.1). The probability of such a  $P$  value arising by chance somewhere in the genome is  $\sim 70\%$ , and thus the observation is not statistically significant. Genomewide significance at the 5% level corresponds to  $P \sim 2 \times 10^{-9}$  (SI Appendix, Section 11.1).



such information, the sample sizes required to detect association will be larger by one to two orders of magnitude. At present, it makes more sense to deploy resources primarily toward whole-exome, rather than whole-genome, sequence. This approach will maximize the number of samples that can be analyzed for coding regions, where the power is currently vastly greater, where the effect sizes are expected to be larger, and where the discoveries are likely to be more immediately actionable.

**Variance Explained.** Finally, the analysis above relates directly to the search for missing heritability. For a disease with prevalence  $\pi$ , the proportion of phenotypic variance (on the observed scale) explained by the null alleles in a gene  $G$  is

$$\text{Var}_{\text{Exp}} \approx 2f_{\text{null}} \frac{\pi}{(1-\pi)} \lambda^2. \quad [4]$$

The case of *LDLR* in early-onset MI discussed above is unusual in that it explains 1.8% of the phenotypic variance (or  $\sim 3.6\%$  of the genetic variance). In contrast, most RVAS findings thus far explain a tiny proportion the phenotypic variance. For example, rare variants in *SLC12A3* (also known as *NCCT*), *SLC12A2* (also known as *NKCC2*), and *KCNJ1* (also known as *ROMK1*) each explain an average of  $<0.17\%$  of the phenotypic variance in risk of hypertension, whereas rare variants in *MTNR1B* similarly explain  $<0.1\%$  of the phenotypic variance in risk of type 2 diabetes (18, 21) (*SI Appendix, Section 13.3*).

From Eqs. 1 and 4, one can calculate the number of cases needed to detect genes explaining a given fraction of the phenotypic variance. To detect a gene explaining 1% of the phenotypic variance based on studying risk-increasing disruptive alleles, the required number of cases should be  $\sim 2,800$ ,  $\sim 4,700$ , and  $\sim 6,500$  for diseases with prevalences of 1%, 5%, and 10%, respectively (*SI Appendix, Section 13.2*). After reaching this sample size, one can reasonably conclude that the remaining genes each explain less than 1% of the variance. (For 0.1% of the variance, the sample size should be 10-fold larger.)

## Discussion

Some early RVAS efforts were premised on the notion that searching for rare variants in small numbers of patients could reveal the genes underlying disease. However, it is now clear that rare variant studies, like common variant studies, will require tens of thousands of cases and careful statistical analysis to achieve adequate power to detect genes underlying disease.

Here, we describe a conceptual framework for thinking about the design of RVAS. Our goal is not to compare specific statistics that have been proposed but rather to extract insight and intuition about how key factors influence RVAS for common disease. For this reason, we focused on a simple situation: a two-class model analyzed with burden tests using frequency cutoffs.

Our main conclusions are as follows.

Disruptive alleles, being a pure class of nulls, provide a key backbone for RVAS. They are powerful and easy to interpret, as the excess in cases directly reflects the effect size.

Missense alleles may potentially play a valuable role as well, by decreasing the required sample size. However, missense alleles are harder to interpret: they are always mixtures of null and neutral alleles, with the proportions depending on the selection coefficient for each gene (which must be inferred), the frequency threshold used (which must be chosen), and the availability and quality of functional predictions (from experimental or computational analysis). Achieving maximal power and accurate inference of effect sizes requires properly accounting for dilution by neutral missense alleles. In practice, the maximal increase in power corresponds to an  $\sim 2.5$ -fold decrease in sample size for our typical gene with  $\alpha = 25\%$ . (The improvement is much smaller for genes with protein sequence under weaker constraint.)

The appropriate sample size for RVAS depends on the mutation rate, selection coefficient, and effect size for null alleles in the gene. Based on Fig. 1, a well-powered RVAS might aim for a discovery sample of at least 25,000 cases for 90% power (or  $\sim 15,000$  cases for 50% power), together with a substantial replication set. This sample size should allow detection of most genes where null alleles confer at least a 10-fold effect, as well as those with 5- and 3-fold effects provided that  $s$  is not too strong ( $s < 2 \times 10^{-2}$  and  $5 \times 10^{-3}$ , respectively). Fortunately, RVAS can begin by sequencing existing sample collections that have been used for CVAS, many of which contain many tens of thousands of cases. Even larger samples will ultimately be desirable, which should be feasible as genomic sequencing becomes a routine part of medical care.

Three strategies may accelerate progress, by enabling early discoveries. First, isolated populations resulting from recent bottlenecks should make it easier to detect a subset of genes. Examples include Finland, Iceland, Ashkenazi Jews, Amish, Bedouins, and various endogamous groups in India. Studies across multiple such populations could prove valuable. Second, early signals may be provided by the study of gene sets that are likely to be enriched for disease-associated loci. The best sets may consist of genes implicated by CVAS. [Initial efforts to identify rare variants in genes identified by CVAS have met only limited success. However, this is likely due to the small discovery sets used—typically, only a few hundred cases (23).] Whereas CVAS and RVAS are sometimes thought of as alternatives, they are likely to be complementary. Third, de novo mutations can be a valuable tool for detecting genes with large effect sizes. This strategy is likely to be most effective for diseases and genes under extremely strong selection (e.g., severe autism).

Extending RVAS to noncoding regions might seem like an obvious next step, given that CVAS has identified so many common variants affecting common traits in noncoding regions. However, major challenges must be overcome before this could become practical. Without a clear scheme for aggregating alleles in noncoding regions, RVAS would require a 10- to 100-fold larger sample size to detect comparable effect size in noncoding vs. coding regions. Moreover, there is reason to expect that rare variants of large effects may be skewed toward coding regions.

Our simple framework was chosen to maximize insight and intuition. However, it has limitations, including that it assumes (i) a two-class model for allelic effects, (ii) constant selection across history, (iii) absolute frequency cutoffs, (iv) unrelated cases rather than families, (v) discrete traits rather than quantitative traits, and (vi) no gene  $\times$  environment interaction.

We elaborate on these points in *SI Appendix, Section 14*. In particular, we show that incorporating hypomorphic alleles would not alter our conclusions significantly. Hypomorphic alleles will typically be common rather than rare owing to weaker selection ( $s$  estimated in the range of  $10^{-3}$ – $10^{-4}$ ) (13, 29, 59) and rare hypomorphic alleles will increase detection power only modestly, owing to their smaller effect size (*SI Appendix, Section 5.1*). Both hypomorphic and countervailing alleles will dilute apparent effect sizes. Although we ignore them for initial gene detection in RVAS, it will be important to consider the possibility of such alleles once a gene has been implicated.

Our paper also addresses certain questions in human population genetics. Contrary to some suggestions, the increase in the number of distinct alleles resulting from the human population explosion over the last  $\sim 1,000$  generations has not led to an increase in the total frequency of disease or a greater role for younger alleles in disease. The paper also raises a number of further research questions in human genetics, including improved ways to estimating  $s$  and  $\alpha$  for each gene and analyzing gene sets comprised of genes with varying properties (60).

There is currently little empirical evidence about (i) whether rare variants associated with a disease will reveal many new

genes beyond those already implicated by common variants and (ii) whether the contribution of rare variants to the heritability of common disease will be large or small. Most of the loci discovered so far account for only a fraction of a percentage point of the phenotypic variance (with a few exceptions such as *LDLR* above), but large, systematic studies will be required to assess the combined contribution across loci. The answer may differ across common diseases, with rare variants likely to

play a greater role in disorders such as schizophrenia and autism and, perhaps, cancer. Regardless of their overall contribution, rare variants in specific genes can enable clinical insights about function.

Assuming that large-scale sequencing gets underway for many diseases, the coming years should be an exciting period for human genetics as we finally are able to probe the full genetic architecture underlying human disease.

- Manolio TA, et al. (2009) Finding the missing heritability of complex diseases. *Nature* 461(7265):747–753.
- Zuk O, Hechter E, Sunyaev SR, Lander ES (2012) The mystery of missing heritability: Genetic interactions create phantom heritability. *Proc Natl Acad Sci USA* 109(4):1193–1198.
- Antonarakis SE, Chakravarti A, Cohen JC, Hardy J (2010) Mendelian disorders and multifactorial traits: The big divide or one for all? *Nat Rev Genet* 11(5):380–384.
- Cohen J, et al. (2005) Low LDL cholesterol in individuals of African descent resulting from frequent nonsense mutations in PCSK9. *Nat Genet* 37(2):161–165.
- Cohen JC, Boerwinkle E, Mosley TH, Jr., Hobbs HH (2006) Sequence variations in PCSK9, low LDL, and protection against coronary heart disease. *N Engl J Med* 354(12):1264–1272.
- Lango Allen H, et al. (2010) Hundreds of variants clustered in genomic loci and biological pathways affect human height. *Nature* 467(7317):832–838.
- Teslovich TM, et al. (2010) Biological, clinical and population relevance of 95 loci for blood lipids. *Nature* 466(7307):707–713.
- van der Harst P, et al. (2012) Seventy-five genetic loci influencing the human red blood cell. *Nature* 492(7429):369–375.
- Lee SH, et al.; Schizophrenia Psychiatric Genome-Wide Association Study Consortium (PGC-SCZ); International Schizophrenia Consortium (ISC); Molecular Genetics of Schizophrenia Collaboration (MGS) (2012) Estimating the proportion of variation in susceptibility to schizophrenia captured by common SNPs. *Nat Genet* 44(3):247–250.
- Yang J, et al. (2010) Common SNPs explain a large proportion of the heritability for human height. *Nat Genet* 42(7):565–569.
- Yang J, et al. (2011) Genome partitioning of genetic variation for complex traits using common SNPs. *Nat Genet* 43(6):519–525.
- Goldstein DB, et al. (2013) Sequencing studies in human genetics: Design and interpretation. *Nat Rev Genet* 14(7):460–470.
- Kryukov GV, Pennacchio LA, Sunyaev SR (2007) Most rare missense alleles are deleterious in humans: Implications for complex disease and association studies. *Am J Hum Genet* 80(4):727–739.
- Pritchard JK (2001) Are rare variants responsible for susceptibility to complex diseases? *Am J Hum Genet* 69(1):124–137.
- Kiezun A, et al. (2012) Exome sequencing and the genetic basis of complex traits. *Nat Genet* 44(6):623–630.
- Farooqi S, O'Rahilly S (2006) Genetics of obesity in humans. *Endocr Rev* 27(7):710–718.
- Ahituv N, et al. (2007) Medical sequencing at the extremes of human body mass. *Am J Hum Genet* 80(4):779–791.
- Bonnefond A, et al.; Meta-Analysis of Glucose and Insulin-Related Traits Consortium (MAGIC) (2012) Rare MTNR1B variants impairing melatonin receptor 1B function contribute to type 2 diabetes. *Nat Genet* 44(3):297–301.
- Cohen JC, et al. (2004) Multiple rare alleles contribute to low plasma levels of HDL cholesterol. *Science* 305(5685):869–872.
- Diogo D, et al.; Consortium of Rheumatology Researchers of North America; Rheumatoid Arthritis Consortium International (2013) Rare, low-frequency, and common variants in the protein-coding sequence of biological candidate genes from GWASs contribute to risk of rheumatoid arthritis. *Am J Hum Genet* 92(1):15–27.
- Ji W, et al. (2008) Rare independent mutations in renal salt handling genes contribute to blood pressure variation. *Nat Genet* 40(5):592–599.
- Johansen CT, et al. (2010) Excess of rare variants in genes identified by genome-wide association study of hypertriglyceridemia. *Nat Genet* 42(8):684–687.
- Rivas MA, et al.; National Institute of Diabetes and Digestive Kidney Diseases Inflammatory Bowel Disease Genetics Consortium (NIDDK IBDGC); United Kingdom Inflammatory Bowel Disease Genetics Consortium; International Inflammatory Bowel Disease Genetics Consortium (2011) Deep resequencing of GWAS loci identifies independent rare variants associated with inflammatory bowel disease. *Nat Genet* 43(11):1066–1073.
- Romeo S, et al. (2009) Rare loss-of-function mutations in ANGPTL family members contribute to plasma triglyceride levels in humans. *J Clin Invest* 119(1):70–79.
- Basu S, Pan W (2011) Comparison of statistical tests for disease association with rare variants. *Genet Epidemiol* 35(7):606–619.
- Stitzel NO, Kiezun A, Sunyaev S (2011) Computational and statistical approaches to analyzing variants identified by exome sequencing. *Genome Biol* 12(9):227.
- Ladouceur M, Dastani Z, Aulchenko YS, Greenwood CM, Richards JB (2012) The empirical power of rare variant association methods: Results from sanger sequencing in 1,998 individuals. *PLoS Genet* 8(2):e1002496.
- Yampolsky LY, Kondrashov FA, Kondrashov AS (2005) Distribution of the strength of selection against amino acid replacements in human proteins. *Hum Mol Genet* 14(21):3191–3201.
- Boyko AR, et al. (2008) Assessing the evolutionary impact of amino acid mutations in the human genome. *PLoS Genet* 4(5):e1000083.
- Nelson MR, et al. (2012) An abundance of rare functional variants in 202 drug target genes sequenced in 14,002 people. *Science* 337(6090):100–104.
- Eyre-Walker A, Keightley PD (2007) The distribution of fitness effects of new mutations. *Nat Rev Genet* 8(8):610–618.
- Eyre-Walker A, Woolfit M, Phelps T (2006) The distribution of fitness effects of new deleterious amino acid mutations in humans. *Genetics* 173(2):891–900.
- Keightley PD, Eyre-Walker A (2007) Joint inference of the distribution of fitness effects of deleterious mutations and population demography based on nucleotide polymorphism frequencies. *Genetics* 177(4):2251–2261.
- Jobling M, Hurles M, Tyler-Smith C (2004) *Human Evolutionary Genetics: Origins, Peoples & Disease* (Garland Science, New York).
- Kimura M (1964) Diffusion models in population genetics. *J Appl Probab* 1(2):177–232.
- Kimura M, Crow JF (1964) The number of alleles that can be maintained in a finite population. *Genetics* 49:725–738.
- Ewens WJ (2004) *Mathematical Population Genetics: I. Theoretical Introduction* (Springer, New York), 2nd Ed.
- Haldane JBS (1927) A mathematical theory of natural and artificial selection. *Math Proc Camb Philos Soc* 23(5):607–615.
- Reich DE, Lander ES (2001) On the allelic spectrum of human disease. *Trends Genet* 17(9):502–510.
- Tennessen JA, et al.; Broad GO; Seattle GO; NHLBI Exome Sequencing Project (2012) Evolution and functional impact of rare coding variation from deep sequencing of human exomes. *Science* 337(6090):64–69.
- Marth GT, Czarbarka E, Murvai J, Sherry ST (2004) The allele frequency spectrum in genome-wide human variation data reveals signals of differential demographic history in three large world populations. *Genetics* 166(1):351–372.
- Keinan A, Clark AG (2012) Recent explosive human population growth has resulted in an excess of rare genetic variants. *Science* 336(6082):740–743.
- Lupski JR, Belmont JW, Boerwinkle E, Gibbs RA (2011) Clan genomics and the complex architecture of human disease. *Cell* 147(1):32–43.
- Li Y, et al. (2010) Resequencing of 200 human exomes identifies an excess of low-frequency non-synonymous coding variants. *Nat Genet* 42(11):969–972.
- Haukka J, Suvisaari J, Lonnqvist J (2003) Fertility of patients with schizophrenia, their siblings, and the general population: A cohort study from 1950 to 1959 in Finland. *Am J Psychiatry* 160(3):460–463.
- Sunyaev SR (2012) Inferring causality and functional significance of human coding DNA variants. *Hum Mol Genet* 21(R1):R10–R17.
- Adzhubei IA, et al. (2010) A method and server for predicting damaging missense mutations. *Nat Methods* 7(4):248–249.
- Goldstein JL, Schrott HG, Hazzard WR, Bierman EL, Motulsky AG (1973) Hyperlipidemia in coronary heart disease. II. Genetic analysis of lipid levels in 176 families and delineation of a new inherited disorder, combined hyperlipidemia. *J Clin Invest* 52(7):1544–1568.
- Levy-Lahad E, et al. (1997) Founder BRCA1 and BRCA2 mutations in Ashkenazi Jews in Israel: Frequency and differential penetrance in ovarian cancer and in breast-ovarian cancer families. *Am J Hum Genet* 60(5):1059–1067.
- Neale BM, et al. (2011) Testing for an unusual distribution of rare variants. *PLoS Genet* 7(3):e1001322.
- Wu MC, et al. (2011) Rare-variant association testing for sequencing data with the sequence kernel association test. *Am J Hum Genet* 89(1):82–93.
- Autism and Developmental Disabilities Monitoring Network Surveillance Year 2008 Principal Investigators; Centers for Disease Control and Prevention; Centers for Disease Control and Prevention (2012) Prevalence of autism spectrum disorders—Autism and Developmental Disabilities Monitoring Network, 14 sites, United States, 2008. *MMWR Surveill Summ* 61(3):1–19.
- O'Roak BJ, et al. (2012) Sporadic autism exomes reveal a highly interconnected protein network of de novo mutations. *Nature* 485(7397):246–250.
- Neale BM, et al. (2012) Patterns and rates of exonic de novo mutations in autism spectrum disorders. *Nature* 485(7397):242–245.
- Lander ES, Botstein D (1989) Mapping mendelian factors underlying quantitative traits using RFLP linkage maps. *Genetics* 121(1):185–199.
- Chen CT, Wang JC, Cohen BA (2007) The strength of selection on ultraconserved elements in the human genome. *Am J Hum Genet* 80(4):692–704.
- Kryukov GV, Schmidt S, Sunyaev S (2005) Small fitness effect of mutations in highly conserved non-coding regions. *Hum Mol Genet* 14(15):2221–2229.
- Morrison AC, et al.; Cohorts for Heart and Aging Research in Genetic Epidemiology (CHARGE) Consortium (2013) Whole-genome sequence-based analysis of high-density lipoprotein cholesterol. *Nat Genet* 45(8):899–901.
- Kryukov GV, Shpunt A, Stamatoyannopoulos JA, Sunyaev SR (2009) Power of deep, all-exon resequencing for discovery of human trait genes. *Proc Natl Acad Sci USA* 106(10):3871–3876.
- Bustamante CD, et al. (2005) Natural selection on protein-coding genes in the human genome. *Nature* 437(7062):1153–1157.

Searching for Missing Heritability -  
Designing Rare Variants Association Studies:  
Supplementary Information



# Contents

<b>List of Figures</b>	<b>4</b>
<b>List of Tables</b>	<b>5</b>
<b>List of Symbols</b>	<b>6</b>
<b>1 Allele Frequency Distribution for Different Populations: Theory</b>	<b>7</b>
1.1 Generalized Wright-Fisher Model . . . . .	7
1.1.1 Model Parameters . . . . .	7
1.1.2 Stochastic Process Formulation . . . . .	8
1.2 Allele Frequency Distribution at Equilibrium: Analytical Formulas . . . . .	9
1.2.1 Individual Allele Frequency Distribution . . . . .	11
1.3 Allele Frequency Distribution for Different Populations: Simulations . . . . .	12
1.3.1 Description of Demographic Models . . . . .	12
1.3.2 Description of Simulations . . . . .	13
<b>2 Allele Frequency Distribution for Different Populations: Empirical Results</b>	<b>17</b>
2.1 Two-Class Model . . . . .	17
2.2 Combined Allele Frequencies . . . . .	18
2.3 Individual Allele Frequencies . . . . .	20
2.4 Age Distribution of Alleles . . . . .	24
2.5 Proportion of Null Alleles among Missense Alleles . . . . .	24
2.6 Mutation Rates for Observable Classes . . . . .	28
<b>3 Calculating Sample Sizes required for RVAS</b>	<b>29</b>
3.1 Estimating Aggregate Effect Size . . . . .	29
3.1.1 Risk for Carriers of Multiple Allele . . . . .	29
3.1.2 Protective Alleles . . . . .	30
3.2 Calculating Sample Size when $f$ is Already Known . . . . .	30
3.3 Calculating Sample Size when $f$ is Unknown . . . . .	35
3.3.1 Using unaffecteds . . . . .	36
3.3.2 Using controls from the population . . . . .	37
3.4 Tests Proposed in the Literature for RVAS . . . . .	38
<b>4 RVAS Strategy 1: Studying Disruptive Alleles</b>	<b>39</b>
<b>5 RVAS Strategy 2: Incorporating Missense Alleles</b>	<b>42</b>
5.1 Heterogeneity of Alleles - Hypomorphs . . . . .	51
<b>6 RVAS Strategy 3: Enriching for Null Missense Alleles</b>	<b>55</b>

<b>7</b>	<b>Effect of Thresholding in a Finite Sample (with <i>LDLR</i> Example)</b>	<b>58</b>
7.1	<i>LDLR</i> Example . . . . .	59
<b>8</b>	<b>RVAS Strategy 4: Isolated Populations</b>	<b>63</b>
<b>9</b>	<b>RVAS Strategy 5: Using Gene Sets</b>	<b>75</b>
<b>10</b>	<b>RVAS Strategy 6: <i>De novo</i> Mutations</b>	<b>76</b>
<b>11</b>	<b>Prospects for RVAS in Non-coding Regions</b>	<b>78</b>
11.1	Multiple Hypothesis Burden for Genome-Wide Testing . . . . .	78
<b>12</b>	<b>Estimating the Parameters <math>s</math> and <math>\alpha</math> in the Two-class Model</b>	<b>81</b>
12.1	Estimating $s$ . . . . .	81
12.2	Estimating $\alpha$ . . . . .	83
<b>13</b>	<b>Estimating Variance Explained by Rare Variants</b>	<b>85</b>
13.1	Calculating Variance Explained . . . . .	85
13.2	Sample Size Required to Detect Loci Explaining a Given Proportion of the Phenotypic Variance . . . . .	85
13.3	Estimating heritability explained by rare variants for two traits . . . . .	86
13.3.1	Blood Pressure [Ji et al 2008] . . . . .	86
13.3.2	Type 2 Diabetes [Bonnenfond et al. 2012] . . . . .	90
<b>14</b>	<b>Consequences and Limitations of our Framework</b>	<b>91</b>

## List of Figures

1	The Combined Allele Frequencies for all Populations . . . . .	19
2	Median of Individual Allele Frequencies for all Populations . . . . .	22
3	Cumulative Allele Frequencies for all Populations . . . . .	23
4	Median of allelic age distribution . . . . .	25
5	Cumulative allelic age distribution . . . . .	26
6	Fraction of missense alleles that are null . . . . .	27
7	Approximating power using the non-centrality parameter . . . . .	32
8	Relationship between effect size and power . . . . .	34
9	Sample size required to detect disruptive alleles . . . . .	40
10	Sample size required to detect protective alleles . . . . .	41
11	Power-gain from using Missense alleles as function of threshold . . . . .	44
12	Power-gain from using Missense alleles as function of threshold for large $\lambda$ . . . . .	45
13	Power-gain from using Missense alleles as function of threshold for small $\lambda$ . . . . .	46
14	Tradeoff between $\Psi_s(T^*)$ and $\rho_s(T^*)$ . . . . .	47
15	Increase in power from using missense hypomorph alleles . . . . .	54
16	Power-gain from functional prediction of missense null alleles . . . . .	57
17	Proportion of null alleles when using a threshold in a finite sample . . . . .	62
18	Variation in Combined Allele Frequency for $s = 10^{-1}$ . . . . .	64
19	Variation in Combined Allele Frequency for $s = 10^{-1.5}$ . . . . .	65
20	Variation in Combined Allele Frequency for $s = 10^{-2}$ . . . . .	66
21	Variation in Combined Allele Frequency for $s = 10^{-2.5}$ . . . . .	67
22	Variation in Combined Allele Frequency for $s = 10^{-3}$ . . . . .	68
23	Power to detect <i>de novo</i> alleles . . . . .	77
24	Confidence intervals around estimated value of $s$ . . . . .	82



## List of Tables

1	Parameters for different demographic models . . . . .	13
2	Combined Allele Frequency for different populations . . . . .	18
3	Median Allele Frequency for different populations . . . . .	21
4	Optimal threshold for Equilibrium model . . . . .	48
5	Optimal threshold for Expansion1 model . . . . .	48
6	Optimal threshold for Expansion2 model . . . . .	49
7	Optimal threshold for Europe model . . . . .	49
8	Optimal threshold for Finland model . . . . .	50
9	Optimal threshold for Iceland model . . . . .	50
10	Contribution of hypomorph alleles under perfect knowledge . . . . .	52
11	Contribution of hypomorph alleles under imperfect knowledge . . . . .	53
12	Association test for <i>LDLR</i> . . . . .	61
13	Variation in $f_D$ for Equilibrium model . . . . .	69
14	Variation in $f_{null}$ for Equilibrium model . . . . .	69
15	Variation in $f_D$ for Expansion1 model . . . . .	70
16	Variation in $f_{null}$ for Expansion1 model . . . . .	70
17	Variation in $f_D$ for Expansion2 model . . . . .	71
18	Variation in $f_{null}$ for Expansion2 model . . . . .	71
19	Variation in $f_D$ for Europe model . . . . .	72
20	Variation in $f_{null}$ for Europe model . . . . .	72
21	Variation in $f_D$ for Finland model . . . . .	73
22	Variation in $f_{null}$ for Finland model . . . . .	73
23	Variation in $f_D$ for Iceland model . . . . .	74
24	Variation in $f_{null}$ for Iceland model . . . . .	74
25	Phenotypic variance explained by rare variants in <i>SCL12A3</i> , <i>SCL12A1</i> , and <i>KCNJ1</i>	88

## List of Symbols

$L$	Target size (number of sites, in nucleotides)	7
$\mu_{C,nc}$	Mutation rate (per-nucleotide per-generation)	7
$\mu_C$	Mutation rate (per-class per-generation)	7
$s$	Selection coefficient	7
$K$	Total number of generations since ancestral population in a demographic model	8
$N$	Effective population Size	8
$S$	Re-scaled selection coefficient ( $S = 4Ns$ )	8
$f$	Derived allele frequency	8
$t_s$	Mean time until fixation/extinction for an allele with selection coefficient $s$	8
$\psi_s$	Density distribution of allele frequency for selection coefficient $s$	8
$\Psi_s$	Cumulative distribution of allele frequency for selection coefficient $s$	9
$A_s$	Probability distribution of age of alleles	9
$\gamma$	Euler's constant, $\gamma \sim 0.5772$	10
$Ei$	Exponential integral function, $Ei(x) \equiv \int_{-\infty}^x \frac{e^t}{t} dt$	10
$\lambda$	Effect size: relative in disease risk conferred by an allele	17
$\alpha$	Fraction of null missense alleles at births	17
$\rho_s$	Fraction of null missense alleles for alleles below a certain frequency	24
$\pi$	Disease prevalence	29
$n$	Number of samples in an RVAS study	29
$d$	Number of observed derived alleles in an RVAS study	29
$\mathcal{LL}$	Log-likelihood	30
$\mathcal{LLR}$	Log-likelihood ratio	30
$NCP$	Non-Centrality-Parameter	30
$V$	Heritability: Total variance explained by a set of alleles	85

## Software

Matlab code performing most of the mathematical calculations and simulations used in the paper is available as part of "heritability calculator" package <http://www.broadinstitute.org/mpg/hc>. A separate software package for simulations of demographic model was written by Stephen Schaffner ([sfs@broadinstitute.org](mailto:sfs@broadinstitute.org)).

## 1 Allele Frequency Distribution for Different Populations: Theory

In this section we show how to compute allele frequency distribution of a class  $C$  of alleles, having a known selection coefficient  $s$ . Throughout the paper, we assume that the dynamics of allele frequencies throughout human demographic history follow a generalized Wright-Fisher model [1, 2].

### 1.1 Generalized Wright-Fisher Model

We assume a generalized Wright-Fisher model incorporating mutation, selection, and changes in population size throughout history; see for example [3]. (Other aspects such as migration and admixture are ignored for simplicity). We consider a target region, which we can imagine to be the coding region of a gene; however, the analysis could apply equally to other targets (such as a set of coding regions, or an extended genomic region). Within the region, each nucleotide (site) is assumed to have two possible alleles: the ancestral allele and the derived allele.

#### 1.1.1 Model Parameters

We consider a class  $C$  of alleles that are functionally and selectively equivalent. (for example, disruptive alleles; silent alleles; or missense alleles that abolish gene function). Our model has the following parameters,

1. Target size:  $L$  denotes the length of the target (measured in nucleotides).
2. Mutation rate:  $\mu_{C,nc}$  denotes the rate per-generation per-nucleotide at which new derived alleles in class  $C$  arise.  $\mu_C$  denotes the rate for the entire target (for example, all mutation in a certain class in a gene), given by  $\mu_C = L\mu_{C,nc}$ .
3. Selection coefficient:  $s$  denotes the selection coefficient for derived alleles in  $C$ . The selection coefficient  $s$  is defined as the relative reduction in the expected number of offspring for carriers of the allele compared to non-carriers. An allele with frequency  $f_t$  in one generation has expected frequency  $f_{t+1} = \frac{(1-s)f_t}{1-f_t s}$  in the next generation. Given that the individual allele frequencies under consideration are tiny,  $f_{t+1} \approx (1-s)f_t$ . (Simulations (see Section 1.3.2) performed with the exact or approximate formula yield essentially indistinguishable results).



We assume an additive model for fitness in which selection on an allele does not depend on the genetic background (that is, the value of other alleles).

4. Population size:  $N^{(k)}$  denotes the population size at generation  $k$ , where  $k$  ranges from 1 to the total number of generations,  $K$ , under consideration. For the special case of population at equilibrium, we denote the effective population size by  $N$  or  $N_{eq}$ .
5. Re-scaled selection coefficient:  $S = 4Ns$  denotes the selection coefficient re-scaled by the population size, where  $N$  is the population size at a given time.

### 1.1.2 Stochastic Process Formulation

We next formulate the generalized Wright-Fisher model as a discrete-time discrete-space stochastic process. We can formulate the process in terms of allele frequencies: we denote the derived allele frequency of a polymorphic allele in the population by  $f$ . More specifically, we define  $f_i^{(k)}$  the allele frequency of the  $i$ -th allele at generation  $k$  ( $i = 1, \dots, L$ ). Similarly, we denote  $X_i^{(k)}$  the number of carriers of the  $i$ -th derived allele at generation  $k$ . Both  $f_i^{(k)}$  and  $X_i^{(k)}$  are random variables, whose distributions are given by the following generative process,

1. Initialize  $X_i^{(0)} = f_i^{(0)} = 0$  for  $i = 1, \dots, L$  - all sites are assumed to carry the ancestral allele.

2. For  $k = 1$  to  $K$ ,

- (a) Draw  $X_i^{(k+1)}$  according to a binomial distribution,

$$X_i^{(k+1)} \sim \text{Binomial}\left(2N^{(k+1)}, f_i^{(k)} \frac{1 - s_i}{1 - f s_i}\right). \quad (1.1)$$

- (b) Set  $f_i^{(k+1)} = \frac{X_i^{(k+1)}}{2N^{(k+1)}} + \mu_{C,nc}$  to account for mutations.

We are interested in several properties of the allele frequency distribution as a function of the parameters of the model defined above.

1. Time spent at each frequency: Each newly born allele spends a certain amount of time (number of generations) in a polymorphic state at each given frequency  $0 < f < 1$  until it is either fixed or becomes extinct. We denote by  $t_s(f)$  the *density* of the mean time the allele spends in a polymorphic state at frequency  $f$ . That is, the number of generations spent between frequencies  $f$  and  $\Delta f$  is  $\int_f^{f+\Delta f} t_s(f') df'$ .
2. Total time spent at polymorphic state: Each newly born allele spends a certain amount of time (number of generations) in a polymorphic state until it is either fixed or becomes extinct. We denote by  $t_s$  the mean time the allele spends in a polymorphic state.
3. Probability density function: We denote the allele frequency probability density function by  $\psi_s$ , where we sample alleles with probability proportional to their derived allele frequencies  $f_i$ . That is, we consider the distribution of allele frequencies obtained when sampling a

random individual from the population, and then sampling a random derived allele from this individual, and denote  $\psi_s(f)$  the density obtained for this distribution.

4. Cumulative distribution function: We denote the cumulative probability function for allele frequencies by  $\Psi_s$ . Here we sample alleles with probability proportional to their derived allele frequencies  $f_i$  as above.
5. Age distribution of alleles: We denote by  $A_s(k)$  the probability that a randomly sampled alleles on a randomly sampled chromosome from the population is of age  $k$ , i.e. was born  $k$  generations ago.

The model parameters  $\mu_C, s$  and  $N^{(k)}$  determine all quantities of interest above.

For population at equilibrium, Kimura solved the Wright-Fisher process analytically in the limit of large population size  $N$ , by using a diffusion approximation; see for example [3–6]. In Section 1.2, we use these solutions to give analytic formulas for the above quantities for a population at equilibrium. For general demographies, there is no known closed form solution, although some partial results and special cases are known (for example [7–9]), and one needs to resort to numerical calculations. In Section 1.3, we compute the quantities above by using simulations for various demographies.

## 1.2 Allele Frequency Distribution at Equilibrium: Analytical Formulas

In this section we compute parameters of interest for a *single* allele using a diffusion approximation for large  $N$ . We assume throughout the generalized Wright-Fisher model from eqs. (2). Kimura and Crow [6] expressed the *expected time* a newly born allele spends at allele frequency  $f$  as,

$$t_s(f) = \frac{2[1 - e^{-S(1-f)}]}{f(1-f)(1 - e^{-S})}. \quad (1.2)$$

This is the density distribution of expected number of generations spent at frequency  $f$  (such that the number of generations spent between frequency  $f$  and  $f + \Delta f$  is the integral of  $t_s(f)$  in this range). From  $t_s(f)$  we can compute all parameters of interest for the model using standard integrations and asymptotic expansions.

For example, we define the mean total *weighted* frequency  $T_s$  that a newly born allele accumulates throughout its life in a polymorphic state, until it is either lost or fixed in the population. The units of  $T_s$  are (frequency  $\times$  generations). For example, for an allele which survive on average three generation as a singleton and two generation as a doubleton on average we will have  $T_s = 3 \times \frac{1}{2N} + 2 \times \frac{2}{2N} = \frac{7}{2N}$ . We have the following for the mean total weighted frequency  $T_s$ ,

**Proposition 1** *The total weighted frequency a newly born allele accumulates throughout its life time, until it dies, is given by, (in units of frequency  $\times$  generations) is*

$$T_s \equiv \int_0^1 f t_s(f) df = \frac{2[\log(-S) + \gamma - Ei(-S)]}{1 - e^{-S}} \quad (1.3)$$

where  $\gamma$  is Euler's constant ( $\gamma \sim 0.5772$ ), and  $Ei$  is the exponential integral function, defined as,

$$Ei(f) \equiv \int_{-\infty}^f \frac{e^x}{x} dx. \quad (1.4)$$

**Proof 1** Using the definition of  $T_s$ , we integrate to get

$$\begin{aligned} T_s &= \int_0^1 f t_s(f) df \\ &= \frac{2}{1 - e^{-S}} \int_0^1 \frac{1 - e^{-S(1-f)}}{(1-f)} df \\ &= \frac{2}{1 - e^{-S}} \left[ -\log(1-f) + e^S Ei(S(f-1)) \right]_{f=0}^1 \\ &= \frac{2}{1 - e^{-S}} \left[ \lim_{x \rightarrow 0} (-\log(x) + e^S Ei(S(-x))) - e^S Ei(-S) \right] \\ &= \frac{2[\log(-S) + \gamma - Ei(-S)]}{1 - e^{-S}}. \end{aligned} \quad (1.5)$$

where here and throughout, we use the following asymptotic expansions for  $Ei(x)$  in different regimes,

$$\begin{aligned} Ei(x) &\sim \log(x) + \gamma + x, \quad x \rightarrow 0 \\ Ei(x) &\sim \frac{e^x}{x} \left( 1 + \frac{1}{x} + \frac{2}{x^2} \right), \quad x \rightarrow \pm\infty \end{aligned} \quad (1.6)$$

■

**Proposition 2** For a class  $C$  of alleles with total mutation rate  $\mu_C$ , the Combined Allele Frequency (CAF) at equilibrium is

$$f_C = 2N\mu_C T_s = \frac{4N\mu_C [\log(-S) - Ei(-S) + \gamma]}{1 - e^{-S}}. \quad (1.7)$$

In addition, we have the following asymptotic approximations for weak selection (nearly-neutral alleles,  $S \rightarrow 0$ ) and very strong selection ( $S \rightarrow \infty$ ),

$$f_C \approx \begin{cases} 4N\mu_C & S \ll 1 \\ \frac{\mu_C}{s} & S \gg 1 \end{cases} \quad (1.8)$$



**Proof 2** The combined allele frequency is given by multiplying the population mutation rate per generation,  $2N\mu_C$ , by the total time spent in polymorphic state for a given allele,  $T_S$ , giving  $f_C = [2N\mu_C]T_S$ . Plugging into eq. (1.3) gives the formula for  $f_C$ .

For the asymptotic relations, we have,

$$\begin{aligned}\lim_{S \rightarrow 0} f_C &= 4N\mu_C \lim_{S \rightarrow 0} \frac{\log(-S) + \gamma - Ei(-S)}{1 - e^{-S}} \\ &= 4N\mu_C \lim_{S \rightarrow 0} \frac{\log(-S) + \gamma - [\log(-S) + \gamma - S]}{S} \\ &= 4N\mu_C.\end{aligned}\tag{1.9}$$

$$\begin{aligned}\lim_{S \rightarrow \infty} f_C &= 4N\mu_C \lim_{S \rightarrow \infty} \frac{\log(-S) + \gamma - Ei(-S)}{1 - e^{-S}} \\ &= 4N\mu_C \lim_{S \rightarrow \infty} \frac{-e^{-S}/S}{-e^{-S}} = \frac{4N\mu_C}{4Ns} \\ &= \frac{\mu_C}{s}.\end{aligned}\tag{1.10}$$

■

For strong selection, the above relation  $f_C \approx \frac{\mu_C}{s}$  can also be obtained by considering mutation-selection balance, as observed early on by Fisher [1] and Haldane [10].

### 1.2.1 Individual Allele Frequency Distribution

We compute here the distribution of individual allele frequencies at equilibrium - recall that we use *weighted* sampling, where individual alleles are sampled with *weight* proportional to their frequency (alternatively, this is the distribution obtained when sampling a random chromosome in the population, sampling a random derived allele from this chromosome, and observing the frequency of this allele). The individual allele frequency distribution is given by the following proposition (the proof is given by simple integration),

**Proposition 3** For a population at equilibrium, at the large  $N$  limit, we have,

1. The probability density function is

$$\psi_s(f) = \frac{ft_s(f)}{\int_0^1 xt_s(x)dx} = \frac{1 - e^{-S(1-f)}}{(1-f)[\gamma - Ei(-S) + \log(-S)]}.\tag{1.11}$$

2. The cumulative distribution function is,

$$\Psi_s(f) = \int_0^f \psi_s(x)dx = \frac{Ei(S(f-1)) - \log(1-f) - Ei(-S) + \log(-S)}{\gamma + \log(-S) - Ei(-S)}.\tag{1.12}$$

**Proof 3** 1. By definition, and plugging in eqs. (1.2, 1.3),

$$\begin{aligned}
\psi_s(f) &= \frac{ft_s(f)}{\int_0^1 xt_s(x)dx} \\
&= \frac{1 - e^{-S(1-f)}}{(1-f)(1 - e^{-S})} \bigg/ \frac{\log(-S) + \gamma - Ei(-S)}{1 - e^{-S}} \\
&= \frac{1 - e^{-S(1-f)}}{(1-f)[\gamma - Ei(-S) + \log(-S)]}.
\end{aligned} \tag{1.13}$$

2. Integrating, we get

$$\begin{aligned}
\Psi_s(f) &= \int_0^f \psi_s(x)dx \\
&= \frac{1}{\gamma - Ei(-S) + \log(-S)} \int_0^f \frac{1 - e^{-S(1-x)}}{1-x} \\
&= \frac{1}{\gamma - Ei(-S) + \log(-S)} \left[ -\log(1-x) + e^S Ei(S(x-1)) \right]_{x=0}^f \\
&= \frac{Ei(S(f-1)) - \log(1-f) - Ei(-S) + \log(-S)}{\gamma + \log(-S) - Ei(-S)}.
\end{aligned} \tag{1.14}$$

■

### 1.3 Allele Frequency Distribution for Different Populations: Simulations

The human population is not at equilibrium, but has changed in size. Recent human evolution has seen an exponential explosion in population size [11]. In addition, migration events, such as the out-of-Africa event [12] or the peopling of isolated regions such as Iceland [13] and Finland [14], have created population bottlenecks. We study several simple demographic models that capture key features of population expansion and bottlenecks. For each model, we used simulations to compute the resulting allele frequency distribution and the parameters of interest.

#### 1.3.1 Description of Demographic Models

We considered six models:

1. **Equilibrium:** The ancestral human population, assumed to have constant population size.
2. **Expansion1:** simple exponential expansion
3. **Expansion2:** two-phase exponential expansion, incorporating a recent period of more rapid growth (as suggested by recent human genetic data).
4. **Europe:** a model of the peopling of Europe, with a bottleneck roughly 1280 generations ago.

5. **Finland:** a model of the peopling of Finland, with a severe bottleneck roughly 100 generations ago
6. **Iceland:** a model of the peopling of Finland, with a severe bottleneck roughly 50 generations ago

All models have an exponential expansion stage, which corresponds to recent expansion in human populations. Some of the models contain bottleneck stages.

The parameters describing the models are as follows,

1.  $\epsilon_1$  - the relative increase in population size, per generation, first stage.
2.  $k_1$  - the number of generations in the first stage.
3.  $N_e(B)$  - the population size (number of individuals) surviving the first bottleneck.
4.  $\epsilon_2$  - the relative increase in population size, per generation, second stage.
5.  $k_2$  - number of generation in second stage, after the population bottleneck.

The parameters used for different models are shown in Table S1.

Model	$\epsilon_1$	$k_1$	$N_e(B)$	$\epsilon_2$	$k_2$	$N_e(final)$
Equilibrium	0.0%	0	-	0.0%	0	10,000
Expnasion1	0.462%	1000	-	0.0%	0	1,000,000
Expansion2	0.197%	1230	-	9.4%	50	10,000,000
Europe <sup>(*)</sup>	0.396%	1230	775	9.4%	50	9,000,000
Finland	0.462%	900	50	12.2%	100	5,000,000
Iceland	0.462%	950	500	13.2%	50	250,000

Table 1: Parameters for different demographic models. We also display the resulting final population size. (\*) For Europe, we assume an *ancient* bottleneck, before the two expansion periods. For Iceland and Finland we assume a *recent* bottleneck, between the two expansion periods. For Europe we stopped the simulation  $\sim 50$  generations ago at a population of  $\sim 9$  millions for computational reasons. The last few generations which have a huge population size and are expected to produce only alleles with tiny frequencies. Since our results all depend on the *weighted* allele frequency distributions, ignoring these generations should not alter our results significantly.

### 1.3.2 Description of Simulations

We initialized the population size of all models to  $N_{eq} = 10,000$ , and run at this constant population size for a "burn-in period" of  $k_B = 20N_{eq} = 200,000$  simulations, to reach equilibrium. The mutation rate (per-chromosome per-generation) was set to  $\mu_D = 1.7 \times 10^{-6}$ . We varied

the selection coefficient on a logarithmic scale with increments of 0.1 in the exponent, getting  $s = 10^{-1}, 10^{-1.1}, 10^{-1.2}, \dots, 10^{-4.9}, 10^{-5}$ , and in addition we used  $s = 0$  representing neutral alleles.

For each selection coefficient and population, we performed  $I = 50,000$  independent simulations (representing histories for 50,000 equivalent genes).

The simulations roughly followed the stochastic process described in Section 1.1.2. Specifically, we describe the Monte-Carlo simulation algorithm we used in Box 1. The values we used for all other parameters not described above are given in Table S1.

**Box 1: Algorithm for Simulating Allele Frequency Distribution****Input Parameters:** $N_{eq}$  - Initial population size at equilibrium $s$  - selection coefficient $\mu_C$  - mutation rate $\epsilon_1, \epsilon_2, k_1, k_2, N_e(B)$  - demographic parameters (see Table S1) $k_B$  - 'burn-in' parameter (number of generations run at ancestral population at equilibrium) $I$  - number of iterations to simulate**Output:** $\hat{f}_C$  - Mean Combined allele frequency $\hat{\Psi}_s(f)$  - Cumulative individual allele frequency distribution $\hat{\psi}_s(f)$  - Density of individual allele frequency distribution $\hat{A}(k)$  - Age probability distribution**Steps:**1. Repeat  $I$  times, for  $i = 1$  to  $I$ ,(a) Initialize  $n_i$ , the counter of the number of derived alleles: set  $n_i = 0$ .(b) Set  $K = k_B + k_1 + k_2$ , the total number of generations to simulate.(c) For  $k = 1$  to  $K$ ,

i. Set population size for next generation,

$$N^{(k+1)} = \begin{cases} N & k < k_B \\ N_e(B) & k = k_B \quad (^*) \text{ only for Europe) } \\ \lfloor N^{(k)}(1 + \epsilon_1) \rfloor & k_B < k < k_B + k_1 \\ N_e(B) & k = k_B + k_1 \quad (\text{only for Iceland and Finland}) \\ \lfloor N^{(k)}(1 + \epsilon_2) \rfloor & k_B + k_1 < k \end{cases} \quad (1.15)$$

ii. For  $j = 1$  to  $n_i$  (all existing derived alleles)A. Draw  $X_{ij}^{(k+1)}$  according to a binomial distribution,

$$X_{ij}^{(k+1)} \sim \text{Binomial}\left(2N^{(k+1)}, f_{ij}(1 - s_i)\right)$$

B. Update the frequency: set  $f_{ij} = \frac{X_{ij}^{(k+1)}}{2N^{(k+1)}}$ iii. A. Draw  $n_{new} \sim \text{Binomial}(2N^{(k+1)}, \mu_C)$ , the number of newly born alleles.



- B. Set singleton frequency for newly born alleles  $f_{ij} = \frac{1}{2N^{(k+1)}}$  for  $j = n_i + 1, \dots, n_i + n_{new}$ .
  - C. Record the generation at which each new allele is born,  $a_{ij} = k$ .
  - D. Update number of polymorphic alleles: set  $n_i = n_i + n_{new}$ .
- (d) Record final individual allele frequencies,  $f_{ij}$  for all  $i = 1, \dots, I$  and  $j = 1, \dots, n_i$ .
2. Compute empirical summary statistics from final outputs:
- (a) Combined allele frequency

$$\hat{f}_C = \frac{1}{I} \sum_{i=1}^I \sum_{j=1}^{n_i} f_{ij} \quad (1.16)$$

- (b) Cumulative individual allele frequency

$$\hat{\Psi}_s(f) = \frac{1}{I\hat{f}_C} \sum_{i=1}^I \sum_{j=1}^{n_i} 1_{\{f_{ij} \leq f\}} f_{ij} \quad (1.17)$$

- (c) Individual allele frequency density: Split the unit interval  $[0, 1]$  into bins  $B_0 = 0 < B_1 < \dots < B_M = 1$ . Then, for  $f \in [B_i, B_{i+1})$ , we have,

$$\hat{\psi}_s(f) = \frac{1}{I\hat{f}_C[B_{i+1} - B_i]} \sum_{i=1}^I \sum_{j=1}^{n_i} 1_{\{B_i \leq f_{ij} < B_{i+1}\}} f_{ij} \quad (1.18)$$

- (d) Age distribution: ( $\hat{A}_s(k)$  is the estimated probability of an allele to be born  $k$  generations before the end of the simulation)

$$\hat{A}_s(k) = \frac{1}{I\hat{f}_C} \sum_{i=1}^I \sum_{j=1}^{n_i} 1_{\{a_{ij} = K - k\}} f_{ij} \quad (1.19)$$

## 2 Allele Frequency Distribution for Different Populations: Empirical Results

We now turn from theory to simulated empirical results.

In section 1 we described the theory needed for computing the properties of a single allele in the population. In practice, we want to use a heterogeneous class of different alleles (namely, missense alleles) having different selection coefficients, different effects on gene function and phenotype, etc. To handle this heterogeneity, we propose a simple two-class model, described in the next section. We then show results for allele frequency distribution under this model and for the different populations describe in Section 1.3.

### 2.1 Two-Class Model

As described in the main text, we adopt a simple two-class model in which all alleles in a gene are either neutral or null. Consider a gene  $G$  and a disease  $D$ . Given an allele in  $G$ , let  $s_{allele}$  denote the selection coefficient for the allele and let  $\lambda_{allele}$  denote the excess relative risk for  $D$  conferred by the allele.

1. Neutral alleles have no effect on selection or on the disease under study - that is  $s_{allele} = \lambda_{allele} = 0$ .
2. Null alleles abolish gene function. We have  $s_{allele} = s$  and  $\lambda_{allele} = \lambda$ , where  $s$  and  $\lambda$  are constant for each gene.

Alleles in the coding region of a gene can be divided into three observable classes.

1. Silent alleles, which do not affect the amino-acid sequence. We assume that all silent alleles are neutral.
2. Disruptive alleles, which produce nonsense, frameshift, and splice-site changes. We assume that all disruptive alleles are null.
3. Missense alleles follow a two-class model. Each newly born missense allele is assumed to be either null (with probability  $\alpha$ ) or neutral (with probability  $(1 - \alpha)$ ).

In the main text, we primarily assume that  $\alpha = 25\%$ , which is the average value across genes [15]. However, the value of  $\alpha$  appears to vary across genes. By comparing the deficit of missense alleles relative to silent alleles in the NHLBI Exome Sequencing Project (<http://evs.gs.washington.edu/EVS>), one can estimate values of  $\alpha = 5\%$  for *BRCA2* and  $\alpha = 50\%$  for *CHD8*.

## 2.2 Combined Allele Frequencies

We computed the (expected) combined allele frequencies for the different populations, and for different selection coefficients, as described in Section 1.3 and shown in Figure 1(a) in the main text, reproduced here in Figure 1.

In Table S2 we give the computed values for selected values of  $s$ , showing that the CAF is very similar for different populations, as previously observed [16].

s	Equilibrium	Expansion1	Expansion2	Europe	Finland	Iceland
0	0.0756	0.076	0.0762	0.0712	0.0708	0.0764
$10^{-5}$	0.0681	0.0695	0.0683	0.0638	0.0625	0.0691
$10^{-4.5}$	0.0533	0.0542	0.0542	0.0506	0.0511	0.0539
$10^{-4}$	0.0236	0.0241	0.0234	0.0231	0.0221	0.0238
$10^{-3.5}$	0.00561	0.00535	0.00516	0.00551	0.00497	0.00521
$10^{-3}$	0.00148	0.00145	0.0014	0.00144	0.00137	0.00137
$10^{-2.5}$	0.000485	0.000467	0.000446	0.000412	0.000469	0.000416
$10^{-2}$	0.000111	0.000162	0.000193	0.000162	0.00017	0.000137
$10^{-1.5}$	6.4e-005	8.24e-005	6.25e-005	7.37e-005	8.12e-005	8.01e-005
$10^{-1}$	2.23e-005	1.77e-005	1.82e-005	1.71e-005	2.06e-005	1.78e-005

Table 2: Combined Allele Frequency for different populations. We assume a mutation rate of  $\mu_c = 1.7 \times 10^{-6}$ . The values are nearly identical for all models, and well approximated by the equilibrium formula in eq. (1.7)

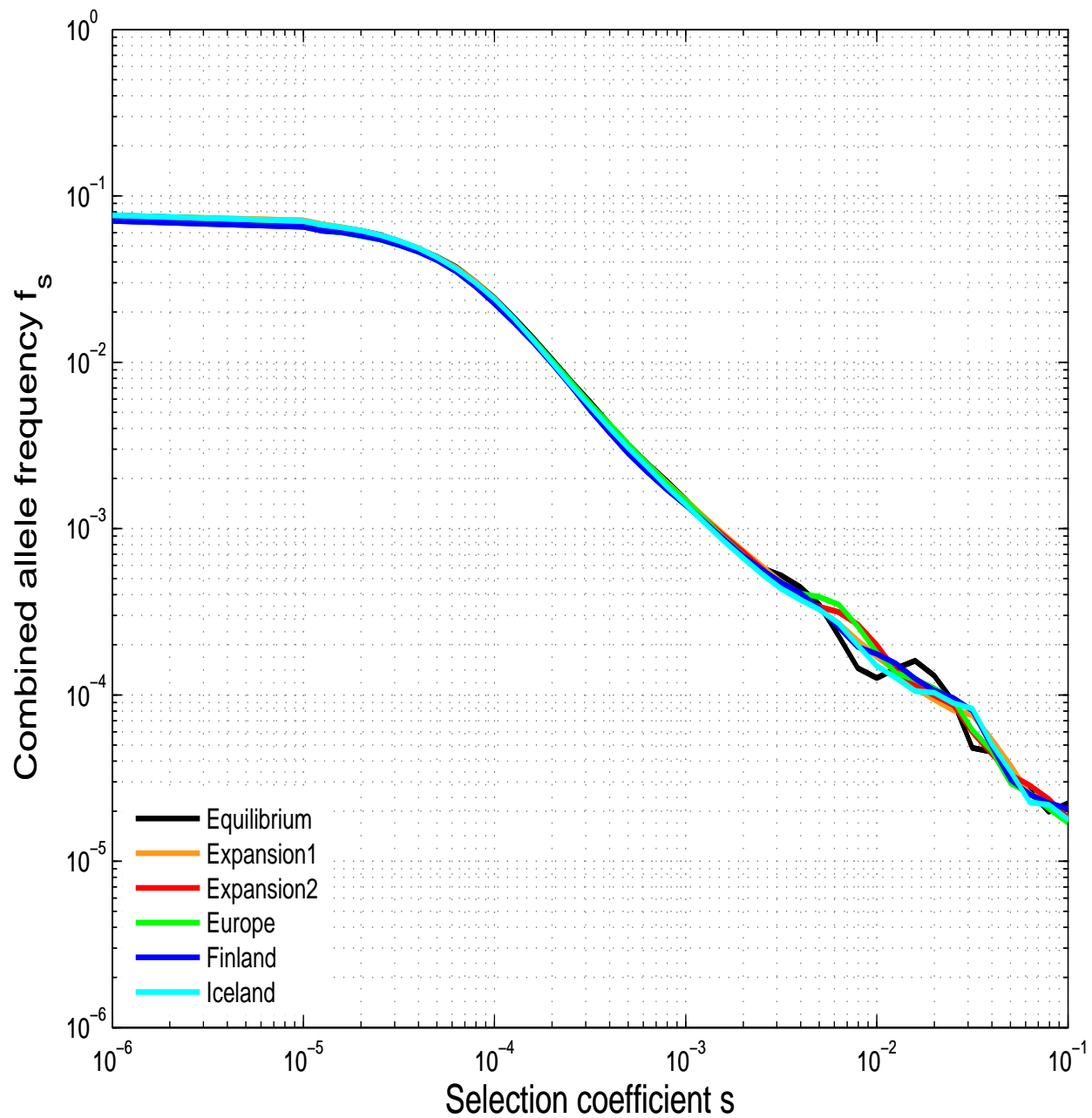


Figure 1: The Combined Allele Frequencies for all populations. Each curve shows the CAF for a different population.

## 2.3 Individual Allele Frequencies

While the combined allele frequency is not sensitive to the demography, different populations show substantial differences in the distribution of individual allele frequencies.

We first demonstrate this by showing the median of the individual allele frequency distribution. Figure S2 shows the median of the individual allele frequency distribution  $\Psi_s(f)$  for different demographic models as a function of the selection coefficient  $s$ , and Table S3 shows the median IAF for representative values of  $s$ . The figure shows very different behaviors for the different models. For large populations with no severe bottlenecks (Expansion1, Expansion2 and Europe), the median IAF is low. For populations with bottleneck (Finland and Iceland), the median IAF is much high, because the (weighted) IAF distribution is dominated by alleles born before the bottleneck and surviving the bottleneck, which therefore have high frequency. For a population at equilibrium, the median IAF is also high, due to variations in genes.

For these three populations, and when selection is strong, the median IAF is even higher than the CAF! for example, for  $s = 10^{-2}$  we have  $f_{null} \approx 0.02\%$  for all populations, but the median IAF for Finland is  $\approx 1.5\%$ . At a first glance it seems impossible that the median IAF, representing the frequency of *one* allele, exceeds the CAF, representing the combined frequency of *all* alleles in a gene; but careful examination of the two quantities can explain this phenomena. Recall that  $f_{null}$  is the *expected* CAF for a gene, and that the IAF distribution represents sampling a random allele from *all* genes on a random chromosome in the population, and hence weights alleles by their frequency. If the CAF was constant across genes - then indeed each individual allele frequency, and in particular the median IAF, would have been lower. However, since there may be substantial variation in the CAF for different genes, a sampled allele will be more likely to be sampled from a gene with high CAF (possibly much higher than the expected CAF), and therefore might have frequency far exceeding the expected CAF. The bottleneck and equilibrium populations show high variation in the CAF, and therefore a high median IAF. We elaborate further on the consequences of variation in CAF in Section S8.

Figure S3 shows the entire cumulative distribution  $\Psi_s(f)$  for different models and different values of the selection coefficient  $s$ . Again, we see clear differences between the different populations.



s	Equilibrium	Expansion1	Expansion2	Europe	Finland	Iceland
0	0.514	0.502	0.514	0.54	0.527	0.502
$10^{-5}$	0.49	0.478	0.478	0.514	0.502	0.478
$10^{-4.5}$	0.434	0.414	0.424	0.467	0.467	0.424
$10^{-4}$	0.243	0.226	0.226	0.302	0.295	0.237
$10^{-3.5}$	0.0707	0.0396	0.0396	0.109	0.118	0.048
$10^{-3}$	0.0211	0.00108	0.00251	0.0113	0.0642	0.00973
$10^{-2.5}$	0.006	9.36e-005	0.000346	0.000547	0.0377	0.00545
$10^{-2}$	0.00175	2.3e-005	4.87e-005	4.53e-005	0.00223	0.0027
$10^{-1.5}$	0.000648	6.54e-006	2.26e-006	3.32e-006	5.14e-006	0.000148
$10^{-1}$	0.000252	2e-006	5.04e-007	5.04e-007	5.97e-007	1.2e-005

Table 3: Median Allele Frequency for different populations. Obtained with 50,000 simulations using  $\mu_C = 1.7 \times 10^{-6}$ , where alleles are sampled with weights proportional to their frequency, as described in Section 1.3. The values are sensitive to the demographic model, except perhaps for neutral alleles. Populations encountering bottleneck, such as Iceland and Finland, exhibit much higher allele frequencies, (yet fewer individual alleles), compared to populations with only expansion.

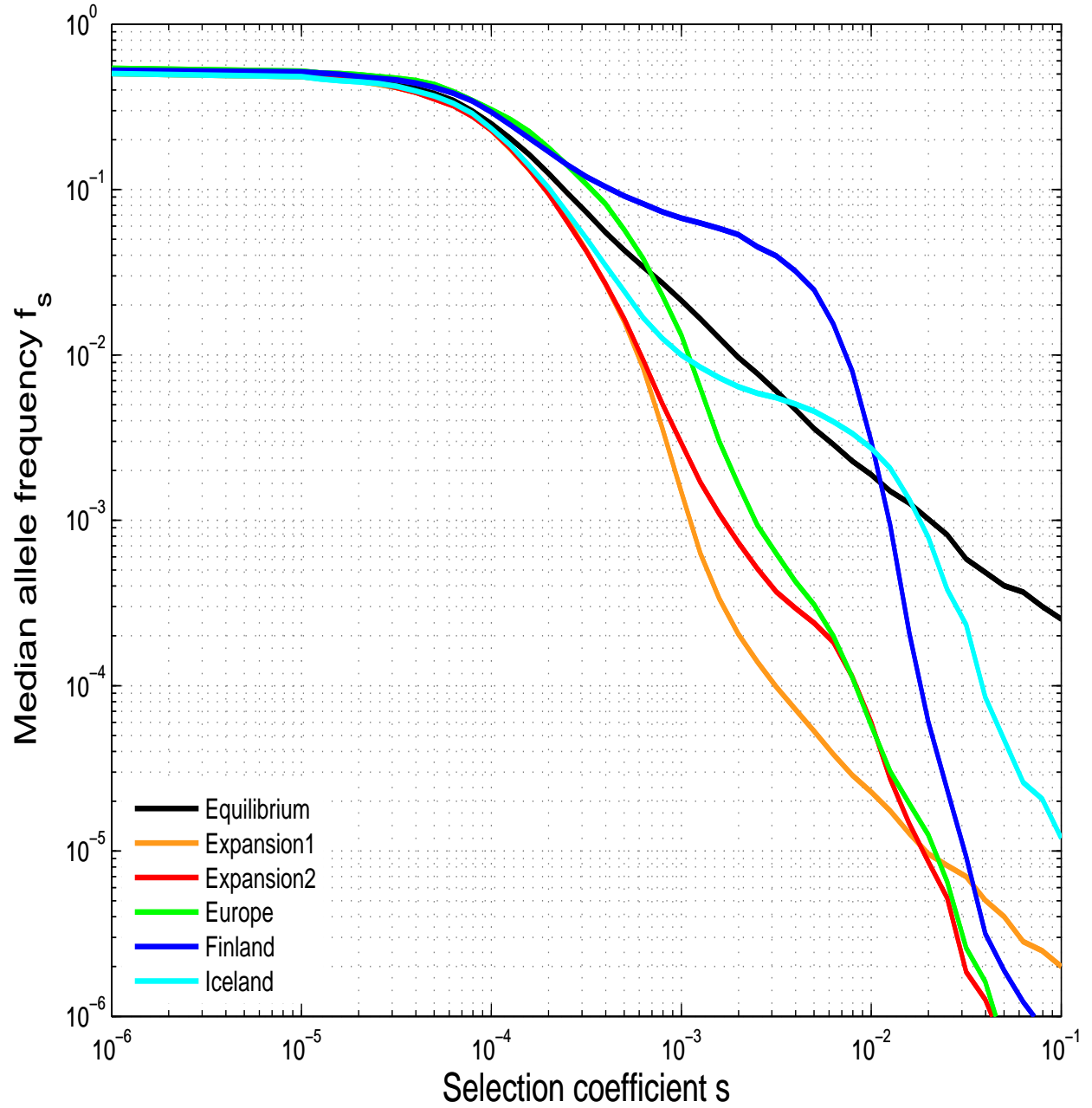


Figure 2: Median Individual Allele Frequencies in Populations for all populations. Each curve shows the median of the IAF distribution for a different population. Obtained with 50,000 simulations using  $\mu_C = 1.7 \times 10^{-6}$ , where alleles are sampled with weights proportional to their frequency, as described in Section 1.3.

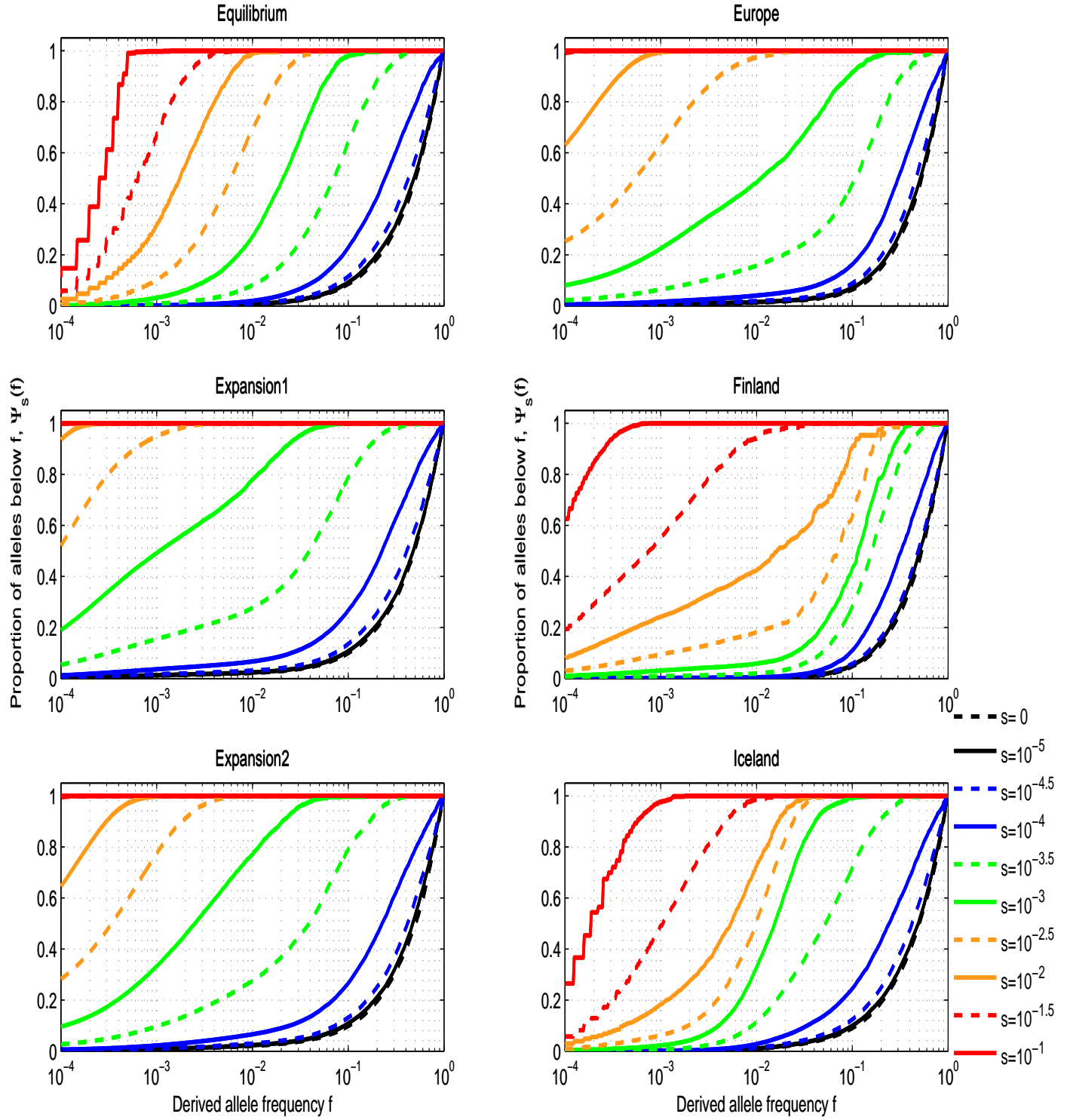


Figure 3: Cumulative Allele Frequencies in Populations for all populations. Each panel shows the cumulative distribution for a different population.

## 2.4 Age Distribution of Alleles

It has been recently suggested that the rapid expansion of the human population has led to a dramatic increase in the role of recent variants in human disease [17]. We explored this suggestion by using the simulations (described in the previous section) to study how the age distribution of alleles is affected by population demography. Figure S4 shows the median age of an allele on a randomly chosen chromosome in the population, as a function of the selection coefficient  $s$ , for the six populations studied. Figure S5 shows the cumulative distribution of allelic age for the different populations and for different selection coefficients. The figures show that the distribution of ages of alleles is essentially *insensitive* to demography - similarly to the situation for the combined allele frequency, and in contrast to the situation for the individual allele frequency distribution.

## 2.5 Proportion of Null Alleles among Missense Alleles

Missense alleles are the most challenging class to interpret, because they are a mixture of both null and neutral alleles - with the proportion varying according to the allele frequency range under consideration. Given (i) the IAF for both null and neutral alleles and (ii) the proportion of newly born missense alleles that are null, we can calculate the proportion  $\rho_s(f)$  of missense alleles with frequency below  $f$  that are null,

$$\rho_s(f) = \rho_s(f; \alpha) = \frac{\alpha \Psi_s(f) f_s}{\alpha \Psi_s(f) f_s + (1 - \alpha) \Psi_0(f) f_0}. \quad (2.1)$$

The proportion is shown in Figure S6, for various populations and selective coefficients.

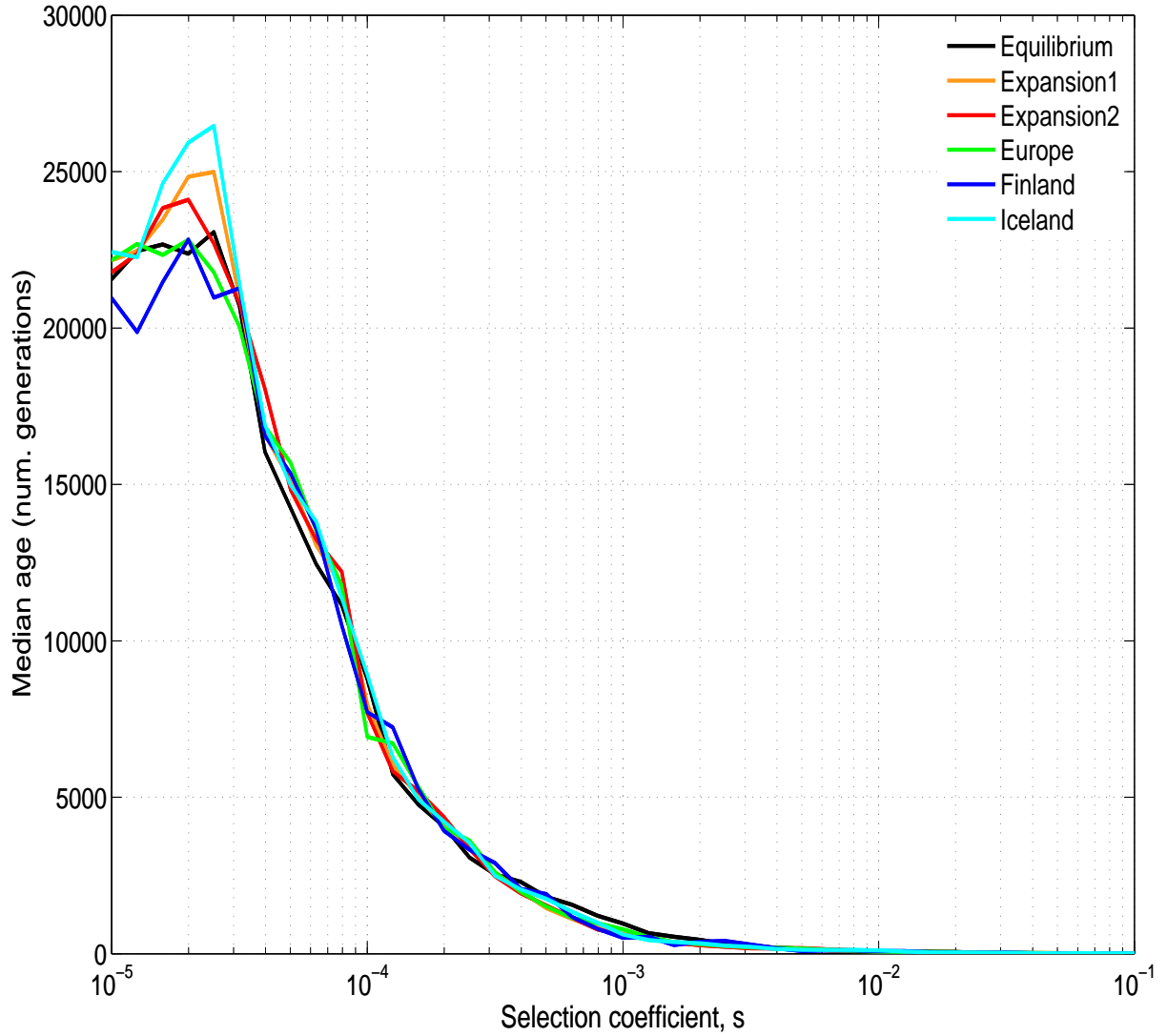


Figure 4: The median age (number of generations) of an allele drawn from a random chromosome in the population is shown as a function of the selection coefficient  $s$ . To generate this plot, alleles were drawn with probability proportional to their frequency. When selection is strong, ( $s > 10^{-3}$ ), alleles survive for a short time in the population, and the distribution is dominated by recent alleles (last  $\sim 1000$  generations). When selection is weak ( $s < 10^{-3}$ ), older alleles are more likely to survive and alleles born more than 10000 generations ago may comprise the majority of the genetic variation. For all values of  $s$ , the median age is very similar for the different populations, hence the effect of demography on the allelic age distribution is minor.



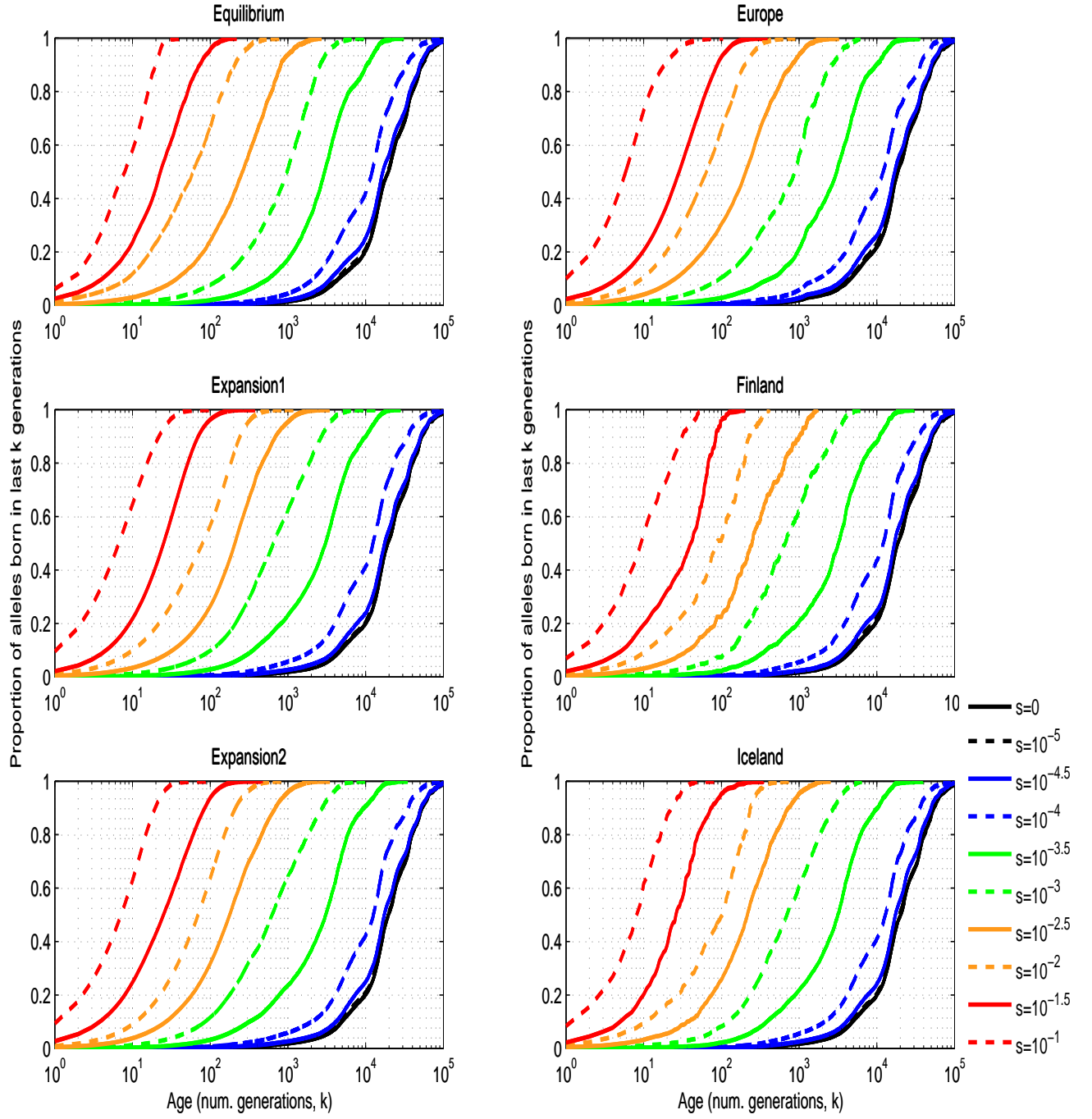


Figure 5: The cumulative age distribution (number of generations) for alleles drawn from a random chromosome in the population is shown for different populations (different panels) and different selection coefficients  $s$  (different colored curves). For strong selection, the distribution is concentrated at recent alleles, and older alleles are likely to survive for weaker selection. The different cumulative distributions are very similar for the different populations, showing that demography does not alter significantly the allelic age distribution.

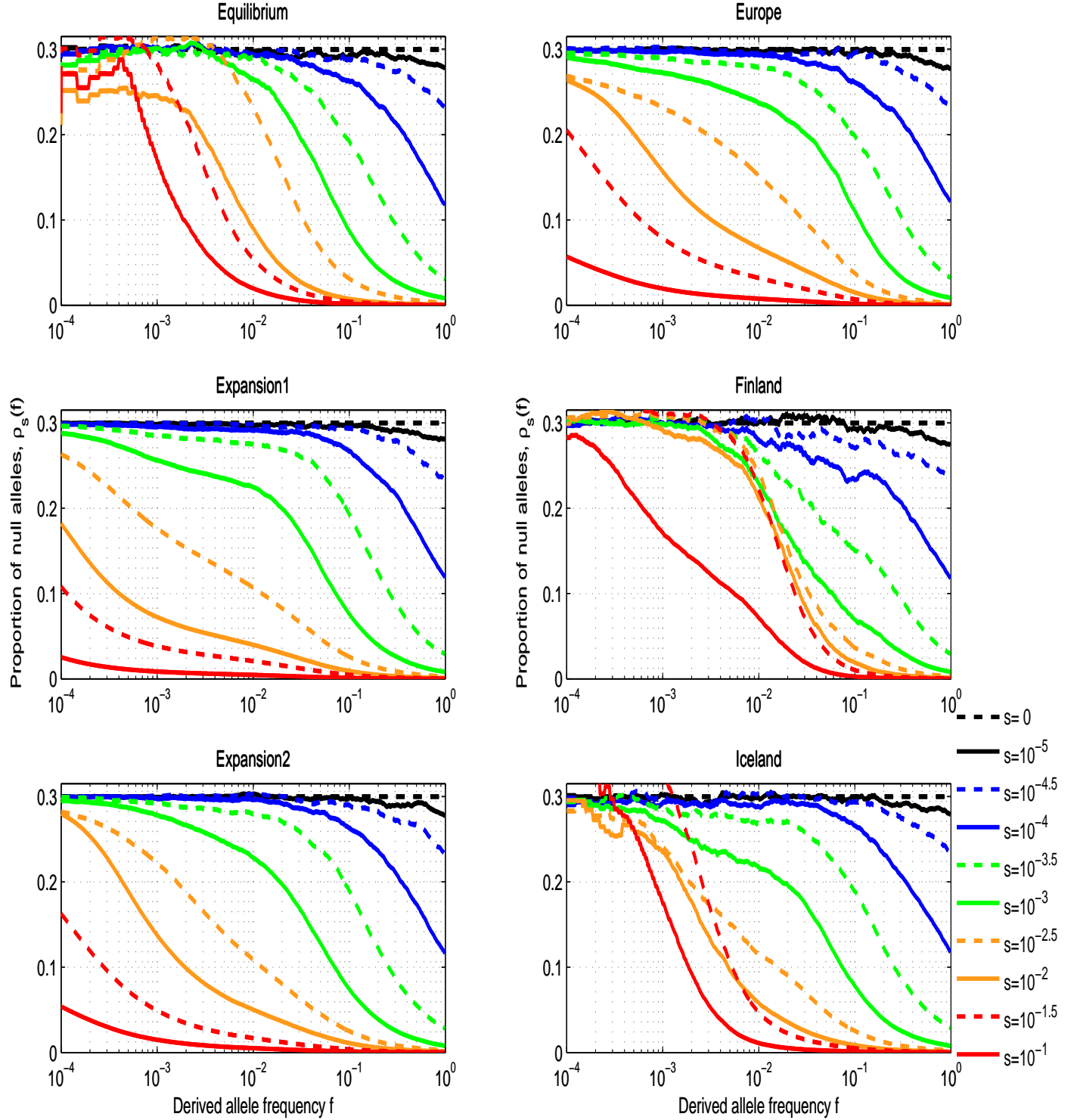


Figure 6: Fraction of missense alleles with frequency less than  $f$  that are null, for various populations. Each panel shows the proportion of null alleles  $\rho_s(f)$  for a randomly sampled allele with frequency  $\leq f$  for a different population. We assume  $\alpha = 0.25$  - that is,  $\frac{1}{4}$  of newly born alleles are null.

## 2.6 Mutation Rates for Observable Classes

For protein-coding regions, three classes of mutations can be directly observed: silent ( $S$ ), missense ( $M$ ) and disruptive ( $D$ , defined as nonsense, splice site and frameshift changes, which severely disrupt protein structure).

For any human gene, we can obtain good estimates of the mutation rates for these observable classes ( $S, M, D$ ) based on (i) the length and sequence composition of the gene and (ii) the rate and mutational spectrum for point mutations in the local region [18–21]. (The latter quantities can be estimated from comparative genomics [18–21], medical genetics [22] or large-scale human parent-offspring trio sequencing studies [23].)

We estimated mutation rates ( $S, M, D$ ) by extending a model [24] that incorporates gene length, sequence context and local variation in mutation rate (as inferred by fixed divergence between human and macaque). Briefly, local sequence context was used to determine the probability of each base in the coding region mutating to any each other possible base and determining the coding impact of each possible mutation.

For power calculations, we focus on a 'typical' human gene with a coding region of 1500 bases and a median mutation rate. For this typical gene, the mutation rates for silent, missense and disruptive mutations are  $5.6 \times 10^{-6}$ ,  $12.8 \times 10^{-6}$ , and  $1.7 \times 10^{-6}$  per chromosome per generation, respectively (Table 1 in the main text).

In the main text, we cite specific mutation rates  $D$  for disruptive mutations in two genes:

- *LDLR* (coding region 2583 bases, including the stop codon) =  $3.8 \times 10^{-6}$ .
- *CHD8* (coding region 7746 bases, including the stop codon) =  $5 \times 10^{-6}$ .

The rate for *LDLR* is slightly higher and for *CHD8* considerably lower than expected by simply adjusting for gene length, with the differences being due to sequence context (largely GC content).

### 3 Calculating Sample Sizes required for RVAS

In order to understand the prospects of RVAS for identifying disease-associated loci, it is important to study the detection power. Power calculations are also useful for guiding the design of RVAS (e.g. what sample size should be used, what populations, what classes of alleles and tests to employ etc.). We describe how to calculate the sample size for RVAS, using a burden test for a class  $C$  of alleles. We start with the simple case of a 'pure' class of alleles with identical effect size (such as disruptive alleles). Then, we build on these sample size calculations to analyze the gains in power achieved by different RVAS strategies.

#### 3.1 Estimating Aggregate Effect Size

We consider a disease  $D$  with prevalence  $\pi$  in the population. We let  $f$  denote the cumulative allele frequency of alleles in class  $C$ , and let  $1 + \lambda$  denote the average relative risk conferred by alleles in  $C$ . (We thus allow the possibility that  $C$  is a mixture of alleles with different properties). By Bayes' formula, the probability that an individual carrying an allele in class  $C$  is affected is  $f(1 + \lambda)$ .

$$Pr(X_C = 1|Z = 1) = \frac{Pr(Z = 1|X_C = 1)Pr(X_C = 1)}{Pr(Z = 1)} = \frac{f\pi(1 + \lambda)}{\pi} = f(1 + \lambda). \quad (3.1)$$

where  $Z$  is an indicator variable for disease status (with 1 indicating that the individual is affected and 0 indicating that the individual is not affected) and  $X_C$  is an indicator variable for carrier status for an allele in class  $C$  (with 1 indicating a carrier and 0 indicating a non-carrier).

Suppose that we gather data from  $n$  affected individuals (cases), and observe  $d$  total alleles of class  $C$ . We can estimate the allele frequency in cases by,  $\hat{f}_{cases} = \frac{d}{2n}$  (where we divide by the total number of *chromosomes*). From the above, we have  $E[\hat{f}_{cases}] = f(1 + \lambda)$ .

##### 3.1.1 Risk for Carriers of Multiple Allele

Our model assumes that a carrier of a null rare allele has risk  $\pi(1 + \lambda)$ , regardless of the number of null alleles carried. We thus assume that individuals who are homozygous (or compound heterozygous) for null alleles have the same disease risk as for heterozygotes. In fact, these individuals are likely to have a greater disease risk. However, because the cumulative frequency of rare alleles is low ( $f \ll 1$ ), the frequency of these individuals is so small (on the order of  $f^2$ ) and their higher disease risk does not significantly affect our calculations. We thus ignore any increased disease risk associated with homozygosity (or compound heterozygosity) for null alleles.

### 3.1.2 Protective Alleles

While the text typically speaks about null alleles increasing disease risk, our mathematical calculations apply equally well to alleles that decrease disease risk (that is, protective alleles) [25, 26]. In this case the parameter  $\lambda$  is simply negative,  $-1 \leq \lambda < 0$ . For example,  $\lambda = -1$  corresponds to fully protective alleles (i.e. carriers are completely immune to the disease). As described in the main text, detecting protective alleles requires larger sample sizes than detecting harmful alleles (see Figure S8).

## 3.2 Calculating Sample Size when $f$ is Already Known

We first suppose that  $f$  is already known to high precision - for example, from a large population survey.

Suppose that we gather data on  $n$  cases, and observe  $d$  total alleles of class  $C$ . We model our observations using a binomial distribution  $d \sim \text{Binomial}(2n, f_{\text{cases}})$ . We use the estimator for the allele frequency in cases,  $\hat{f}_{\text{cases}} = \frac{d}{2n}$ , and perform a simple hypothesis test, with,

$$\begin{aligned} H_0 : f_{\text{cases}} &= f, \\ H_1 : f_{\text{cases}} &> f \end{aligned} \tag{3.2}$$

We use the likelihood-ratio test statistic

$$\begin{aligned} 2\mathcal{LLR}(d, n; f) &= 2[LL(d, n; \hat{f}_{\text{cases}}) - \mathcal{LL}(d, n; f)] \\ &= 2[d \log \frac{\hat{f}_{\text{cases}}}{f} + (2n - d) \log \frac{1 - \hat{f}_{\text{cases}}}{1 - f}] \end{aligned} \tag{3.3}$$

where  $\mathcal{LL}$  denotes the Log-Likelihood and  $\mathcal{LLR}$  denotes the Log-Likelihood-Ratio. Under the null hypothesis  $H_0$ , the test statistic  $2\mathcal{LLR}$  has a  $\chi^2(1)$  distribution. Under the alternative  $H_1$ , it has a non-central  $\chi^2(1; NCP)$  distribution, with the non-centrality parameter  $NCP$ ,

$$\begin{aligned} NCP &= NCP(n, \lambda, f) = E[2\mathcal{LLR}] \\ &= n \left[ (1 + \lambda) f \log(1 + \lambda) + (1 - (1 + \lambda)f) \log \frac{1 - (1 + \lambda)f}{1 - f} \right]. \end{aligned} \tag{3.4}$$

The power to detect an allele, when setting a significance threshold  $a$  (for example,  $a = 2.5 \times 10^{-6}$  to get 0.05 false-positives and account for testing 20,000 genes), is approximately

$$1 - b = 1 - b(n, \lambda) = 1 - F_{\chi^2} \left( F_{\chi^2}^{-1}(1 - a, 1), 1, NCP \right) \tag{3.5}$$



where  $b$  is defined as the false-negatives rate (type-2 error).

We checked that the above formula provides an excellent analytic approximation to power, by comparing it to Fisher's exact test (Figure S7). Similarly good approximations are obtained for the other tests described in the next sections.

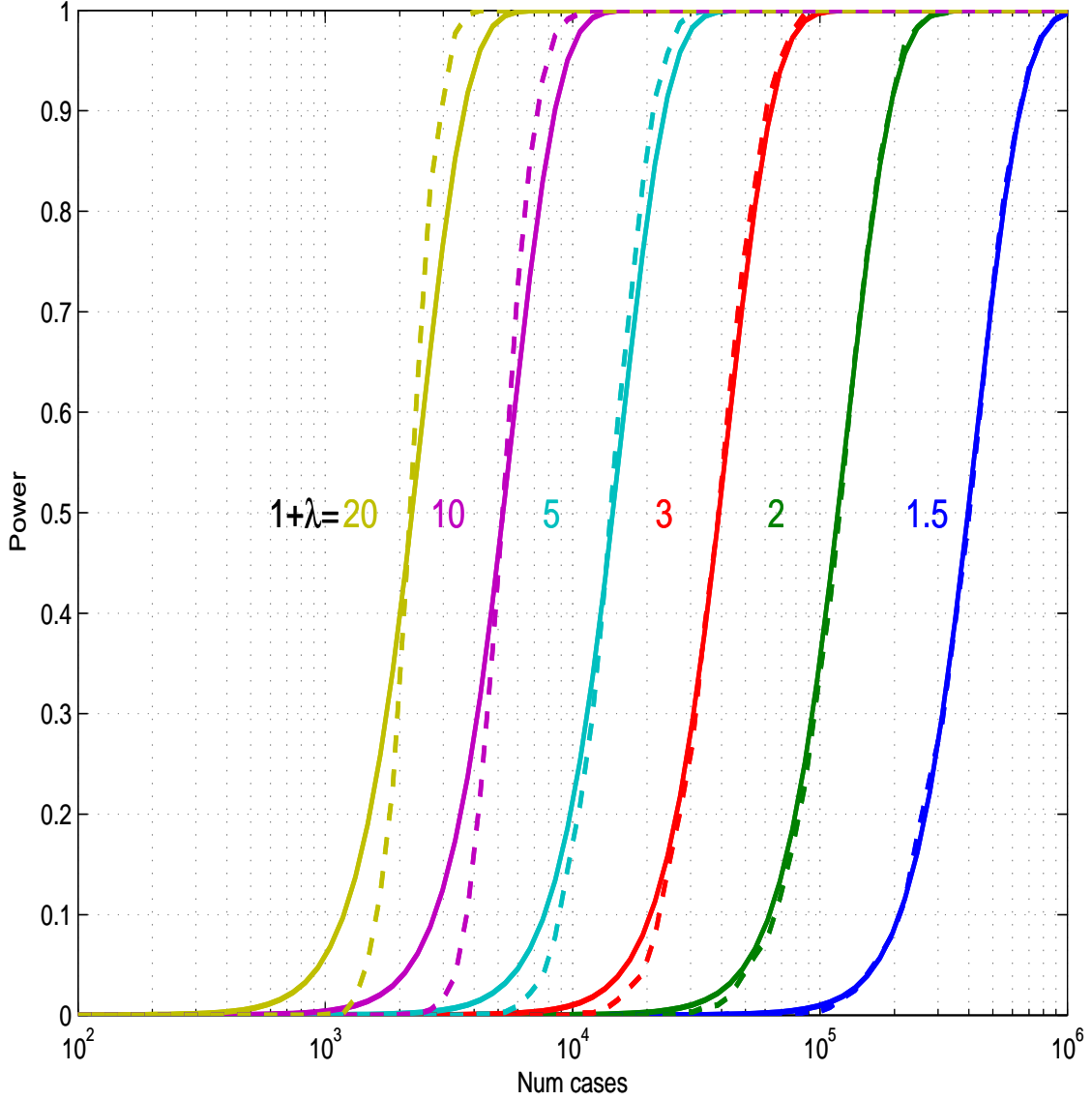


Figure 7: Power to detect an association as function of sample size (x-axis, number of cases) and effect size (different colored curves), comparing the analytic approximation from eq. (3.5) (solid curves) and simulations using Fisher's exact test (dashed curves). For each value of the sample size (number of cases), we simulated 1000 different realization of cases and computed the empirical power as the fraction of simulations in which the test statistics exceeded the threshold set by the significance level  $\alpha$ . (We assumed cumulative allele frequency  $f = 0.1\%$ , significance level  $\alpha = 0.05/20,000$  and a disease prevalence of  $5\%$ .) Overall, there is a very good agreement between the analytic approximation and empirical power, especially for small effect sizes and for intermediate power ( $\sim 50\%$ ). For large effect sizes, the analytic approximation slightly under-estimates power for high power (e.g.  $\sim 90\%$ ), and slightly over-estimates power for low power (e.g.  $\sim 10\%$ ).

For given type-1 error  $a$  and type-2 error  $b$ , we introduce a specific value of a non-centrality parameter denoted by  $\nu_{a,b}$ . We define  $\nu_{a,b}$  to be the value such that if a test statistic has a non-central  $\chi^2(1; \nu_{a,b})$  distribution under the alternative hypothesis  $H_1$ , then testing under  $H_0$  using this test statistic, assuming a  $\chi^2(1)$  distribution, and setting the significance level to  $a$ , would indeed give power of  $1 - b$ . The specific value  $\nu_{a,b}$  for given  $a$  and  $b$  is obtained by solving equation (3.5) above for  $NCP$ . It depends only on the type-1 and type-2 errors. We can compute the required sample size by matching this value to the NCP actually obtained in a given study for a given effect size and sample size. Specifically, from eq. (3.4), the sample size is then simply given by,

$$n_{a,b} = \frac{\nu_{a,b}}{4[(1+\lambda)f \log(1+\lambda) + (1-(1+\lambda)f) \log \frac{1-(1+\lambda)f}{1-f}]}. \quad (3.6)$$

When  $f$  is small,  $f \ll 1$ , we can approximate  $n_{a,b}$  by,

$$n_{a,b} \approx \frac{\nu_{a,b}}{4f[(1+\lambda) \log(1+\lambda) - \lambda]} = \frac{\nu_{a,b}}{4fg(\lambda)}. \quad (3.7)$$

where we define

$$g(\lambda) \equiv (1+\lambda) \log(1+\lambda) - \lambda. \quad (3.8)$$

Thus, the sample size (number of cases) is roughly inversely proportional to the combined allele frequency  $f$  and the value of  $g(\lambda)$ . The function  $g(\lambda)$  is plotted in Figure S8 for both harmful ( $1+\lambda > 1$ ) and protective ( $1+\lambda < 1$ ) alleles.

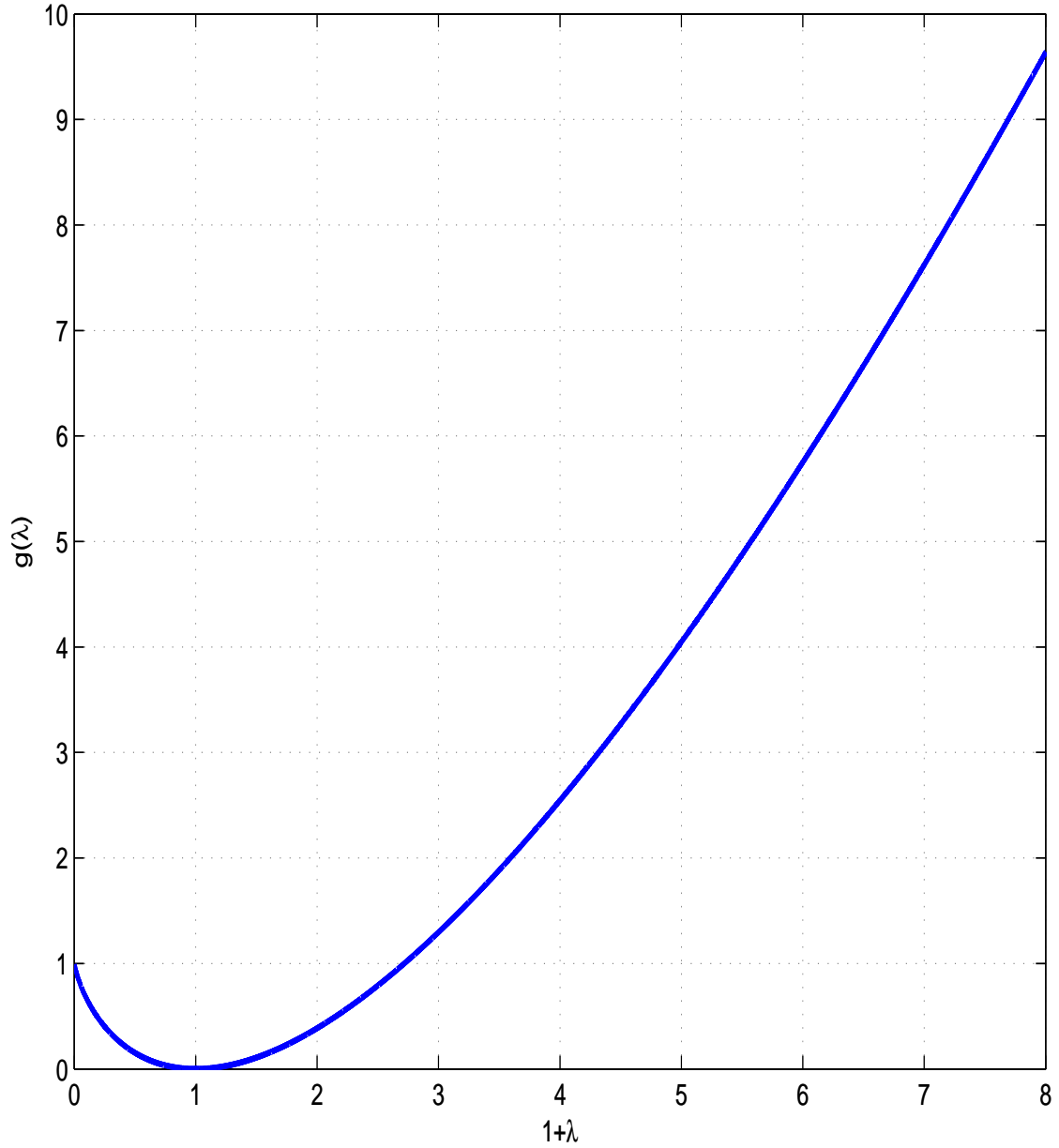


Figure 8: The function  $g(\lambda)$ , representing power, which is proportional to the inverse sample size as a function of  $\lambda$ , the effect size.  $g(\lambda)$  is shown on the y-axis, plotted against the relative disease risk  $1 + \lambda$ , shown on the x-axis for both harmful and protective alleles. In general, the function is  $g(\lambda)$  is lower for protective alleles ( $1 + \lambda < 1$ ) than for harmful alleles ( $1 + \lambda > 1$ ), hence protective alleles have lower detection power and will require larger sample sizes for detection. For example, for a completely protective allele ( $\lambda = -1$ ) we have  $g(-1) = g(e) = 1$ , for  $e \approx 2.718$ , thus the power to detect a completely protective allele is roughly equal to the power to detect a harmful allele with a relative risk of  $\approx 2.7$ .

Under strong selection, we have  $f = \frac{\mu_C}{s}$  from eq. (1.8). This gives,

$$n_{a,b} \approx \frac{\nu_{a,b}s}{4\mu_C g(\lambda)}. \quad (3.9)$$

Thus, the sample size is (approximately) directly proportional to the selection coefficient.

When  $\lambda$  is relatively small,  $\lambda \ll 1$ , the above two formulas further simplify to,

$$n_{a,b} \approx \frac{\nu_{a,b}}{2f\lambda^2} \approx \frac{\nu_{a,b}s}{2\mu_C\lambda^2}. \quad (3.10)$$

Thus, the sample size is proportional to  $\frac{1}{\lambda^2}$ , which is the same as given by a simple z-score approximation (see next). However, when  $\lambda$  is large, this z-score approximation over-estimates power. In fact, the true power is inversely proportional to roughly  $\lambda \log(\lambda)$  (and not  $\lambda^2$ ), from eq. (3.7).

We can compare this to the following crude approximation, based on a z-score,

$$n_{a,b} \approx \frac{[\Phi^{-1}(a) - \sqrt{1+\lambda}\Phi^{-1}(b)]^2}{2\lambda^2 f} \quad (3.11)$$

which simplifies when  $\lambda \ll 1$  to,

$$n_{a,b} \approx \frac{[\Phi^{-1}(a) - \Phi^{-1}(b)]^2}{2\lambda^2 f}. \quad (3.12)$$

For example:

1. If we take  $b = 0.1$  (i.e. 90% power) and  $a = 2.5 \times 10^{-6}$ , we get,  $\nu_{a,b} = 35.9$ . For small  $\lambda$  and  $f$ , we get  $n \approx \frac{17.9}{\lambda^2 f}$ . The crude approximation gives us  $n \approx \frac{17.1}{\lambda^2 f}$ , which is slightly optimistic.
2. If we are satisfied with a nominal significance level  $a = 0.05$  (that is, if we were certain that we would only ever test a single gene), we could use  $\nu_{a,b} = 10.5$ . For small  $\lambda$  and  $f$ , the required sample size is then roughly 3.5-fold lower at  $\frac{5.3}{\lambda^2 f}$ .

### 3.3 Calculating Sample Size when $f$ is Unknown

In the above calculations, we assumed that the population frequency  $f$  is known precisely. If  $f$  is unknown, we can estimate it by performing a case-control study or a case-unaffected study. Here "controls" refer to random individuals in the general population and "unaffecteds" to individuals known not to have the disease (based on the diagnostic criteria in use).

### 3.3.1 Using unaffecteds

We begin by considering a case-unaffected study. The control frequency  $f_{unaffected}$  satisfies  $f = (1 - \pi)f_{unaffected} + \pi f_{cases}$ , which gives

$$\begin{aligned} f_{unaffected} &= \frac{1 - \pi - \pi\lambda}{1 - \pi} f, \\ f_{cases} &= \left(1 + \frac{\lambda}{1 - \pi - \pi\lambda}\right) f_{unaffected}. \end{aligned} \quad (3.13)$$

The observed numbers of carriers in cases and controls have the following binomial distributions,

$$\begin{aligned} d_{cases} &\sim \text{Binomial}(2n_{cases}, f_{cases}), \\ d_{controls} &\sim \text{Binomial}(2n_{controls}, f_{unaffected}). \end{aligned} \quad (3.14)$$

This time, we test the hypothesis,

$$\begin{aligned} H_0 : f_{cases} &= f_{unaffected}, \\ H_1 : f_{cases} &> f_{unaffected}. \end{aligned} \quad (3.15)$$

i.e. we test whether the parameters of two binomial random variables are equal. Again, we write the likelihood ratio statistic

$$\begin{aligned} 2\mathcal{LLR}(n_{cases}, d_{cases}, n_{controls}, d_{controls}) \\ &= 2 \left[ LL(n_{cases}, d_{cases}, n_{controls}, d_{controls}; (\hat{f}_{cases}, \hat{f}_{unaffected})) \right. \\ &\quad \left. - LL(n_{cases}, d_{cases}, n_{controls}, d_{controls}; \hat{f}) \right] \end{aligned} \quad (3.16)$$

with,

$$\begin{aligned} \hat{f}_{cases} &= \frac{d_{cases}}{2n_{cases}}, \\ \hat{f}_{unaffected} &= \frac{d_{controls}}{2n_{controls}}, \\ \hat{f} &= \frac{d_{cases} + d_{controls}}{2(n_{cases} + n_{controls})}. \end{aligned} \quad (3.17)$$

The non-centrality parameter is

$$\begin{aligned} NCP = E[2\mathcal{LLR}] &= 4n_{cases}h_b(f_{cases}) + 4n_{controls}h_b(f_{unaffected}) \\ &\quad - 4(n_{cases} + n_{controls})h_b\left(\frac{f_{cases}n_{cases} + f_{unaffected}n_{controls}}{n_{cases} + n_{controls}}\right) \end{aligned} \quad (3.18)$$

where  $h_b$  is the binary entropy function (with logarithm taken at the natural basis):

$$h_b(x) = -[x \log(x) + (1 - x) \log(1 - x)]. \quad (3.19)$$

We assume that the case-controls ratio is  $\rho : (1 - \rho)$ , and define  $n_{cases,a,b}, n_{controls,a,b}$  the number of cases and controls, respectively, required to reach false-positive and false-negative rates  $a$  and  $b$ , respectively. The overall sample size (cases+controls) is  $n_{a,b} = n_{cases,a,b} + n_{controls,a,b}$  with  $n_{cases,a,b} = \rho n_{a,b}$  and  $n_{controls,a,b} = (1 - \rho)n_{a,b}$ . From eq. (3.18) we get,

$$n_{a,b} = \frac{\nu_{a,b}}{4 \left\{ \rho h_b((1 + \lambda)f) + (1 - \rho) h_b\left(\frac{1 - \pi + \pi\lambda}{1 - \pi} f\right) - h_b([\rho(1 + \lambda) + (1 - \rho)\frac{1 - \pi + \pi\lambda}{1 - \pi}]f) \right\}}. \quad (3.20)$$

When  $f$  is small, we get the following approximate formula,

$$n_{a,b} \approx \frac{\nu_{a,b}}{4f[\rho g(\frac{\lambda}{1 - \pi - \pi\lambda}) - g(\frac{\rho\lambda}{1 - \pi - \pi\lambda})]} \quad (3.21)$$

When the effect size  $\lambda$  is also small, Taylor expansion gives,

$$n_{a,b} \approx \frac{\nu_{a,b}(1 - \pi)^2}{2f\rho(1 - \rho)\lambda^2} \quad (3.22)$$

and the number of cases is,

$$n_{cases,\alpha,\beta} \approx \frac{\nu_{a,b}(1 - \pi)^2}{2f(1 - \rho)\lambda^2}. \quad (3.23)$$

### 3.3.2 Using controls from the population

If we perform a case-control study (where individuals from the the control group are taken from the general population), the control frequency is simply  $f$ . Formula (3.20) changes to,

$$n_{a,b} = \frac{\nu_{a,b}}{4 \left\{ \rho h_b((1 + \lambda)f) + (1 - \rho) h_b(f) - h_b((1 + \rho\lambda)f) \right\}}. \quad (3.24)$$

When  $f$  is small, we get the following approximate formula,

$$n_{a,b} \approx \frac{\nu_{a,b}}{4f[\rho g(\lambda) - g(\rho\lambda)]}. \quad (3.25)$$

When the effect size  $\lambda$  is also small, Taylor expansion gives,

$$n_{a,b} \approx \frac{\nu_{a,b}}{2f\rho(1 - \rho)\lambda^2} \quad (3.26)$$



and the number of cases is,

$$n_{cases,\alpha,\beta} = \rho n_{a,b} \approx \frac{\nu_{a,b}}{2f(1-\rho)\lambda^2}. \quad (3.27)$$

Compared to the case-only test (eq. (3.7)), the number of cases required increases by roughly a factor of  $1 - \rho$ . For example, if we take a balanced case-control study ( $n_{cases} = n_{controls}$ ), for  $a = 2.5 \times 10^{-6}, b = 0.1$  we get  $n_{cases,a,b} = \frac{35.9}{f\lambda^2}$ , compared to  $n_{a,b} \approx \frac{17.9}{f\lambda^2}$  for the case-only test with known  $f$  (when effect size  $\lambda$  is small). The resulting number of cases is increased  $\sim 2$ -fold (the overall sample size is increased 4-fold since we also need to genotype controls).

When the disease is rare ( $\pi \ll 1$ ) we have  $f \approx f_{unaffected}$ ,  $f_{cases} = (1 + \lambda)f \approx (1 + \lambda)f_{unaffected}$  and the formulas for the case-control and case-unaffected studies coincide.

### 3.4 Tests Proposed in the Literature for RVAS

Given the early stage of the field, the analytical methodology for RVAS remains in flux. Many authors have proposed a rich collection of possible statistics (e.g. [27–35]; reviewed in [36] and [37]; tests compared in [38]. Our goal here is neither to evaluate their relative merits nor to propose alternatives. The tests include ’burden’ tests, designed to detect allelic effects in the same direction, and ’overdispersion’ tests, designed to detect bi-directional allelic effects [27, 39, 40]. One can incorporate weights based on allele frequency [41–43], apparent effect size [39, 44] and presumed functional significance [39, 42, 45].

## 4 RVAS Strategy 1: Studying Disruptive Alleles

The simplest strategy would be to study just the disruptive alleles, which we assumed to be a homogenous class of null alleles with equal effect size and selection coefficient. To compute power, we can use the formulas for Section 3. In Figure S9 (reproduced Figure 2(a) from the main text) we show the power to detect harmful disruptive alleles as a function of either the selection coefficient  $s$  or the combined allele frequency  $f_D$  (assumed to be interchangeable through the expectation  $f_D = \frac{\mu_D}{s}$ ) and their effect size  $\lambda$ . Similarly, in Figure S10 (reproduced Figure 2(b) from the main text) we show the power to detect protective disruptive alleles.

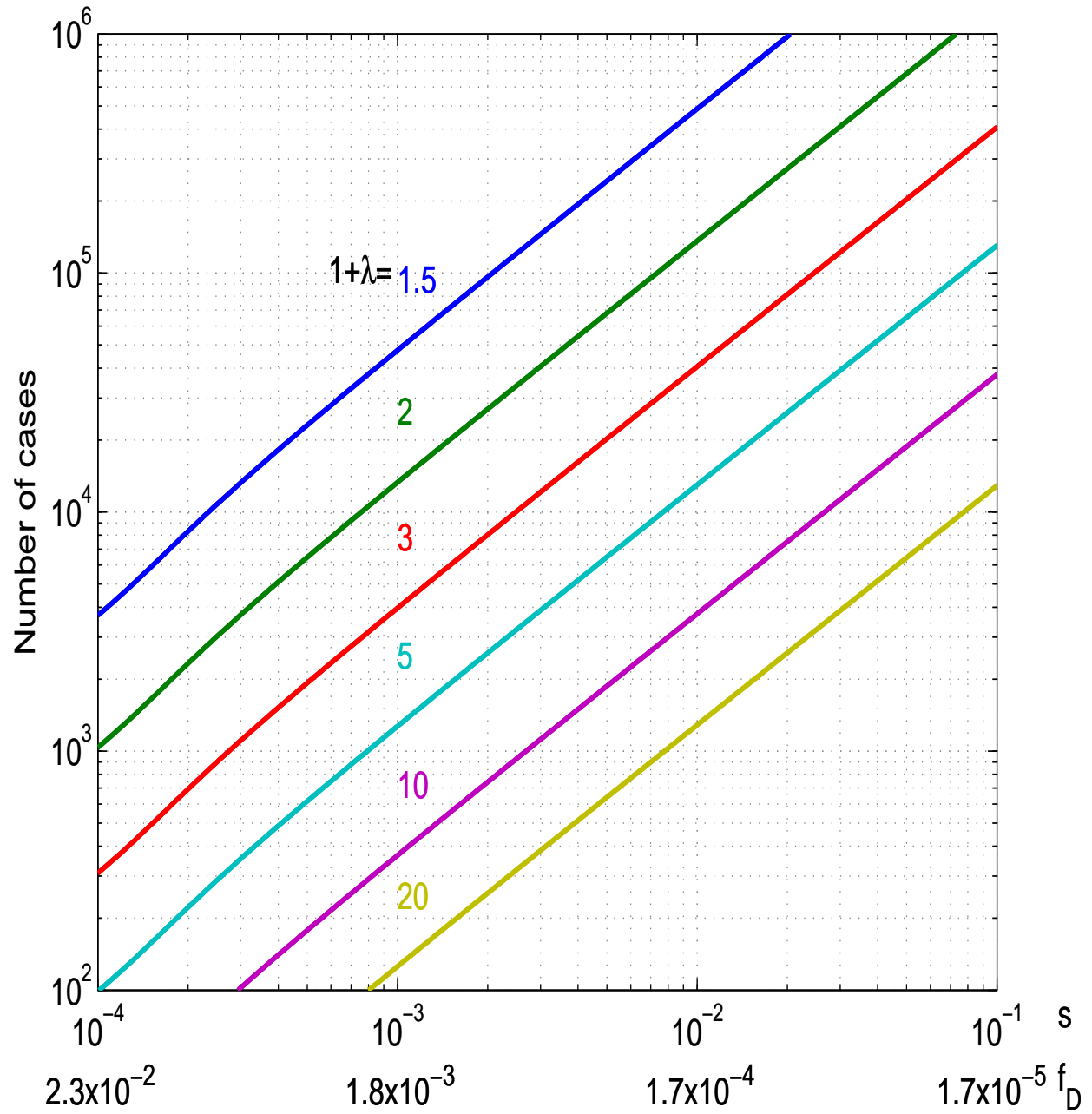


Figure 9: Sample size (number of cases) required to detect association using disruptive alleles in a case-only study with known population allele frequency, as function of the either  $f_D$ , the combined allele frequency or  $s$ , the selection coefficient (x-axis), and  $\lambda$ , the effect size (different colored curves) (Figure 2(a) in main text).

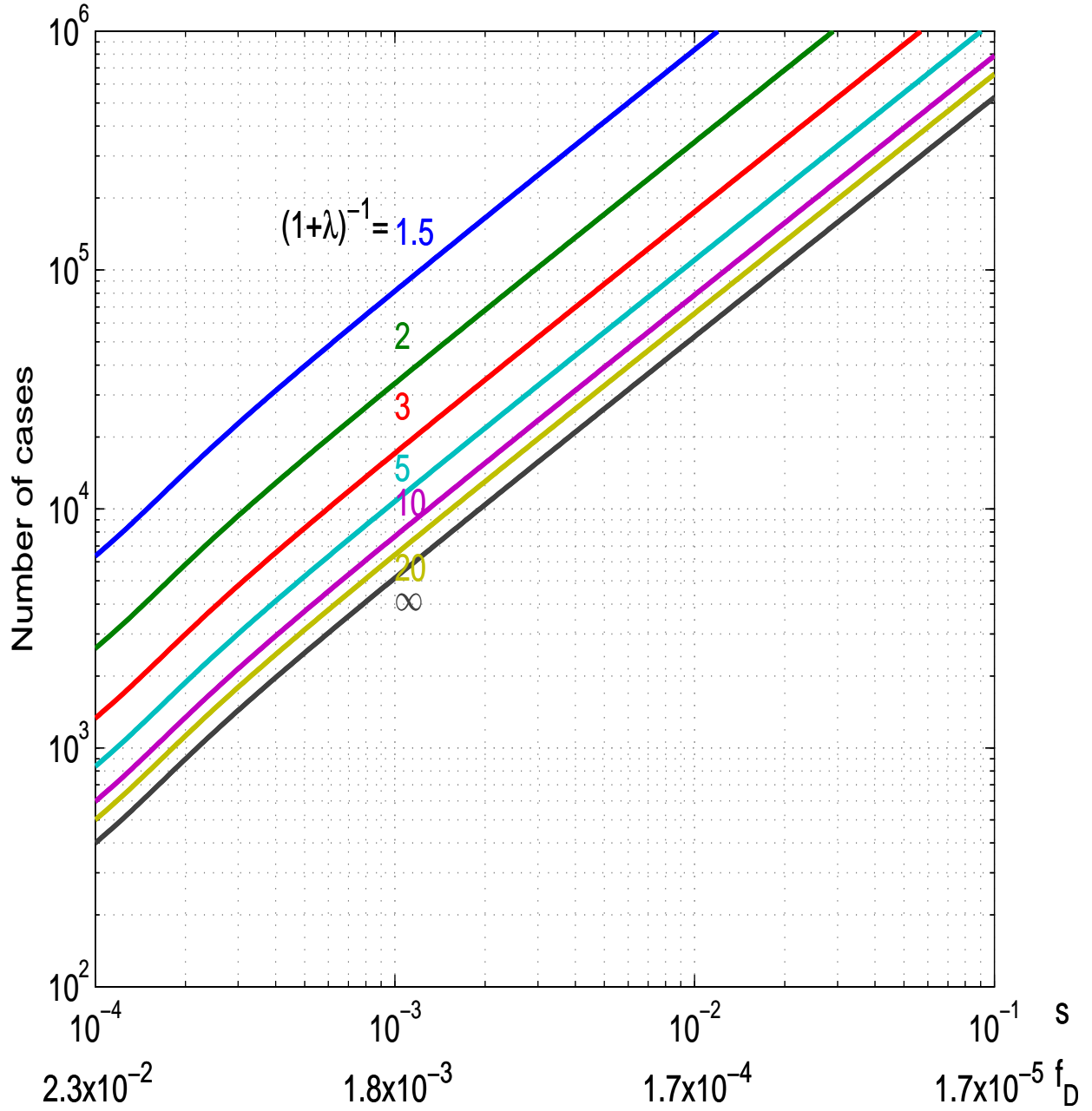


Figure 10: Sample size required to detect association using disruptive protective alleles, as function of the either  $f_D$ , the combined allele frequency or  $s$ , the selection coefficient (x-axis), and effect size  $\lambda$  (different colored curves) (Figure 2(b) in main text). For protective alleles, the effect size  $\lambda$  is negative - for example  $\lambda = -0.95$  for a  $(1 + \lambda)^{-1} = 20$ -fold depletion. The sample size needed to detect the depletion of rare protective alleles in cases is considerably higher than the sample size needed to detect the excess of rare harmful alleles (Figure S9). As protection increases, the sample size curve converges to a curve representing completely protective alleles (corresponding to  $(1 + \lambda)^{-1} = \infty$ ), and is roughly equal to the sample size required to detect alleles increasing disease probability by a factor of  $e \approx 2.718$ .

## 5 RVAS Strategy 2: Incorporating Missense Alleles

One attractive way to increase power is to incorporate missense alleles into the burden analysis. Only a fraction  $\alpha$  of missense alleles are null and thereby contribute to disease association. If we could perfectly identify this subset, we could simply include both disruptives and missense-null alleles in our burden test. This would be advantageous because the number of missense-null alleles typically exceeds the number of disruptive alleles. Specifically, the expected ratio of null missense alleles to disruptive alleles is  $\frac{\mu_{M-null}}{\mu_D} = \frac{\alpha\mu_M}{\mu_D}$ . For our 'typical' gene with  $\alpha = 0.25$  and  $\frac{\mu_M}{\mu_D} = 7.3$  (Table 1 in the main text), this ratio is  $\sim 2.8$ .

The problem is that we cannot readily distinguish the missense nulls from missense neutrals. The latter are more abundant (because they are not under purifying selection) and thus may swamp the former. We can try to avoid this problem by focusing only on missense alleles with frequency below a specified threshold  $T$ . There are two considerations:

1. The ratio of such alleles in cases vs controls will be smaller than the true effect size  $1 + \lambda$ . Instead, we will see an "apparent" effect size of  $1 + \rho_s(T)\lambda$ , because the signal is diluted by neutral alleles.
2. The total number of alleles under consideration is reduced to  $\Psi_s(T)f_M$ .

There is an important trade-off. Decreasing the frequency threshold  $T$  (1) enriches for missense null alleles and thereby increases the apparent effect size (although it never exceeds  $1 + \alpha\lambda$ ) but (2) decreases the total number of alleles under consideration. Our goal then is to choose the optimal threshold  $T^*$  maximizing power. The optimal value depends on  $s, \alpha, \lambda$  and demography.

For a given threshold  $T$ , the non-centrality-parameter is

$$\begin{aligned}
 NCP_{missense}(T) &= E[\mathcal{L}\mathcal{L}\mathcal{R}_{missense}(T)] \\
 &\approx 4n \left[ (1 + \lambda\rho_s(T)) \frac{\mu_M}{\mu_D} f \log(1 + \lambda\rho_s(T)) \right. \\
 &\quad \left. + (1 - (1 + \lambda\rho_s(T)) \frac{\mu_M}{\mu_D} f) \log \frac{1 - (1 + \lambda\rho_s(T)) \frac{\mu_M}{\mu_D} f}{1 - \frac{\mu_M}{\mu_D} f} \right] \quad (5.1)
 \end{aligned}$$

where we take the target size of missense alleles to be roughly  $\frac{\mu_M}{\mu_D}$  times the target size of disruptive alleles. The optimal threshold is,

$$T^* \equiv \underset{T}{argmax} NCP_{missense}(T). \quad (5.2)$$

We will assume that selection is strong enough that the total allele frequency  $f$  is quite low. In this case, we can approximate the power ratio as follows,

$$\frac{E[\mathcal{L}\mathcal{L}\mathcal{R}_{missense}(T^*)]}{E[\mathcal{L}\mathcal{L}\mathcal{R}_D]} \sim \frac{\mu_M \alpha \Psi_s(T^*) g(\rho_s(T^*) \lambda)}{\mu_D \rho_s(T^*) g(\lambda)}. \quad (5.3)$$

For small effect sizes ( $\lambda \rightarrow 0$ ), we get,

$$\frac{E[\mathcal{L}\mathcal{L}\mathcal{R}_{missense}]}{E[\mathcal{L}\mathcal{L}\mathcal{R}_D]} \sim \frac{\mu_M}{\mu_D} \alpha \Psi_s(T^*) \rho_s(T^*). \quad (5.4)$$

For large  $\lambda$  (but with the constraint  $f\lambda \ll 1$ , that is, the risk of disease in carriers is significantly smaller than 100%), we get,

$$\frac{E[\mathcal{L}\mathcal{L}\mathcal{R}_{missense}]}{E[\mathcal{L}\mathcal{L}\mathcal{R}_D]} \sim \frac{\mu_M}{\mu_D} \alpha \Psi_s(T^*). \quad (5.5)$$

For large values of  $\lambda$ , the dilution  $\rho_s(T^*)$  has little effect on power: the power is similar to the ideal situation where we can perfectly recognize null missense alleles. The reason is that when effect sizes are very large, the combined allele frequency in cases is barely altered due to the dilution effect.

In general, as the effect size  $\lambda$  increases, the effect of dilution  $\rho_s(T^*)$  decreases, and it becomes more beneficial to set a higher threshold  $T^*$ , (up to the maximum frequency of  $T^* = 1$ ).

Figures S11, S12 and S13 show the relative value of the set of missense alleles (normalized to the value of disruptive mutations), as a function of the frequency threshold  $T$  used to filter the missense alleles. The three figures correspond to medium, large and small effect sizes ( $1 + \lambda = 4, 16$  and  $1.5$ ); the six panels within each figure correspond to different population models; and the curves within each panel correspond to different values of  $s$ .

The value of missense alleles is sensitive to the choice of  $T$ , and the optimal value  $T^*$  depends on the value of  $s$ . Although the optimal value  $T^*$  varies with  $s$ , the power achieved at this threshold is fairly similar across values of  $s$ . For medium effect size ( $1 + \lambda = 4$ ), the optimal threshold  $T^*$  results in missense alleles contributing roughly an equal amount of information as disruptive alleles - that is, the peak is typically around 1.0. (When combining information from both disruptive and missense alleles, the sample size is thus 1.5 – 2.0-fold smaller). For large effect size, the contribution is larger ( $\sim 1.5$ -fold) for large effect size and smaller ( $\sim 0.60$ -fold). The optimal threshold  $T^*$  itself is relatively insensitive to the effect size (increasing only slightly with  $\lambda$ ).

The optimal threshold  $T^*$  typically occurs around the 80% percentile of the IAF for null alleles (that is, we retain  $\Psi(T^*) \sim 80\%$  of the null alleles) and the proportion of nulls among all missense alleles below this frequency threshold tends to be  $\rho_s(T^*) \sim 15\% - 20\%$  (see Tables S4-S9). Figure S14 shows how the optimal threshold  $T^*$  relates to  $\Psi(T^*)$  and  $\rho_s(T^*)$ .

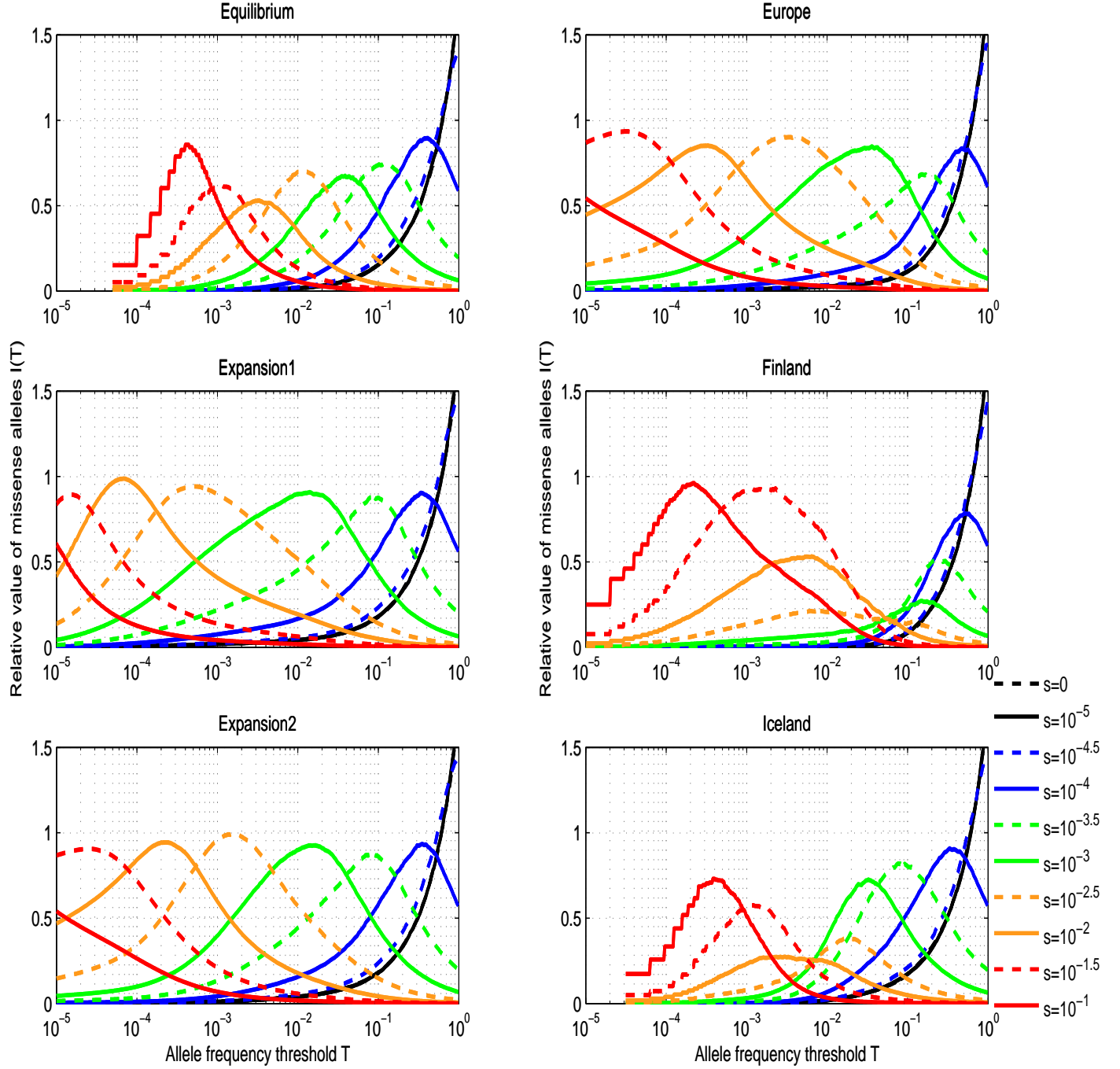


Figure 11: The relative contribution of missense alleles to power as function of threshold used, for different demographic models (shown in different panels), and different selection coefficients (colored curves). The precise value of threshold used depends heavily on the population and the selection coefficient, and is usually at the  $\sim 80\%$  quantile of the allele frequency distribution. The relative power of missense alleles from using the optimal threshold is, however, more stable, at around 0.5 – 1 fold in most cases, leading to a 1.5 – 2-fold improvement over using only disruptive alleles. We assume that the proportion of null alleles among newborn missense alleles is  $\alpha = 0.25$ , and an effect size of  $1 + \lambda = 4$ .



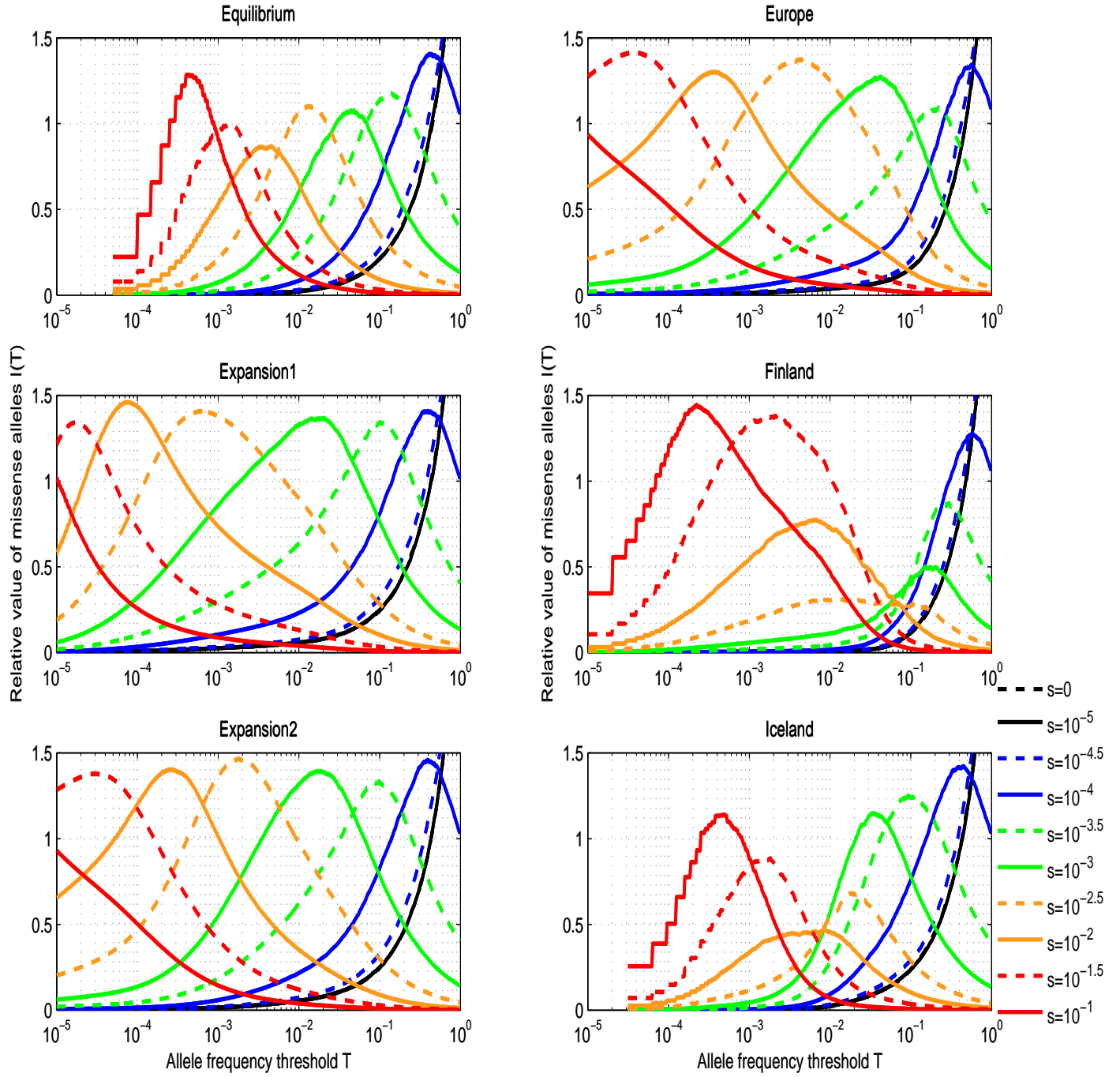


Figure 12: Similar to Figure S11, but for larger effect size ( $1 + \lambda = 16$ ). For large effects, missense alleles are more beneficial, giving  $\sim 1 - 1.5$ -fold the power of disruptive alleles at the optimal threshold, thus using them, in combination with disruptive alleles, leads to a  $\sim 2 - 2.5$ -fold increase in power.

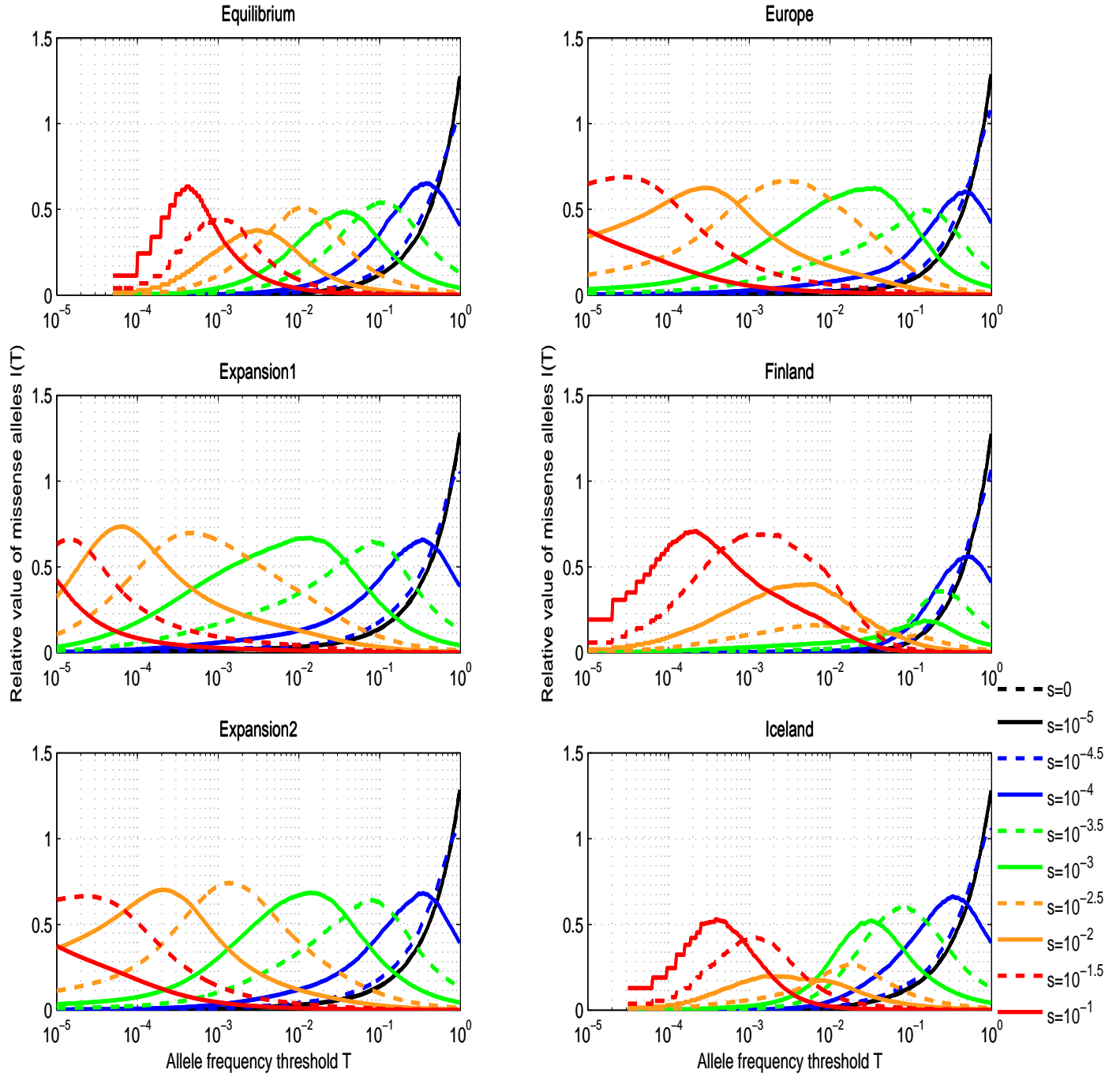


Figure 13: Similar to Figure S11, but for smaller effect size ( $1 + \lambda = 1.5$ ). For small effects, missense alleles are less beneficial, giving  $\sim 0.5$ -fold the power of disruptive alleles at the optimal threshold, thus using them, in combination with disruptive alleles, leads only to a  $\sim 1.5$ -fold increase in power.

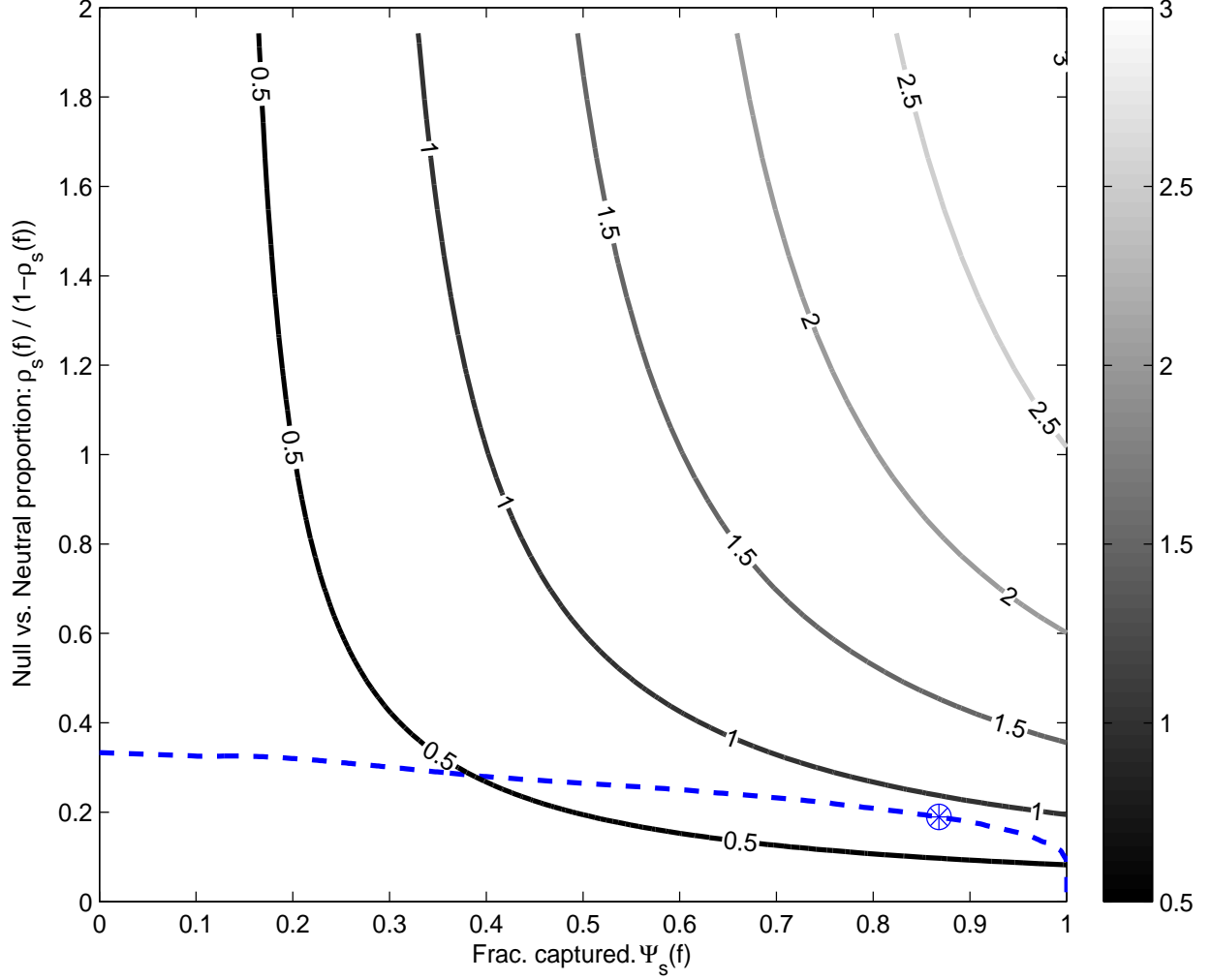


Figure 14: Relation between the fraction of null alleles which are included ( $\Psi_s(T^*)$ ) to the fraction of null alleles among the set of included alleles ( $\rho_s(T^*)$ ) as we vary the threshold  $T^*$  for the European population. The contour plots represent iso-power curves, where the value is the ratio of the contribution of missense alleles relative to disruptive alleles. The x-axis displays the fraction of null alleles captured, and the y-axis represent the proportion of null alleles among all missense alleles. Varying the threshold  $T$  corresponds to moving along the blue curve. The circled blue dot represents the values obtained for the optimal threshold. We have used  $1 + \lambda = 4$ ,  $\alpha = 0.25$ , and  $s = 0.01$ . The behavior for different populations and different selection coefficients is not significantly different.

s	0	$10^{-5}$	$10^{-4.5}$	$10^{-4}$	$10^{-3.5}$	$10^{-3}$	$10^{-2.5}$	$10^{-2}$	$10^{-1.5}$	$10^{-1}$
$f_{1/2}$	0.51	0.49	0.43	0.24	0.071	0.021	0.006	0.0018	0.00065	0.00025
$T^*$	0.99	0.99	0.96	0.38	0.1	0.039	0.011	0.0032	0.0012	0.0004
$\rho_s(T^*)$	0.25	0.25	0.2	0.16	0.16	0.13	0.15	0.12	0.13	0.17
$\Psi_s(T^*)$	1	1	1	0.86	0.76	0.8	0.76	0.72	0.78	0.81
$\rho_s(1\%)$	0.25	0.25	0.25	0.25	0.23	0.2	0.16	0.054	0.019	0.0081
$\Psi_s(1\%)$	0.011	0.011	0.015	0.042	0.13	0.35	0.72	0.98	1	1
$\rho_s(0.1\%)$	0.25	0.25	0.25	0.25	0.24	0.24	0.24	0.18	0.13	0.081
$\Psi_s(0.1\%)$	0.001	0.001	0.0013	0.0039	0.013	0.039	0.11	0.33	0.72	0.99

Table 4: Optimal threshold for Equilibrium model. The tables show the optimal threshold  $T^*$ , compared to the median allele frequency  $f_{1/2}$ . In addition, we show the cumulative allele frequency  $\Psi_s$  and the proportion of null alleles  $\rho_s$  at the optimal threshold  $T^*$ , as well as the frequencies 0.1% and 1%. At the optimal threshold  $T^*$ , the cumulative frequency is in the range of 0.7 – 0.9, and the proportion of null alleles is around 0.15 – 0.2. Using a fixed threshold of 0.1% or 1% is sub-optimal, and may lead to severe dilution of null alleles (low  $\rho_s$  for strong selection.)

s	0	$10^{-5}$	$10^{-4.5}$	$10^{-4}$	$10^{-3.5}$	$10^{-3}$	$10^{-2.5}$	$10^{-2}$	$10^{-1.5}$	$10^{-1}$
$f_{1/2}$	0.50	0.48	0.41	0.23	0.040	0.0011	9.4e-005	2.3e-005	6.5e-006	2e-006
$T^*$	0.99	0.99	0.96	0.33	0.08	0.014	0.00048	6.2e-005	1.4e-005	3.9e-006
$\rho_s(T^*)$	0.25	0.25	0.21	0.16	0.18	0.17	0.18	0.19	0.18	0.16
$\Psi_s(T^*)$	1	1	1	0.86	0.81	0.86	0.85	0.86	0.81	0.8
$\rho_s(1\%)$	0.25	0.25	0.25	0.24	0.23	0.18	0.078	0.028	0.0089	0.0026
$\Psi_s(1\%)$	0.03	0.03	0.038	0.12	0.33	0.8	1	1	1	1
$\rho_s(0.1\%)$	0.25	0.25	0.25	0.25	0.24	0.22	0.15	0.061	0.02	0.0059
$\Psi_s(0.1\%)$	0.013	0.013	0.017	0.053	0.16	0.46	0.94	1	1	1

Table 5: Optimal threshold for Expansion1 model. Similar to Table S4.

s	0	$10^{-5}$	$10^{-4.5}$	$10^{-4}$	$10^{-3.5}$	$10^{-3}$	$10^{-2.5}$	$10^{-2}$	$10^{-1.5}$	$10^{-1}$
$f_{1/2}$	0.51	0.48	0.42	0.23	0.040	0.0025	0.00035	4.9e-005	2.3e-006	5.0e-007
$T^*$	0.99	0.99	0.94	0.36	0.072	0.012	9.6e-005	7.6e-006	1.5e-006	5e-007
$\rho_s(T^*)$	0.25	0.25	0.21	0.16	0.18	0.18	0.18	0.17	0.16	0.15
$\Psi_s(T^*)$	1	1	1	0.87	0.8	0.86	0.84	0.86	0.82	0.86
$\rho_s(1\%)$	0.25	0.25	0.25	0.25	0.23	0.18	0.073	0.024	0.0075	0.0026
$\Psi_s(1\%)$	0.031	0.031	0.041	0.12	0.36	0.84	1	1	1	1
$\rho_s(0.1\%)$	0.25	0.25	0.25	0.25	0.24	0.21	0.12	0.042	0.013	0.0045
$\Psi_s(0.1\%)$	0.018	0.018	0.024	0.068	0.21	0.56	0.99	1	1	1

Table 6: Optimal threshold for Expansion2 model. Similar to Table S4.

s	0	$10^{-5}$	$10^{-4.5}$	$10^{-4}$	$10^{-3.5}$	$10^{-3}$	$10^{-2.5}$	$10^{-2}$	$10^{-1.5}$	$10^{-1}$
$f_{1/2}$	0.54	0.51	0.47	0.30	0.11	0.011	0.00055	4.5e-005	3.3e-006	5.0e-007
$T^*$	0.99	0.99	0.94	0.47	0.15	0.036	0.0025	0.00027	2.9e-005	8.4e-007
$\rho_s(T^*)$	0.25	0.25	0.21	0.15	0.15	0.18	0.18	0.17	0.17	0.18
$\Psi_s(T^*)$	1	1	0.98	0.86	0.73	0.79	0.82	0.83	0.9	0.84
$\rho_s(1\%)$	0.25	0.25	0.25	0.25	0.24	0.22	0.12	0.037	0.013	0.0039
$\Psi_s(1\%)$	0.019	0.019	0.024	0.071	0.21	0.57	0.99	1	1	1
$\rho_s(0.1\%)$	0.25	0.25	0.25	0.25	0.25	0.25	0.21	0.1	0.04	0.012
$\Psi_s(0.1\%)$	0.0064	0.0063	0.0081	0.024	0.073	0.23	0.62	0.99	1	1

Table 7: Optimal threshold for Europe model. Similar to Table S4.

s	0	$10^{-5}$	$10^{-4.5}$	$10^{-4}$	$10^{-3.5}$	$10^{-3}$	$10^{-2.5}$	$10^{-2}$	$10^{-1.5}$	$10^{-1}$
$f_{1/2}$	0.53	0.50	0.47	0.30	0.12	0.064	0.038	0.0023	5.1e-006	6.0e-007
$T^*$	0.99	0.99	0.99	0.5	0.23	0.15	0.0076	0.0053	0.0011	0.00021
$\rho_s(T^*)$	0.25	0.25	0.21	0.14	0.1	0.056	0.21	0.2	0.2	0.17
$\Psi_s(T^*)$	1	1	1	0.86	0.77	0.72	0.17	0.44	0.78	0.91
$\rho_s(1\%)$	0.25	0.26	0.26	0.25	0.22	0.2	0.19	0.16	0.1	0.036
$\Psi_s(1\%)$	0.0023	0.0025	0.003	0.0086	0.023	0.066	0.18	0.48	0.96	1
$\rho_s(0.1\%)$	0.25	0.26	0.25	0.25	0.25	0.24	0.25	0.25	0.2	0.097
$\Psi_s(0.1\%)$	0.00081	0.00083	0.001	0.0031	0.0095	0.029	0.093	0.27	0.76	1

Table 8: Optimal threshold for Finland model. Similar to Table S4.

s	0	$10^{-5}$	$10^{-4.5}$	$10^{-4}$	$10^{-3.5}$	$10^{-3}$	$10^{-2.5}$	$10^{-2}$	$10^{-1.5}$	$10^{-1}$
$f_{1/2}$	0.50	0.48	0.42	0.24	0.048	0.010	0.0054	0.0027	0.00015	1.2e-005
$T^*$	0.99	0.99	0.96	0.33	0.076	0.033	0.017	0.0016	0.0011	0.00038
$\rho_s(T^*)$	0.25	0.25	0.21	0.17	0.18	0.13	0.074	0.17	0.17	0.15
$\Psi_s(T^*)$	1	1	1	0.85	0.76	0.86	0.79	0.26	0.55	0.8
$\rho_s(1\%)$	0.25	0.25	0.26	0.25	0.24	0.19	0.095	0.048	0.022	0.0048
$\Psi_s(1\%)$	0.012	0.013	0.016	0.047	0.14	0.34	0.52	0.75	0.97	1
$\rho_s(0.1\%)$	0.25	0.25	0.25	0.25	0.24	0.23	0.2	0.2	0.18	0.08
$\Psi_s(0.1\%)$	0.00065	0.00065	0.00083	0.0026	0.008	0.024	0.066	0.2	0.51	0.97

Table 9: Optimal threshold for Iceland model. Similar to Table S4.

## 5.1 Heterogeneity of Alleles - Hypomorphs

Our basic two class model focuses only on neutral and null alleles. We ignore the possibility of hypomorphic alleles with effect size and selection coefficients lying between neutral and null alleles. We can refine the model to include a third class of hypomorphic alleles. This three-class model has

1. Null alleles with selection coefficient  $s$  and effect size  $1 + \lambda$  as before. with fraction  $\alpha$  at birth.
2. Hypomorphic alleles with selection coefficient  $\delta s$  and effect size  $1 + \lambda\delta$  for some  $0 < \delta < 1$  and fraction  $\beta$  at birth.
3. Neutral alleles with selection coefficient 0 and no effect, with frequency  $1 - \alpha - \beta$  at birth.

The above model assumes direct selection - that is, the proportional decrease in effect size for hypomorph alleles (compared to null alleles) is the same as the proportional decrease in the selective coefficient.

We can compute the effect of adding hypomorphs alleles on power. We consider two scenarios:

### 1. Perfect knowledge.

In this idealized scenario, we assume that we can perfectly recognize whether a missense allele is null, hypomorphic or neutral. In this case, we can simply calculate the contribution to the likelihood ratio of hypomorphic alleles:

$$E[2\mathcal{L}\mathcal{R}_H] = 4n \frac{\beta\mu_M}{\delta s} g(\delta\lambda). \quad (5.6)$$

The proportional contribution of missense alleles, relative to disruptive alleles, becomes:

$$\begin{aligned} \frac{E[2\mathcal{L}\mathcal{R}_M]}{E[2\mathcal{L}\mathcal{R}_D]} &= \frac{E[2\mathcal{L}\mathcal{R}_{M,null} + 2\mathcal{L}\mathcal{R}_H]}{E[2\mathcal{L}\mathcal{R}_D]} \\ &= \frac{\alpha\mu_M}{\mu_D} \left[ 1 + \frac{\beta}{\alpha} \frac{g(\delta\lambda)}{\delta g(\lambda)} \right]. \end{aligned} \quad (5.7)$$

Here, the first term in the brackets represents the contribution of null missense alleles and the second term represents hypomorphic missense alleles. For small values of  $\lambda$ , we have  $g(\lambda) \sim \frac{\lambda^2}{2}$ , and the additional relative contribution of hypomorphs is  $\sim \frac{\beta}{\alpha} \delta$ . For large effect size  $\lambda$ , we have  $g(\lambda) \sim \lambda \log(\lambda)$  and the additional contribution of hypomorphs is  $\sim \frac{\beta}{\alpha} [1 + \frac{\log(\delta)}{\log(\lambda)}]$ . In both cases, the relative additional contribution to power is insensitive to the selective coefficient (provided that the assumption of strong selection holds).

Table S10 below shows the relative contribution of hypomorphic alleles in this idealized case. We considered our typical gene with  $\alpha = 0.25$  and  $\frac{\mu_M}{\mu_D} = 7.3$ . We assumed that hypomorphic missense alleles are born at twice the rate of null missense alleles - that is,  $\beta = 0.5$ . [15].

We suppose that null alleles increase disease risk by either 3-fold or 11-fold ( $\lambda = 2$  or 10) and that hypomorphic alleles decrease the effect size and selection coefficient by either 5-fold or 10-fold ( $\delta = 0.2$  or 0.1). (For example, with  $\lambda = 10$  and  $\delta = 0.1$ , hypomorphic alleles increase disease risk by  $1 + \delta\lambda = 2$ -fold.)

		Reduction in sample size by supplementing disruptive alleles with:		
$\lambda$	$\delta$	Null missense only	Null and hypomorphic missense	Improvement
10	0.2	2.83-fold	4.27-fold	51.1%
10	0.1	2.83-fold	3.69-fold	30.5%
2	0.2	2.83-fold	3.83-fold	35.4%
2	0.1	2.83-fold	3.35-fold	18.7%

Table 10: The relative contribution of missense null and hypomorph alleles for different values of  $\lambda$  and  $\delta$  under perfect knowledge. The relative contribution is shown here for the European population.

With perfect knowledge, hypomorphic alleles can contribute usefully when the effect size is large.

## 2. Imperfect knowledge.

In this realistic scenario, we assume that we cannot distinguish whether a missense allele is null, hypomorphic or neutral. Instead, we must select a single optimal frequency threshold  $T^*$  and count only those alleles with frequency  $\leq T^*$ . One challenge is that hypomorphic and null missense alleles have different selection coefficients and hence different allele frequencies, and thus a single threshold will be sub-optimal in terms of capturing these two groups of alleles. In addition, the two classes have different effect sizes, and thus the observed effect size will represent an average value (overweighted toward hypomorphic alleles, because they are more frequent due to a higher birth rate and weaker selection), leading to further loss of power.

We computed the total effect of hypomorphic alleles for the same parameters as above, for the European population, and for different selection coefficients. Figure S15 shows the results for various threshold values  $T$ , for intermediate effect size ( $1 + \lambda = 4$ ). Table S11 shows the maximal contribution, achieved when using the optimal threshold  $T^*$ . For the reasons discussed above, the proportional contribution of hypomorphic alleles to power is much smaller than in the idealized case. In the examples shown, they typically reduce the required sample size by less than 10%.



		Reduction in sample size by supplementing disruptive alleles with:		
$\lambda$	$\delta$	Null missense only	Null and hypomorphic missense	Improvement
10	0.2	1.44 – 1.59-fold	1.58 – 1.79-fold	7.1 – 13.5%
10	0.1	1.44 – 1.59-fold	1.48 – 1.63-fold	2.1 – 3.9%
2	0.2	1.25 – 1.35-fold	1.31 – 1.44-fold	4.0 – 7.3%
2	0.1	1.25 – 1.35-fold	1.26 – 1.37-fold	1.1 – 1.7%

Table 11: The relative contribution of missense null and hypomorph alleles for different values of  $\lambda$  and  $\delta$ , in the situation of imperfect knowledge, where we choose the threshold  $T^*$  maximizing power. The relative contribution is shown here for the European population. The relative contribution depends on the selection coefficient  $s$  (see Figure S15). For each value of  $\lambda$  and  $\delta$ , we display the range of relative contributions, when varying  $s$  in the range  $10^{-4} - 10^{-1}$ . The relative contributions of hypomorph alleles are tiny, unless the effect size  $\lambda$  and the proportionality constant  $\delta$  are large.

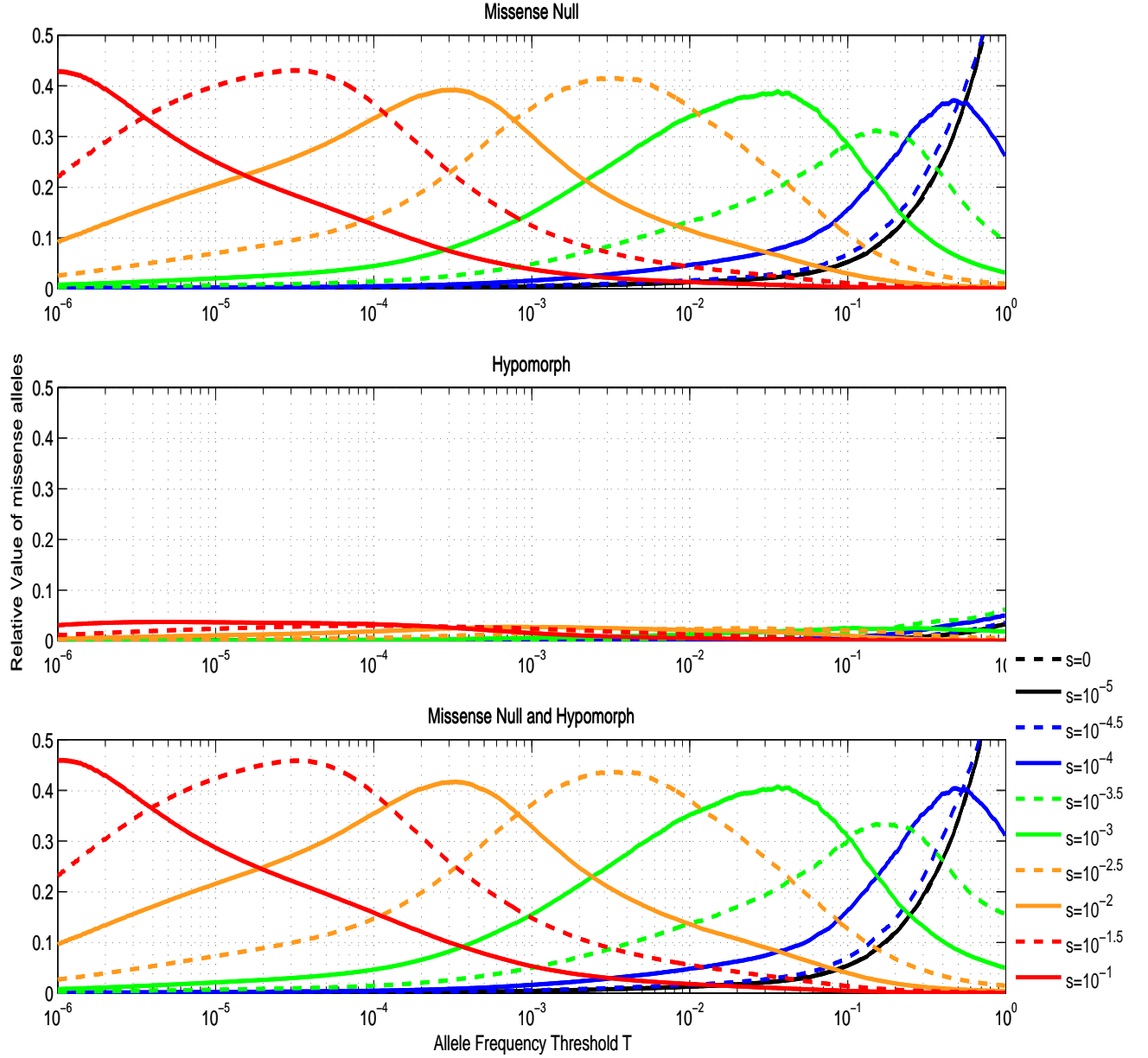


Figure 15: Increase in power from using both null and hypomorph missense alleles. The figures show the contribution of missense alleles to power, compared to the contribution of disruptive alleles, as function of the threshold  $T$  for the European population, and with the parameters,  $1 + \lambda = 4$ ,  $\alpha = 0.25$ ,  $\beta = 0.5$ ,  $\delta = 0.1$ . The top plot shows the contribution of only null missense alleles. The middle plot shows the contribution of hypomorph missense alleles. The bottom plot shows the contribution of all missense alleles. Overall, the relative additional contribution of hypomorph alleles to power is  $< 10\%$  of the contribution of missense null alleles.

## 6 RVAS Strategy 3: Enriching for Null Missense Alleles

One might seek to enrich for null missense alleles by using computational programs, such as PolyPhen-2 [46], SIFT [47], and MutationTaster [48], that predict which missense changes are "damaging" - based on the biochemical nature of the substitution and evolutionary conservation of the site (but not allele frequency). A common approach is to use such programs to filter the alleles and analyze only the damaging alleles.

We can summarize the accuracy of such programs with two terms: (i) the false positives rate  $\gamma_{neutral}$  (the probability that a neutral missense allele will be incorrectly classified as null allele), and (ii) the true positives rate  $\gamma_{null}$  (the probability that a null missense allele will be correctly classified as a null allele). We next calculate the gain in power as a function of the parameters  $\gamma_{neutral}$  and  $\gamma_{null}$ , where we combine the strategy from the previous section (of enriching further for null alleles by using only alleles below a frequency threshold) with the strategy of using functional predictions.

Considering only alleles with frequency below threshold  $T$ , we define  $\Psi_s^{(\gamma_{neutral}, \gamma_{null})}(T)$  to be the cumulative allele frequency of null alleles predicted to be damaging, and  $\rho_s^{(\gamma_{neutral}, \gamma_{null})}(T)$  to be the fraction of null alleles among all damaging alleles. The values are given by

$$\begin{aligned}\rho_s^{(\gamma_{neutral}, \gamma_{null})}(T) &= \frac{\rho_s(T)\gamma_{null}}{\rho_s(T)\gamma_{null} + (1 - \rho_s(T))\gamma_{neutral}} \\ \Psi_s^{(\gamma_{neutral}, \gamma_{null})}(T) &= \gamma_{null}\Psi_s(T).\end{aligned}\tag{6.1}$$

To compute power, we can simply plug these values in eq. (5.3), instead of  $\rho_s(T^*)$  and  $\Psi_s(T^*)$ , giving:

$$\frac{E[\mathcal{L}\mathcal{R}_{missense}^{(\gamma_{neutral}, \gamma_{null})}(T^*)]}{E[\mathcal{L}\mathcal{R}_D]} \sim \frac{\mu_M \alpha \Psi_s^{(\gamma_{neutral}, \gamma_{null})}(T^*) g(\rho_s^{(\gamma_{neutral}, \gamma_{null})}(T^*) \lambda)}{\mu_D \rho_s^{(\gamma_{neutral}, \gamma_{null})}(T^*) g(\lambda)}.\tag{6.2}$$

We can then search for optimal threshold maximizing power in the above equation, which we denote as  $T^*(\gamma_{neutral}, \gamma_{null})$ . This threshold is different from the optimal threshold  $T^*$  for the case in which we lack functional prediction (see previous section), and will typically be higher, allowing us to capture more missense null alleles, while still maintaining them at high proportion.

There is a simple formula relating the proportion of null alleles  $\rho_s$ , without functional predictions to the proportion of null alleles  $\rho_s^{(\gamma_{neutral}, \gamma_{null})}(T)$  with functional prediction,

$$\frac{\rho_s^{(\gamma_{neutral}, \gamma_{null})}(T)}{1 - \rho_s^{(\gamma_{neutral}, \gamma_{null})}(T)} = \frac{\gamma_{null}}{\gamma_{neutral}} \frac{\rho_s(T)}{1 - \rho_s(T)}.\tag{6.3}$$

In Figure S16 we show the advantage of using functional prediction.

If we have perfect prediction, ( $\gamma_{neutral} = 0, \gamma_{null} = 1$ ), we get  $\rho_s^{(0,1)}(T) = 1, \forall T \in [0, 1]$ , and the above ratio in eq. (6.3) diverges to infinity. In this case, the optimal threshold will be  $T^* = 1$ , taking all null missense alleles, and simply get (using  $\Psi_s(1) = 1$ ),

$$\frac{E[\mathcal{LLR}_{missense}^{(0,1)}(1)]}{E[\mathcal{LLR}_D]} \sim \frac{\mu_M \alpha}{\mu_D}. \quad (6.4)$$

For a typical gene with  $\frac{\mu_M}{\mu_D} = 7.3$  and  $\alpha = 0.25$ , we get that missense contribute roughly 1.8-fold as much information as disruptives, thus in this ideal case we can decrease the sample size by roughly 2.8-fold.

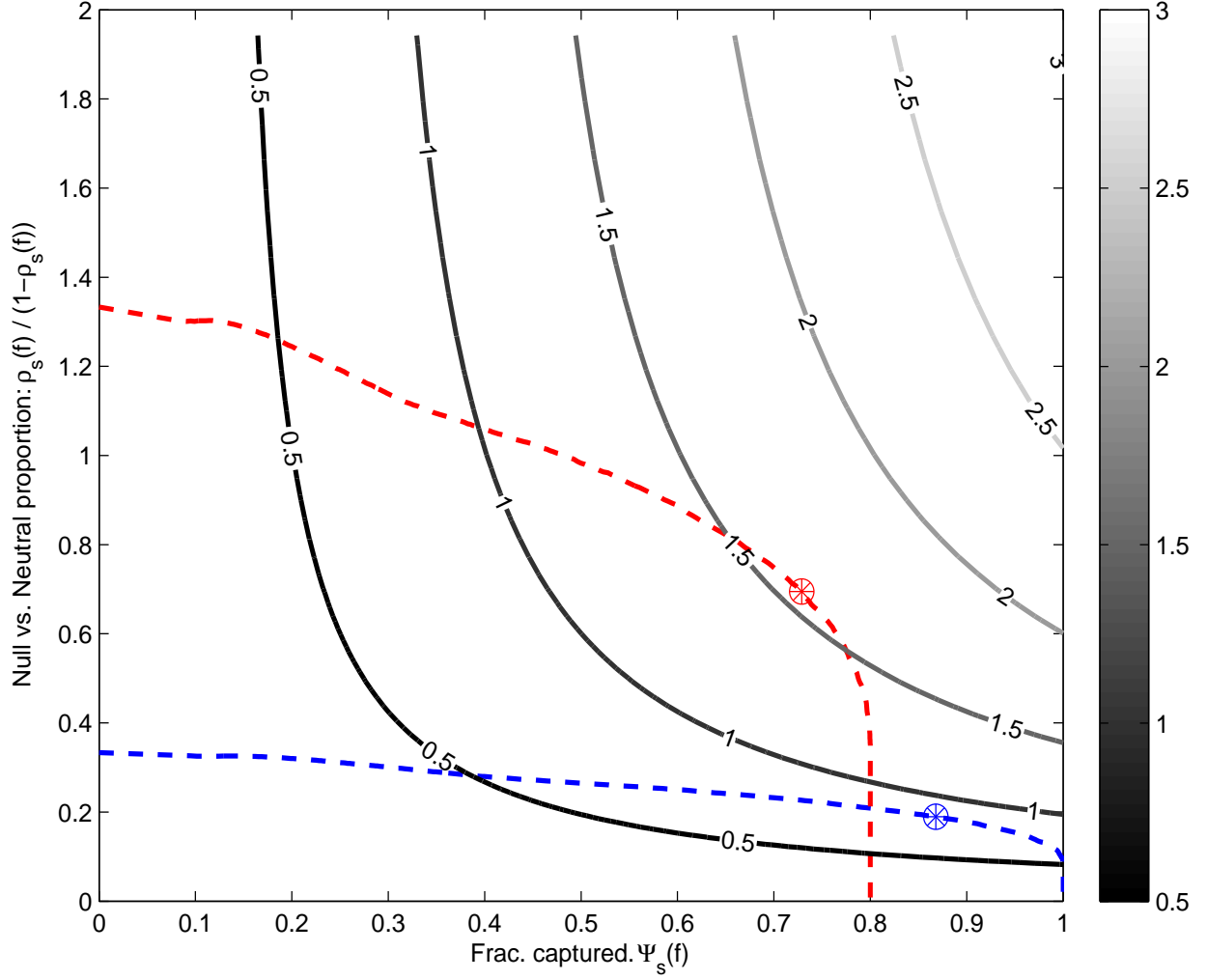


Figure 16: Power-gain from functional prediction of missense null alleles for the equilibrium population. As in Figure S14, the contour plots represent iso-power curves. The x-axis displays the fraction of null alleles captured, and the y-axis represent the proportion of null alleles among all missense alleles. Varying the threshold  $T$  corresponds to moving along the colored curves. The blue curve shows results without functional prediction (strategy 2) and the red curve shows results with a functional prediction with  $\gamma_{null} = 0.8, \gamma_{neutral} = 0.2$ . The circled dots on each curve represent the values obtained for the optimal threshold. When using functional prediction, we see a shift in the feasible curve, and thus an almost 2-fold increase in relative contributions, from 0.85 to 1.56. We have used  $1 + \lambda = 4$ ,  $\alpha = 0.25$ , and  $s = 0.01$ .

## 7 Effect of Thresholding in a Finite Sample (with *LDLR* Example)

The burden analyses in Sections 5 and 6 assume an idealized case, in which we know the precise population frequency of each allele based on a large population survey. In this case, we can filter alleles based on their frequency, and enrich for null alleles, with  $\rho(T)$  of missense alleles below a threshold  $T$  being null.

Here, we consider the situation where we don't know the allele frequencies based on a large population survey, but have only the sample data from a case-control or case-unaffected study with a total on  $n$  individuals. In this case, we can filter alleles based on their frequency in the sample.

Given a threshold  $T$ , we can retain alleles that have at most  $\lfloor 2nT \rfloor$  occurrences in the sample. We denote  $\rho_s(T; n)$  to be the expected fraction of nulls when we consider only alleles with frequency below  $T$  in a *sample* of  $n$  individuals. We have:

$$\rho_s(T; n) = \frac{\int_{x=0}^1 \alpha f_s \psi_s(x) B(\lfloor 2nT \rfloor, 2n, x) dx}{\int_{x=0}^1 [\alpha f_s \psi_s(x) + (1 - \alpha) f_0 \psi_0(x)] B(\lfloor 2nT \rfloor, 2n, x) dx} \quad (7.1)$$

where we denote by  $B(k, n, p)$  the cumulative binomial distribution (minus the value at zero):

$$B(k, n, p) = \sum_{i=1}^k \binom{2n}{i} p^i (1 - p)^{2n-i}. \quad (7.2)$$

For example, if we take only singleton alleles (i.e. setting  $T = \frac{1}{2n}$ ) we get,

$$\rho_s\left(\frac{1}{2n}; n\right) = \frac{\int_{x=0}^1 \alpha f_s \psi_s(x) x(1 - x)^{2n-1} dx}{\int_{x=0}^1 [\alpha f_s \psi_s(x) + (1 - \alpha) f_0 \psi_0(x)] x(1 - x)^{2n-1} dx} \quad (7.3)$$

When we set the frequency threshold based on cases, we need to be more careful with the choice of threshold, since the frequency in cases is higher,  $(1 + \lambda)f$  for null alleles with population frequency  $f$ . If we set the same threshold for cases and population controls, i.e. take all alleles with frequency at least  $T$  in either cases or controls, (assuming equal number of cases and controls), then

$$\begin{aligned} \rho_s(T; n, \lambda) &\approx \int_{x=0}^1 \alpha f_s \psi_s(x) \left[ B(\lfloor 2nT \rfloor, 2n, x) + B(\lfloor 2nT \rfloor, 2n, x(1 + \lambda)) \right. \\ &\quad \left. - B(\lfloor 2nT \rfloor, 2n, x) B(\lfloor 2nT \rfloor, 2n, x(1 + \lambda)) \right] dx \\ &\quad \Bigg/ \int_{x=0}^1 \left\{ \alpha f_s \psi_s(x) \left[ B(\lfloor 2nT \rfloor, 2n, x) + B(\lfloor 2nT \rfloor, 2n, x(1 + \lambda)) \right. \right. \\ &\quad \left. \left. - B(\lfloor 2nT \rfloor, 2n, x) B(\lfloor 2nT \rfloor, 2n, x(1 + \lambda)) \right] \right. \\ &\quad \left. + (1 - \alpha) f_0 \psi_0(x) \left[ 2B(\lfloor 2nT \rfloor, 2n, x) - B(\lfloor 2nT \rfloor, 2n, x)^2 \right] \right\} dx. \end{aligned} \quad (7.4)$$

The fraction of nulls,  $\rho_s$ , thus depends on  $\lambda$ ; large values of  $\lambda$  increase  $\rho_s$ .

## 7.1 *LDLR* Example

To illustrate the results in the paper (including the issues with finite samples), we use an example taken from an exome-wide RVAS of Early-Onset Myocardial Infarction (EOMI Study).

Briefly, several of the authors of this paper are involved in a large-scale exome-wide RVAS for EOMI, including analysis of 2743 cases and 2465 controls. The study subjects were taken from the National Heart Lung and Blood Institute’s Exome Sequencing Project (NHLBI ESP) EOMI Study (1027 cases, 946 controls) and the Italian Atherosclerosis, Thrombosis and Vascular Biology (ATVB) study (1716 cases, 1519 controls) funded by the National Human Genome Research Institute. In the NHLBI ESP study, cases were individuals with MI at age  $\leq 50$  for males and age  $\leq 60$  for females and controls were individuals of advanced age ( $\geq 60$  for men and  $\geq 70$  for women) who had not suffered Myocardial Infarction (MI). The Italian ATVB Study ascertained 1716 survivors of acute MI before the age of 45 from 125 intensive care units across Italy between 1998 – 2001. Controls were individuals without a personal history of thrombotic disease and were matched to cases for age, gender, and geographic location. The EOMI study employed the commonly used definition of rare variants as being alleles with frequency  $\leq 1\%$  in the general population.

The full results from the EOMI Study will be published elsewhere. Here, we focus only on the results for the *LDLR* gene (coding region of 2583 base pairs, including the stop codon).

The results (Table S12) show strong enrichment for disruptive alleles ( $1 + \lambda_D = 18.1$ ) but much weaker enrichment for missense alleles ( $1 + \lambda_M = 1.5$ ). The low enrichment seen for missense alleles is explained under our two-class model by the fact that null alleles in *LDLR* are under strong selection ( $s \approx 10^{-1.7}$ ). Given such strong selection, the optimal threshold is very low:  $T^* = 10^{-4}$ . With the much higher threshold of  $T = 1\%$ , missense null alleles are swamped by missense neutral alleles. The relative risk for missense alleles with frequency  $\leq 1\%$  is expected to be  $1 + \lambda_M = 1.3$ , which is very close to the observed value of 1.5. For the optimal threshold of  $T^* = 10^{-4}$ , the relative risk would be expected to be higher:  $1 + \lambda_M = 3.8$  (although this is still lower than seen with disruptive alleles, which is a pure class of null alleles).

There is a practical problem, however, with using the optimal threshold  $T^* = 10^{-4}$ . Given the relatively small sample size (and no additional population survey data), we can’t tell which alleles actually have population frequency  $\leq 10^{-4}$ . The best alternative is to study only the singleton alleles - that is, the alleles that appear exactly once in the sample.

For the EOMI study, counting singletons turns out to be almost as good as if we could identify precisely the alleles with frequency  $\leq 10^{-4}$ . (The expected value of  $1 + \lambda_M$  is 3.7 in the former case vs 3.8 in the latter; Table S12). This is because the EOMI study just happens to involve  $\sim 10^4$  chromosomes (more precisely,  $2 \times (2743 + 2465) = 10,420$ ) - that is, singletons correspond to a frequency of  $\sim 10^{-4}$  in the sample.

If the EOMI study involved a much smaller sample, the use of singletons would be less effective at enriching for null alleles. With only 1000 chromosomes, the expected relative risk is 2.1. With only 100 chromosomes, the expected relative risk is only 1.4. (Table S12). Figure S17 shows how the proportion of nulls among missense alleles varies with sample size.



Allelic-Class	Cases	Controls	$\Psi_s(T)$	$\rho_s(T)$	$1 + \lambda$
n	2743	2465			
<u>Disruptive:</u>					
Observed	20	1			18.1
Expected					18.1
<u>Missense(<math>f \leq 1\%</math>):</u>					
Observed	172	102			1.5
Expected (population)			100.0%	2.0%	1.3
Expected ( $n = 5208$ )			100.0%	2.0%	1.3
<u>Missense(<math>f \leq 0.01\%</math>):</u>					
Observed	37	19			1.8
Expected (population)			90.9%	16.6%	3.8
Expected ( $n = 5208$ , singletons)			86.8%	16.0%	3.7
Expected ( $n = 500$ , singletons)			100.0%	6.5%	2.1
Expected ( $n = 50$ , singletons)			100.0%	2.3%	1.4
<u>Missense-polyphen(<math>f \leq 1\%</math>):</u>					
Observed	89	32			2.5
Expected (population)			100.0%	7.7%	2.3
Expected ( $n = 5208$ , singletons)			100.0%	7.7%	2.3
<u>Missense-polyphen-Singletons(<math>f \leq 0.01\%</math>):</u>					
Observed	19	6			2.8
Expected (population)			90.9%	44.4%	8.6
Expected ( $n = 5208$ , singletons)			86.8%	39.0%	7.7

Table 12: Values observed in an association test for *LDLR* with EOMI. The table shows observed counts and expected values of  $\rho_s(T)$  and  $1 + \lambda$ . 'Expected (population)' refers to the situation when allele frequencies are known precisely. 'Expected ( $n = \dots$ , singletons)' refers to the situation when the sample size is  $n$  and only singletons are counted. Calculations assume that the true relative risk for null alleles is  $1 + \lambda = 18.1$  (based on the observed value for disruptive alleles), the selection coefficient is  $s = 10^{-1.7}$  (based on the observed frequency of disruptive alleles),  $\alpha = 0.25$ , the population follows the European model, and the functional prediction model misclassifies 20% of null and 20% of neutral alleles.

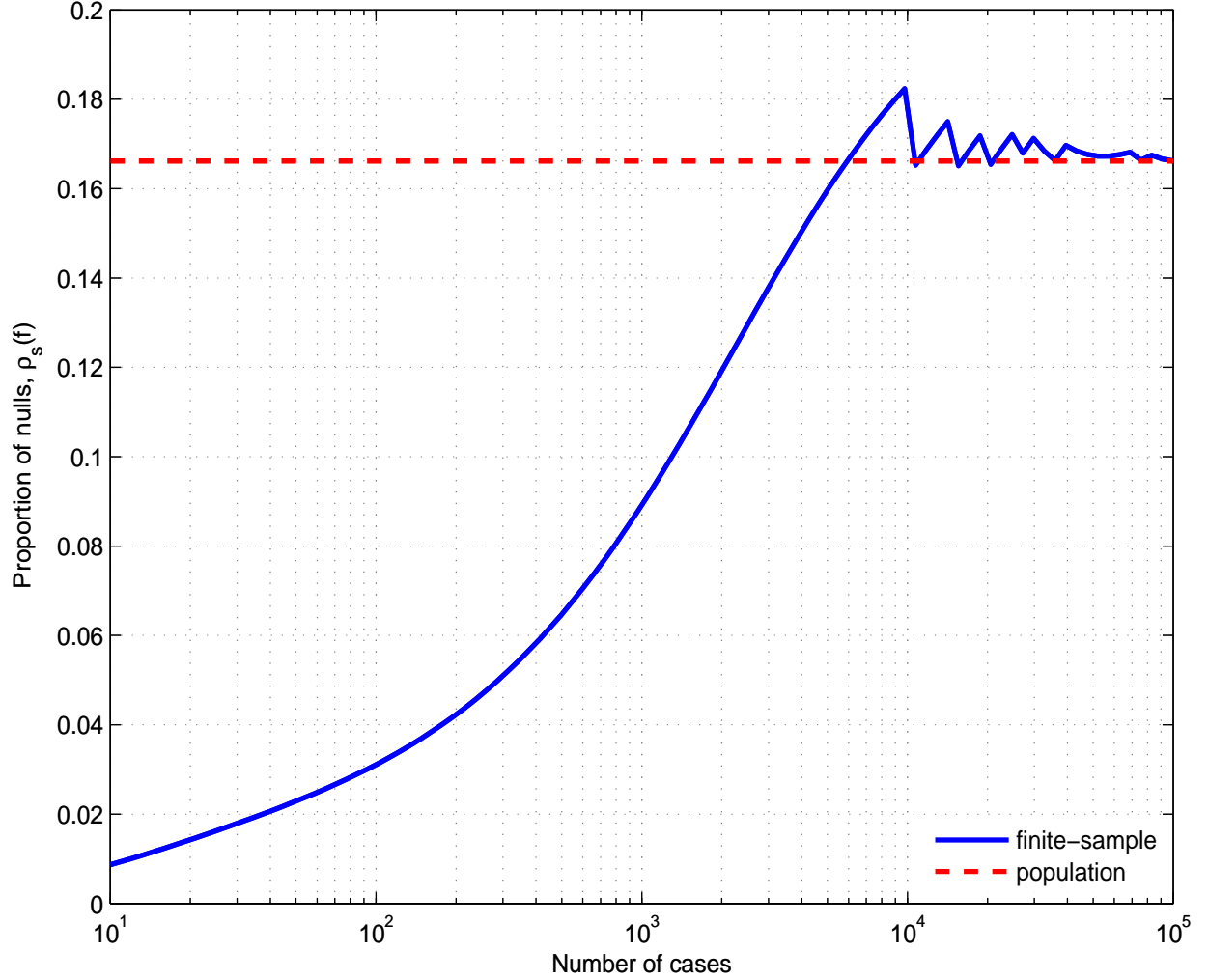


Figure 17: Proportion  $\rho_s(f)$  of missense alleles that are null, as a function of the number  $n$  of cases, for the EOMI study with assumptions as in Table S12. The red dashed line shows the proportion of missense alleles that are null when allele frequencies are known precisely and one uses the optimal threshold  $T^* \sim 10^{-4}$ . The blue curve shows the proportion of missense alleles that are null if allele frequencies are not known precisely and one instead uses (i) singletons, if  $J = 0$  and (ii) only alleles with  $J$  counts, if  $J > 0$ , where  $J = \lfloor 2nT^* \rfloor$ . The proportion of nulls reaches the dashed red curve when the number of cases is  $\sim 5000$ , corresponding to 10,000 chromosomes. For smaller sample sizes, the proportion of missense alleles that are null is much smaller (necessitating a much larger sample size).

## 8 RVAS Strategy 4: Isolated Populations

Another potential approach is to exploit the inherent variation in combined allele frequencies across different populations and genes, with the hope that, for certain genes associated with disease, the CAF will happen to be large in the population tested, making it possible to detect association in a smaller sample. To study this variation, we computed the CAF for various populations using simulations, as described in Section 1.3. Specifically, we recorded the CAF for each gene in each individual simulation, to obtain an overall distribution of the CAF for different populations, shown in Figure 3 in the main text for all null alleles ( $\mu_{null} = 5 \times 10^{-6}$ ).

Here, we describe results for both null alleles ( $\mu_{null} = 5 \times 10^{-6}$ ) and disruptive alleles ( $\mu_D = 1.7 \times 10^{-6}$ ). For large populations without bottlenecks, the distribution is in general tightly concentrated around the mean value, as shown in Tables S15-S18. For such populations we can thus largely ignore variations in the CAF, and simply use the mean value (Table S2). However, for populations that have experienced recent severe bottlenecks, the variation in CAF is much larger, as shown in Tables S21- S24 and in Figures S18-S22.

Figures S18-S22 show results for (i) all null alleles (as shown in Figure 3 in the main text) and (ii) disruptive alleles. Models with severe and recent bottlenecks (Finland and Iceland) show substantially higher variation in the CAF, compared to the Expansion1 model with a large population and no severe bottleneck, whereas the behaviour for Europe is intermediate.

The distributions depend on the bottleneck size, number of generations since expansion, mutation rate of the allelic class and selection coefficient. With a tighter bottleneck (e.g., 100 chromosomes in Finland vs. 1000 chromosomes in Iceland), the probability that a rare variant passes through the bottleneck is lower but those rare alleles that are lucky enough to pass jump to a higher frequency (1% vs 0.1%). Consequently, the proportion of genes at intermediate deviations (e.g., 5- to 10-fold) is often higher in Iceland, but the proportion of genes at high deviations (e.g., 30-fold or more) is typically higher in Finland. The curves also depend on the absolute mutation rate, and thus differ for all null alleles vs. disruptive alleles.

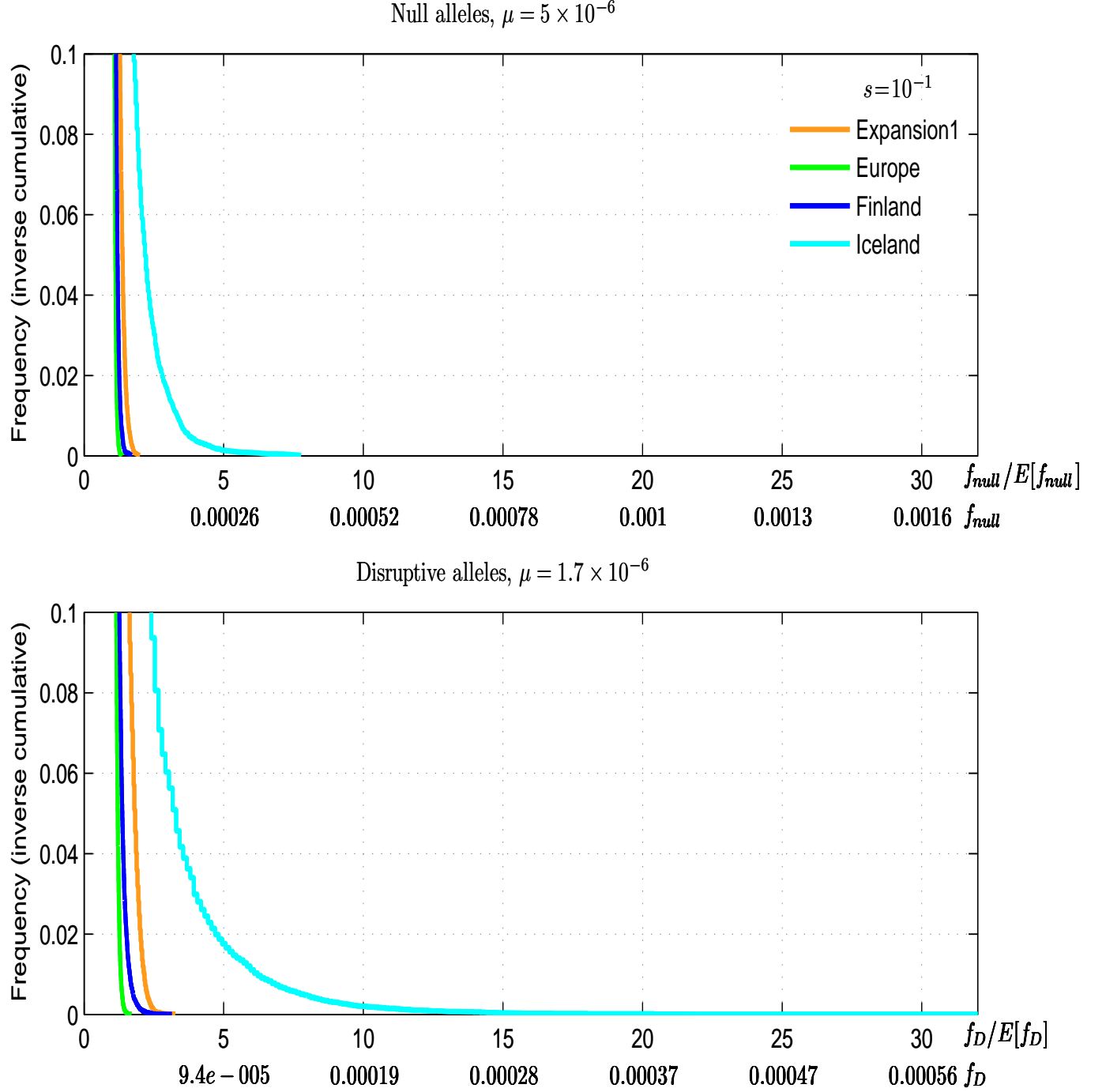


Figure 18: The inverse cumulative distribution of the Combined Allele Frequency (CAF) for  $s = 10^{-1}$ . Obtained by simulating 50,000 genes for each demographic model. The top panel represents null alleles ( $\mu_{null} = 5 \times 10^{-6}$ ), as in Figure 3 in the main text, and the bottom panel represents disruptive alleles ( $\mu_D = 1.7 \times 10^{-6}$ ). The x-axis shows both the CAF itself ( $f_{null}$ ,  $f_D$ ), and the CAF normalized to have mean 1 ( $f_{null}/E[f_{null}]$ ,  $f_D/E[f_D]$ ). The figures show the right tail of the distributions. While the mean CAF is essentially the same for all models (see Figure 1), different models show different distributions.

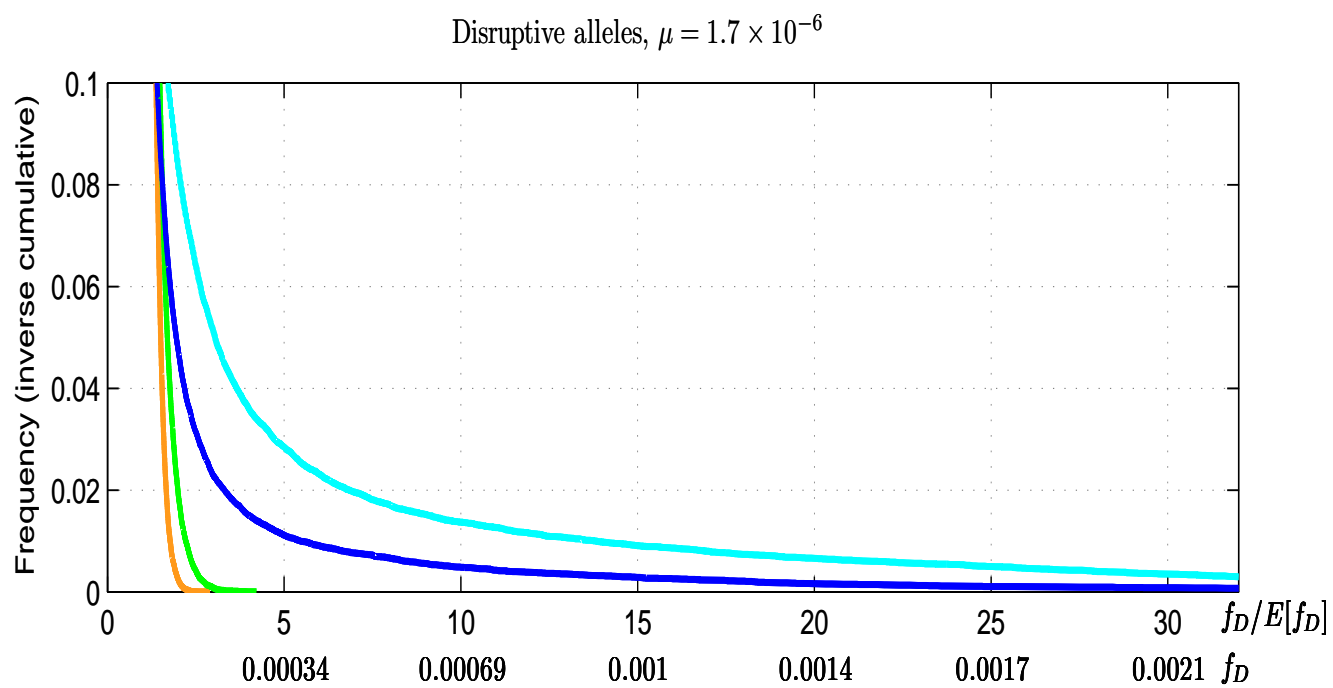
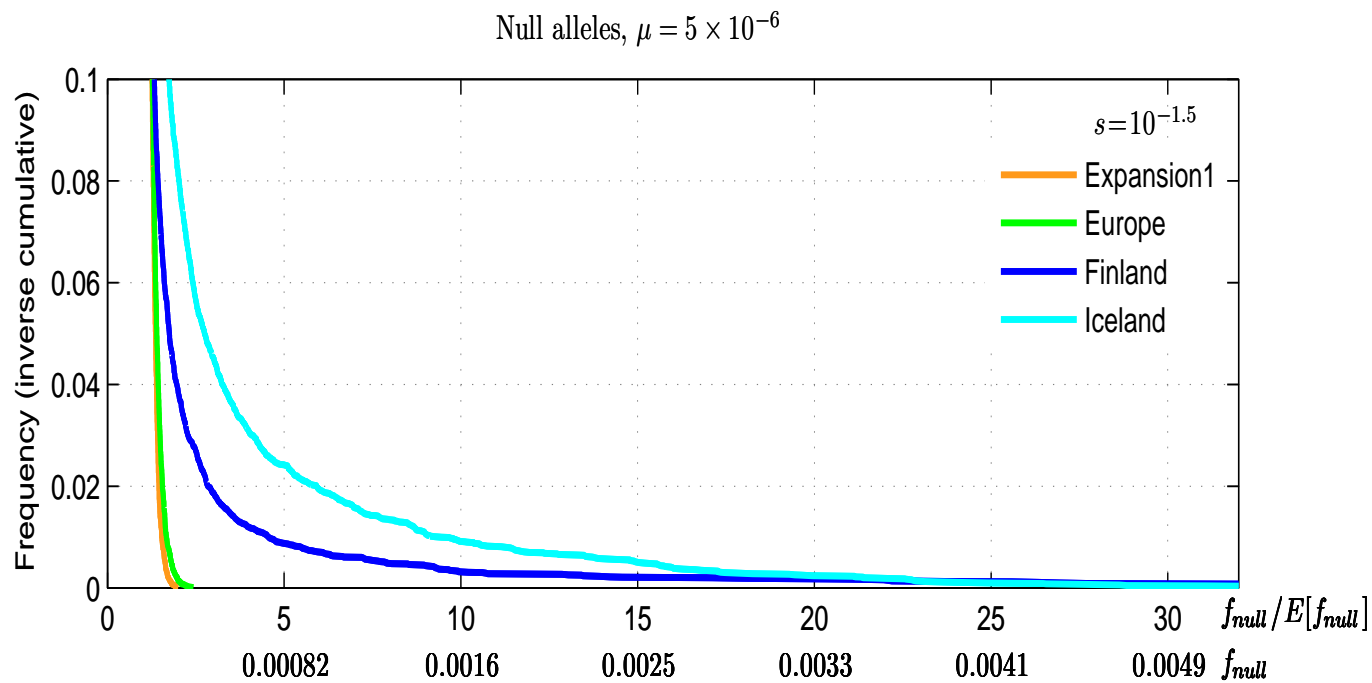


Figure 19: The inverse cumulative distribution of the Combined Allele Frequency (CAF) for  $s = 10^{-1.5}$ . Similar to Figure S18.

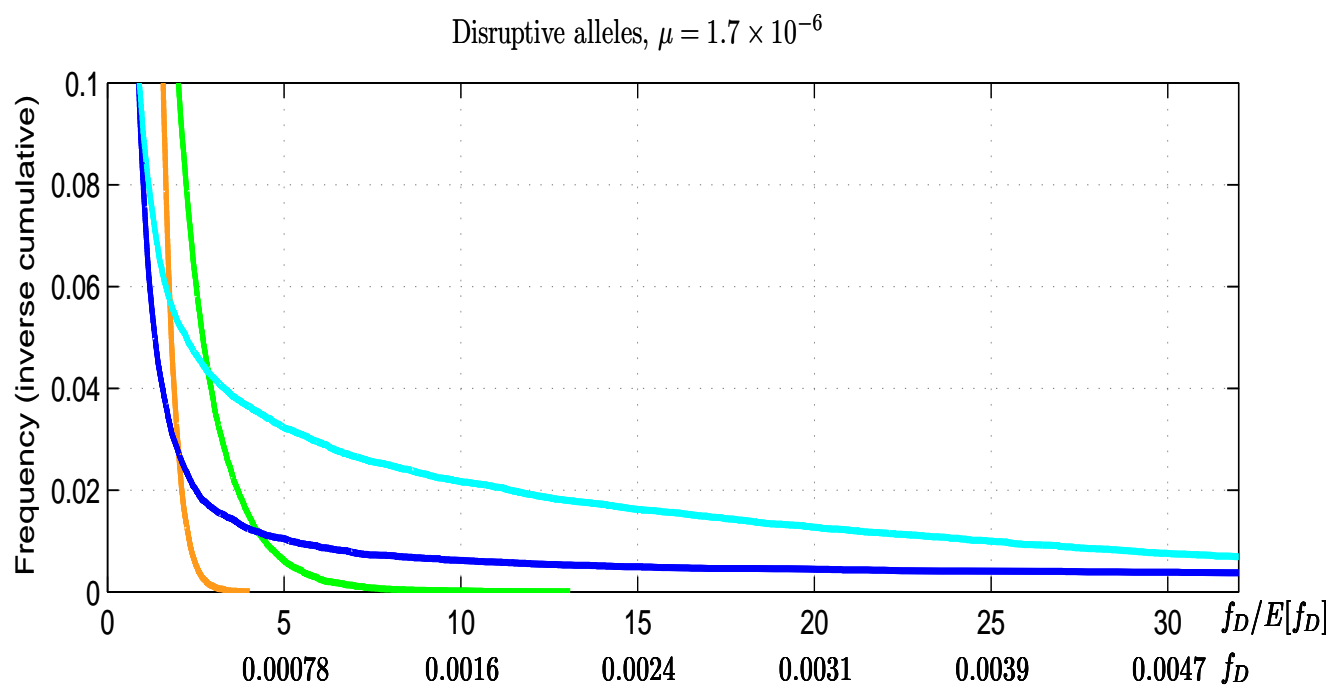
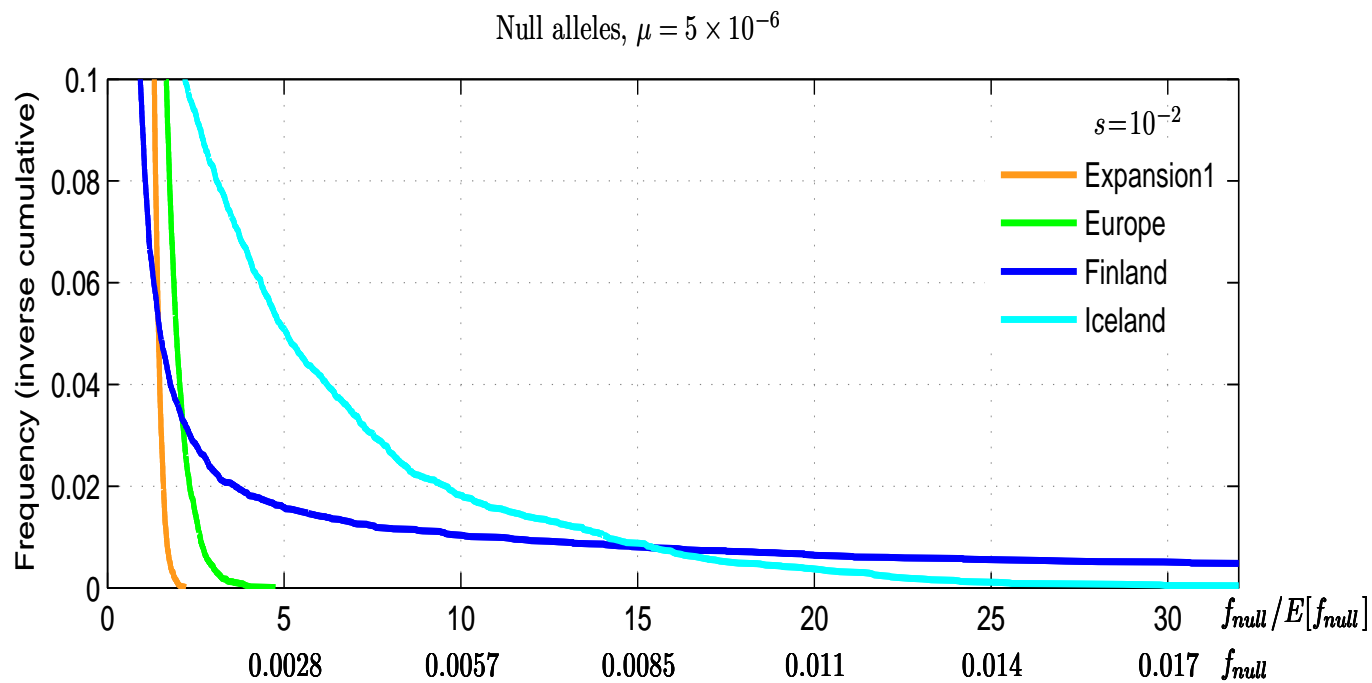


Figure 20: The inverse cumulative distribution of the Combined Allele Frequency (CAF) for  $s = 10^{-2}$ . Similar to Figure S18.

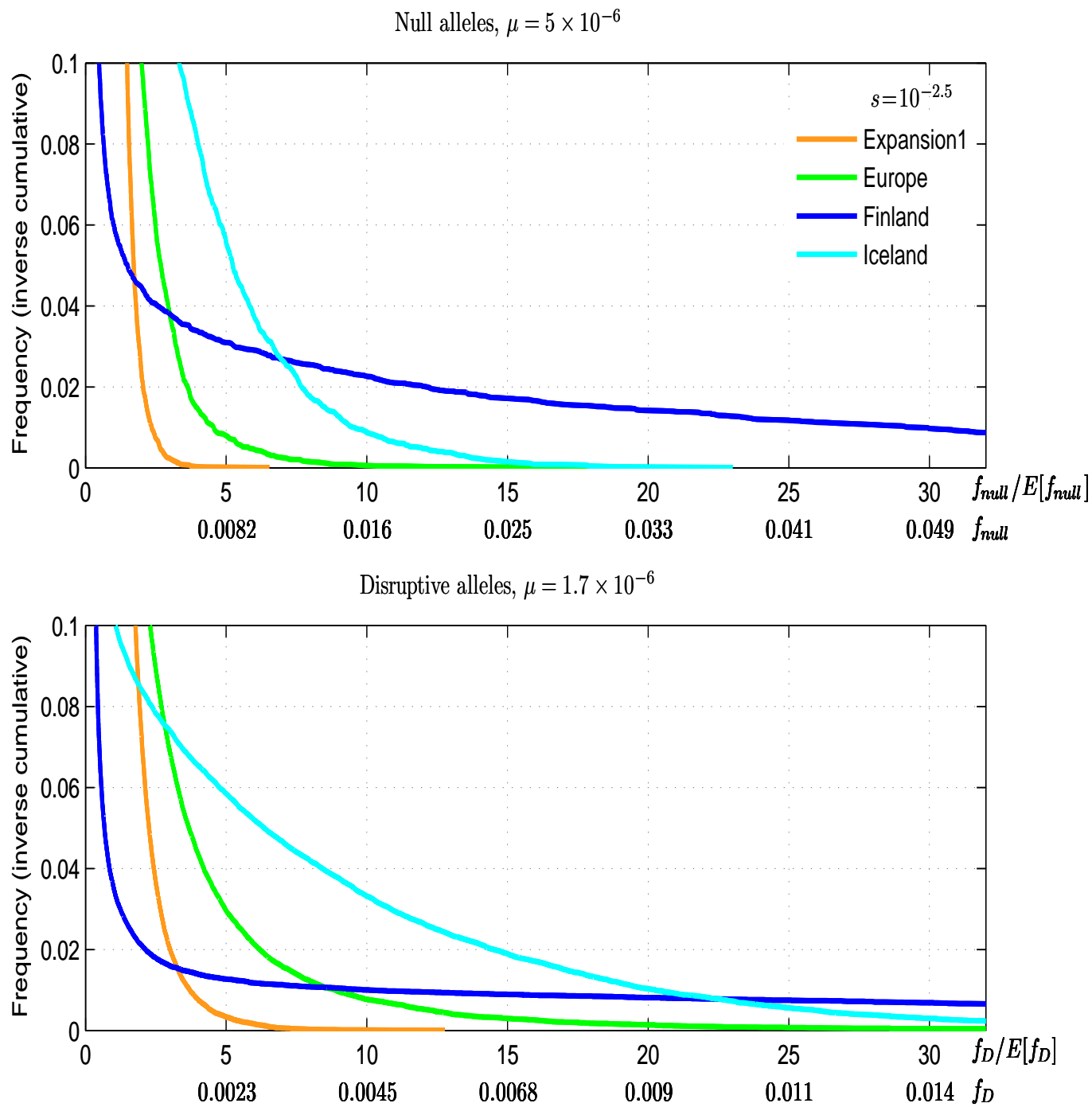


Figure 21: The inverse cumulative distribution of the Combined Allele Frequency (CAF) for  $s = 10^{-2.5}$ . Similar to Figure S18.

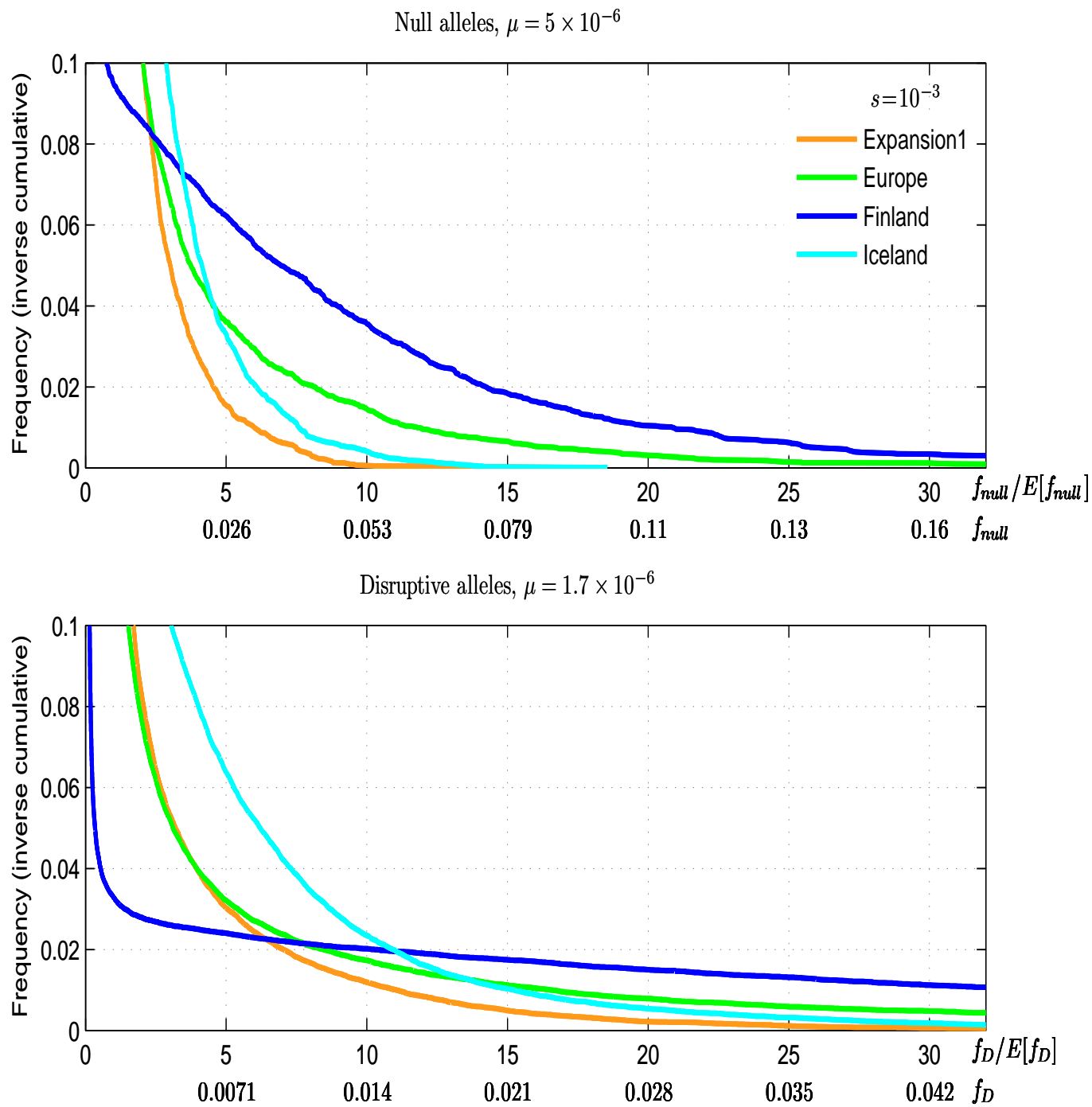


Figure 22: The inverse cumulative distribution of the Combined Allele Frequency (CAF) for  $s = 10^{-3}$ . Similar to Figure S18.



s	0	$10^{-5}$	$10^{-4.5}$	$10^{-4}$	$10^{-3.5}$	$10^{-3}$	$10^{-2.5}$	$10^{-2}$	$10^{-1.5}$	$10^{-1}$
Mean	0.076	0.068	0.053	0.024	0.0056	0.0015	0.00049	0.00011	6.4e-005	2.2e-005
St.d.	0.2	0.18	0.16	0.086	0.023	0.0065	0.0021	0.00053	0.00024	7.7e-005
1%	0	0	0	0	0	0	0	0	0	0
5%	0	0	0	0	0	0	0	0	0	0
10%	0	0	0	0	0	0	0	0	0	0
25%	0	0	0	0	0	0	0	0	0	0
50%	0	0	0	0	0	0	0	0	0	0
75%	0.019	0.013	0.007	0.0012	0.0002	0	0	0	0	0
90%	0.27	0.23	0.16	0.054	0.0095	0.0021	0.00085	0.00015	0.0002	0.0001
95%	0.55	0.5	0.38	0.15	0.033	0.0082	0.0027	0.00055	0.0004	0.0002
99%	0.93	0.9	0.82	0.47	0.12	0.033	0.01	0.0026	0.0012	0.0004

Table 13: The mean, standard deviation, and different quantiles of the distribution of CAF for disruptive alleles ( $\mu_D = 1.7 \times 10^{-6}$ ) across different simulations for a population at equilibrium. Values were obtained by simulating 50,000 realizations corresponding to 50,000 different simulated genes (see Section 1.3).

s	0	$10^{-5}$	$10^{-4.5}$	$10^{-4}$	$10^{-3.5}$	$10^{-3}$	$10^{-2.5}$	$10^{-2}$	$10^{-1.5}$	$10^{-1}$
Mean	0.22	0.19	0.15	0.073	0.018	0.0052	0.0015	0.00065	0.0002	5.7e-005
St.d.	0.33	0.31	0.26	0.15	0.041	0.012	0.0035	0.0013	0.0004	0.00012
1%	0	0	0	0	0	0	0	0	0	0
5%	0	0	0	0	0	0	0	0	0	0
10%	0	0	0	0	0	0	0	0	0	0
25%	0.0013	0.00075	0.00035	0.0001	5e-005	0	0	0	0	0
50%	0.051	0.039	0.025	0.0086	0.0019	0.00045	0.00015	0.0001	5e-005	0
75%	0.32	0.27	0.19	0.071	0.017	0.0048	0.0013	0.0007	0.0002	5e-005
90%	0.73	0.66	0.51	0.23	0.057	0.015	0.0045	0.0019	0.00065	0.0002
95%	0.93	0.88	0.73	0.39	0.091	0.027	0.0083	0.0031	0.001	0.0003
99%	1.4	1.3	1.1	0.74	0.2	0.056	0.017	0.0064	0.002	0.0006

Table 14: The mean, standard deviation, and different quantiles of the distribution of CAF for all null alleles ( $\mu_D = 5 \times 10^{-6}$ ) across different simulations for a population at equilibrium. Values were obtained by simulating 50,000 realizations corresponding to 50,000 different simulated genes (see Section 1.3).

s	0	$10^{-5}$	$10^{-4.5}$	$10^{-4}$	$10^{-3.5}$	$10^{-3}$	$10^{-2.5}$	$10^{-2}$	$10^{-1.5}$	$10^{-1}$
Mean	0.076	0.07	0.054	0.024	0.0054	0.0015	0.00047	0.00016	8.2e-005	1.8e-005
St.d.	0.19	0.18	0.15	0.084	0.018	0.0031	0.00033	7.1e-005	2.4e-005	7.5e-006
1%	0.00019	0.00019	0.00019	0.00018	0.00017	0.00014	9.6e-005	4.9e-005	3.4e-005	6.5e-006
5%	0.00033	0.00032	0.00032	0.0003	0.00028	0.00023	0.00015	6.9e-005	4.6e-005	8.5e-006
10%	0.00044	0.00043	0.00043	0.0004	0.00036	0.00029	0.00018	8.2e-005	5.3e-005	9.5e-006
25%	0.00074	0.00072	0.00071	0.00065	0.00057	0.00044	0.00026	0.00011	6.6e-005	1.2e-005
50%	0.0015	0.0015	0.0014	0.0012	0.00099	0.00072	0.00038	0.00015	8.1e-005	1.6e-005
75%	0.018	0.014	0.0087	0.0036	0.0021	0.0012	0.00057	0.0002	9.7e-005	2.2e-005
90%	0.27	0.23	0.16	0.051	0.0084	0.0025	0.00083	0.00026	0.00011	2.9e-005
95%	0.54	0.5	0.38	0.14	0.026	0.0046	0.001	0.0003	0.00012	3.2e-005
99%	0.92	0.91	0.82	0.46	0.09	0.015	0.0017	0.00038	0.00015	3.8e-005

Table 15: Variation in disruptive alleles combined allele frequency  $f_D$  for the Expansion1 model. Similar to Table S13.

s	0	$10^{-5}$	$10^{-4.5}$	$10^{-4}$	$10^{-3.5}$	$10^{-3}$	$10^{-2.5}$	$10^{-2}$	$10^{-1.5}$	$10^{-1}$
Mean	0.22	0.2	0.16	0.07	0.017	0.0052	0.0016	0.00049	0.00015	4.9e-005
St.d.	0.33	0.31	0.26	0.14	0.032	0.0057	0.00062	0.00012	2.9e-005	1.1e-005
1%	0.0017	0.0017	0.0016	0.0016	0.0015	0.0012	0.00068	0.00026	9e-005	2.7e-005
5%	0.0024	0.0024	0.0023	0.0022	0.0019	0.0015	0.00086	0.00031	0.0001	3.2e-005
10%	0.003	0.003	0.0029	0.0026	0.0023	0.0018	0.00096	0.00034	0.00011	3.5e-005
25%	0.0057	0.0054	0.0049	0.0039	0.0032	0.0023	0.0012	0.0004	0.00012	4.1e-005
50%	0.052	0.041	0.029	0.011	0.0054	0.0033	0.0015	0.00048	0.00014	4.9e-005
75%	0.32	0.29	0.2	0.064	0.016	0.0055	0.0019	0.00056	0.00016	5.6e-005
90%	0.73	0.68	0.53	0.21	0.044	0.011	0.0024	0.00065	0.00018	6.3e-005
95%	0.95	0.9	0.75	0.36	0.073	0.016	0.0027	0.00071	0.0002	6.8e-005
99%	1.4	1.3	1.1	0.7	0.15	0.031	0.0038	0.00082	0.00022	7.7e-005

Table 16: Variation in null alleles combined allele frequency  $f_{null}$  for the Expansion1 model. Similar to Table S14.

s	0	$10^{-5}$	$10^{-4.5}$	$10^{-4}$	$10^{-3.5}$	$10^{-3}$	$10^{-2.5}$	$10^{-2}$	$10^{-1.5}$	$10^{-1}$
Mean	0.076	0.068	0.054	0.023	0.0052	0.0014	0.00045	0.00019	6.3e-005	1.8e-005
St.d.	0.2	0.18	0.16	0.083	0.018	0.0032	0.00055	0.00014	2.5e-005	2e-006
1%	7.1e-005	7.2e-005	7.2e-005	6.9e-005	6.7e-005	6.3e-005	5.2e-005	5.1e-005	3.2e-005	1.4e-005
5%	0.00011	0.00011	0.00011	0.00011	9.9e-005	8.9e-005	6.9e-005	6.4e-005	3.6e-005	1.5e-005
10%	0.00016	0.00016	0.00016	0.00015	0.00013	0.00012	8.5e-005	7.4e-005	3.9e-005	1.6e-005
25%	0.00039	0.00038	0.00036	0.00032	0.00027	0.00021	0.00013	9.7e-005	4.5e-005	1.7e-005
50%	0.0014	0.0014	0.0012	0.00099	0.00072	0.0005	0.00026	0.00015	5.6e-005	1.8e-005
75%	0.018	0.014	0.0093	0.0043	0.0023	0.0013	0.00053	0.00024	7.3e-005	2e-005
90%	0.27	0.23	0.16	0.047	0.0089	0.0031	0.001	0.00038	9.5e-005	2.1e-005
95%	0.55	0.49	0.38	0.14	0.024	0.0055	0.0015	0.00048	0.00011	2.2e-005
99%	0.93	0.9	0.83	0.45	0.088	0.015	0.0027	0.00073	0.00015	2.3e-005

Table 17: Variation in disruptive alleles combined allele frequency  $f_D$  for the Expansion2 model. Similar to Table S13.

s	0	$10^{-5}$	$10^{-4.5}$	$10^{-4}$	$10^{-3.5}$	$10^{-3}$	$10^{-2.5}$	$10^{-2}$	$10^{-1.5}$	$10^{-1}$
Mean	0.23	0.19	0.15	0.072	0.017	0.0048	0.0016	0.00057	0.00017	5e-005
St.d.	0.33	0.3	0.25	0.14	0.03	0.006	0.0011	0.00028	3.5e-005	3.3e-006
1%	0.00064	0.00063	0.00059	0.00054	0.00045	0.00035	0.00027	0.00019	0.00011	4.3e-005
5%	0.0013	0.0013	0.0011	0.001	0.00079	0.00059	0.0004	0.00024	0.00013	4.5e-005
10%	0.002	0.002	0.0018	0.0015	0.0011	0.00082	0.00051	0.00028	0.00013	4.6e-005
25%	0.0057	0.0051	0.0043	0.0032	0.0022	0.0014	0.00079	0.00037	0.00015	4.8e-005
50%	0.051	0.04	0.028	0.012	0.0052	0.0027	0.0013	0.00051	0.00017	5e-005
75%	0.34	0.27	0.19	0.067	0.016	0.0056	0.002	0.00072	0.00019	5.2e-005
90%	0.74	0.64	0.52	0.22	0.045	0.011	0.003	0.00095	0.00022	5.4e-005
95%	0.95	0.85	0.72	0.37	0.074	0.016	0.0037	0.0011	0.00024	5.6e-005
99%	1.4	1.2	1.1	0.73	0.15	0.03	0.0057	0.0015	0.00028	5.8e-005

Table 18: Variation in null alleles combined allele frequency  $f_{null}$  for the Expansion2 model. Similar to Table S14.

s	0	$10^{-5}$	$10^{-4.5}$	$10^{-4}$	$10^{-3.5}$	$10^{-3}$	$10^{-2.5}$	$10^{-2}$	$10^{-1.5}$	$10^{-1}$
Mean	0.071	0.064	0.051	0.023	0.0055	0.0014	0.00041	0.00016	7.4e-005	1.7e-005
St.d.	0.19	0.18	0.16	0.091	0.028	0.0069	0.00082	0.00014	2.7e-005	2.1e-006
1%	5.3e-005	5.3e-005	5.3e-005	5.2e-005	5e-005	4.7e-005	4.4e-005	4.4e-005	3.3e-005	1.2e-005
5%	7.1e-005	7.2e-005	7.2e-005	7e-005	6.5e-005	6e-005	5.2e-005	5.3e-005	4e-005	1.4e-005
10%	9.2e-005	9.2e-005	9.2e-005	8.8e-005	8e-005	7.3e-005	6e-005	6e-005	4.5e-005	1.5e-005
25%	0.00018	0.00017	0.00017	0.00016	0.00014	0.00012	8.4e-005	7.7e-005	5.5e-005	1.6e-005
50%	0.00058	0.00056	0.00052	0.00043	0.00034	0.00026	0.00017	0.00011	6.9e-005	1.7e-005
75%	0.005	0.0039	0.003	0.0017	0.0011	0.00072	0.00041	0.00019	8.7e-005	1.8e-005
90%	0.26	0.22	0.15	0.029	0.0044	0.0021	0.00095	0.00032	0.00011	2e-005
95%	0.54	0.49	0.38	0.15	0.016	0.0043	0.0015	0.00044	0.00012	2.1e-005
99%	0.93	0.91	0.84	0.5	0.14	0.026	0.0037	0.00073	0.00016	2.2e-005

Table 19: Variation in disruptive alleles combined allele frequency  $f_D$  for the European model. Similar to Table S13.

s	0	$10^{-5}$	$10^{-4.5}$	$10^{-4}$	$10^{-3.5}$	$10^{-3}$	$10^{-2.5}$	$10^{-2}$	$10^{-1.5}$	$10^{-1}$
Mean	0.21	0.19	0.15	0.068	0.019	0.0055	0.0016	0.00065	0.00017	4.7e-005
St.d.	0.33	0.3	0.27	0.15	0.051	0.013	0.0015	0.00032	3.7e-005	3.4e-006
1%	0.00029	0.00029	0.00028	0.00027	0.00025	0.00025	0.00027	0.0002	0.00012	3.9e-005
5%	0.0005	0.0005	0.00046	0.00043	0.00038	0.00036	0.00037	0.00027	0.00013	4.1e-005
10%	0.00076	0.00076	0.00069	0.00061	0.00053	0.00048	0.00046	0.00031	0.00013	4.2e-005
25%	0.002	0.0019	0.0017	0.0013	0.001	0.00088	0.00069	0.00042	0.00015	4.4e-005
50%	0.02	0.014	0.0091	0.0039	0.0025	0.0019	0.0012	0.00058	0.00017	4.7e-005
75%	0.31	0.26	0.18	0.046	0.0088	0.0044	0.002	0.0008	0.00019	4.9e-005
90%	0.71	0.64	0.55	0.24	0.048	0.011	0.0032	0.0011	0.00022	5.1e-005
95%	0.93	0.87	0.78	0.4	0.11	0.02	0.0043	0.0013	0.00024	5.2e-005
99%	1.4	1.3	1.1	0.74	0.26	0.064	0.0072	0.0017	0.00029	5.5e-005

Table 20: Variation in null alleles combined allele frequency  $f_{null}$  for the European model. Similar to Table S14.

s	0	$10^{-5}$	$10^{-4.5}$	$10^{-4}$	$10^{-3.5}$	$10^{-3}$	$10^{-2.5}$	$10^{-2}$	$10^{-1.5}$	$10^{-1}$
Mean	0.073	0.065	0.053	0.024	0.0052	0.0014	0.00046	0.00016	5.8e-005	1.8e-005
St.d.	0.2	0.18	0.16	0.091	0.027	0.01	0.0051	0.0016	0.00014	3.7e-006
1%	2.7e-005	2.7e-005	2.7e-005	2.7e-005	2.7e-005	2.7e-005	2.6e-005	2e-005	2.1e-005	1.1e-005
5%	3.4e-005	3.4e-005	3.3e-005	3.3e-005	3.3e-005	3.2e-005	3.2e-005	2.5e-005	2.4e-005	1.2e-005
10%	3.8e-005	3.8e-005	3.8e-005	3.7e-005	3.7e-005	3.7e-005	3.6e-005	2.8e-005	2.7e-005	1.3e-005
25%	5e-005	5e-005	5e-005	4.8e-005	4.7e-005	4.6e-005	4.6e-005	3.6e-005	3.2e-005	1.5e-005
50%	7.9e-005	7.7e-005	7.6e-005	7.1e-005	6.6e-005	6.4e-005	6.2e-005	5.2e-005	4.1e-005	1.7e-005
75%	0.00062	0.00035	0.00024	0.00015	0.00011	0.0001	9.5e-005	8.2e-005	5.6e-005	2e-005
90%	0.27	0.22	0.16	0.047	0.00037	0.0002	0.00017	0.00014	8.2e-005	2.2e-005
95%	0.55	0.48	0.39	0.15	0.024	0.0005	0.00032	0.00022	0.00011	2.4e-005
99%	0.93	0.9	0.84	0.49	0.14	0.047	0.0044	0.0009	0.00034	2.9e-005

Table 21: Variation in disruptive alleles combined allele frequency  $f_D$  for the Finland model. Similar to Table S13.

s	0	$10^{-5}$	$10^{-4.5}$	$10^{-4}$	$10^{-3.5}$	$10^{-3}$	$10^{-2.5}$	$10^{-2}$	$10^{-1.5}$	$10^{-1}$
Mean	0.21	0.2	0.15	0.069	0.017	0.0055	0.0019	0.00051	0.00016	5.5e-005
St.d.	0.33	0.31	0.27	0.15	0.049	0.022	0.01	0.0032	0.00031	6.1e-006
1%	0.00014	0.00014	0.00014	0.00014	0.00013	0.00013	0.00012	0.0001	7.1e-005	4.3e-005
5%	0.00017	0.00017	0.00017	0.00017	0.00016	0.00015	0.00014	0.00012	8e-005	4.6e-005
10%	0.0002	0.0002	0.0002	0.00019	0.00017	0.00017	0.00016	0.00013	8.7e-005	4.7e-005
25%	0.00029	0.0003	0.00027	0.00024	0.00022	0.00021	0.00019	0.00015	0.0001	5e-005
50%	0.035	0.031	0.0051	0.00049	0.00032	0.00028	0.00025	0.0002	0.00012	5.4e-005
75%	0.3	0.28	0.19	0.064	0.0012	0.0005	0.00039	0.00028	0.00015	5.8e-005
90%	0.71	0.67	0.53	0.23	0.061	0.004	0.00089	0.00047	0.00021	6.2e-005
95%	0.91	0.87	0.76	0.39	0.11	0.038	0.0028	0.00076	0.00027	6.5e-005
99%	1.4	1.3	1.1	0.77	0.24	0.12	0.054	0.0054	0.00071	7.2e-005

Table 22: Variation in null alleles combined allele frequency  $f_{null}$  for the Finland model. Similar to Table S14.

s	0	$10^{-5}$	$10^{-4.5}$	$10^{-4}$	$10^{-3.5}$	$10^{-3}$	$10^{-2.5}$	$10^{-2}$	$10^{-1.5}$	$10^{-1}$
Mean	0.077	0.069	0.054	0.024	0.0054	0.0014	0.00044	0.00014	6.3e-005	1.4e-005
St.d.	0.2	0.18	0.16	0.085	0.02	0.0044	0.0017	0.00072	0.00021	2.1e-005
1%	0	0	0	0	0	0	0	0	0	0
5%	0	0	0	0	0	0	0	0	0	0
10%	4e-006	4e-006	4e-006	4e-006	4e-006	2e-006	2e-006	0	2e-006	0
25%	1.8e-005	1.8e-005	1.6e-005	1.4e-005	1.2e-005	1e-005	8e-006	8e-006	8e-006	4e-006
50%	0.00015	0.00012	9.4e-005	6.4e-005	4.4e-005	3e-005	2.2e-005	2e-005	2e-005	8e-006
75%	0.02	0.016	0.011	0.0051	0.0016	0.00016	6.8e-005	5e-005	4.8e-005	1.8e-005
90%	0.28	0.23	0.16	0.048	0.012	0.0042	0.00049	0.00012	0.00011	3.6e-005
95%	0.55	0.49	0.37	0.14	0.028	0.0084	0.0029	0.00031	0.0002	5e-005
99%	0.93	0.9	0.83	0.46	0.098	0.021	0.0089	0.0034	0.00081	9.6e-005

Table 23: Variation in disruptive alleles combined allele frequency  $f_D$  for the Iceland model. Similar to Table S13.

s	0	$10^{-5}$	$10^{-4.5}$	$10^{-4}$	$10^{-3.5}$	$10^{-3}$	$10^{-2.5}$	$10^{-2}$	$10^{-1.5}$	$10^{-1}$
Mean	0.22	0.2	0.16	0.073	0.018	0.0054	0.0017	0.00054	0.00013	5.5e-005
St.d.	0.33	0.3	0.27	0.15	0.034	0.0086	0.0034	0.0014	0.00025	3.6e-005
1%	3.9e-005	3.6e-005	3.4e-005	2.8e-005	2.2e-005	1.8e-005	1.4e-005	1.2e-005	1.2e-005	6e-006
5%	0.0001	9.8e-005	9.2e-005	7.6e-005	6e-005	4.6e-005	3.2e-005	2.3e-005	2e-005	1e-005
10%	0.00026	0.00024	0.00018	0.00014	9.6e-005	6.6e-005	4.6e-005	3.2e-005	2.8e-005	1.8e-005
25%	0.0057	0.0052	0.0037	0.0019	0.00042	0.00015	8.2e-005	6.4e-005	4.2e-005	3.2e-005
50%	0.053	0.044	0.028	0.014	0.0058	0.0016	0.0002	0.00013	7e-005	4.8e-005
75%	0.31	0.27	0.2	0.07	0.019	0.0072	0.0015	0.0003	0.00013	7e-005
90%	0.73	0.67	0.55	0.22	0.051	0.015	0.0055	0.0012	0.00022	9.8e-005
95%	0.92	0.88	0.78	0.37	0.084	0.022	0.0087	0.0027	0.00035	0.00012
99%	1.4	1.3	1.2	0.74	0.17	0.041	0.016	0.0076	0.0012	0.00018

Table 24: Variation in null alleles combined allele frequency  $f_{null}$  for the Iceland model. Similar to Table S14.

## 9 RVAS Strategy 5: Using Gene Sets

Another attractive strategy is to move beyond single genes and study gene-sets. By aggregating signal from multiple genes, we may potentially enhance the association signal and improve power. Consider a simple approach for testing association with gene-sets, where we test for burden of disruptive alleles in all genes in the set in cases vs. controls. Consider a set  $S$  with  $m$  genes, with disruptive CAF  $f_1, \dots, f_m$  and effect sizes  $\lambda_1, \dots, \lambda_m$  on disease. We define the total cumulative frequency in the set  $f_S = \sum_i f_i$ , and the average excess effect size for the set is  $\lambda_{avg} = \frac{\sum_i f_i \lambda_i}{f_S}$ .

Then, the sample size required to detect association is similar to eq. (3.6) for one gene, with the frequency  $f$  replaced by  $\sum_i f_i$ , and with the effect size  $\lambda$  replaced by  $\beta\lambda$ , where  $\beta$  is the (weighted) fraction of genes having an effect,  $\beta \equiv \frac{\sum_i f_i 1_{\{\lambda_i=\lambda\}}}{\sum_i f_i}$ , giving:

$$n_{a,b} = \frac{\nu_{a,b}}{4[(1 + \lambda_{avg})f_S \log(1 + \lambda_{avg}) + (1 - (1 + \lambda_{avg})f_S) \log \frac{1 - (1 + \lambda_{avg})f_S}{1 - f_S}]}. \quad (9.1)$$

Compared to a single gene with cumulative frequency  $f_C$  and effect size  $\lambda$ , the ratio of the two sample sizes is,

$$\frac{n_{a,b}(f_C, \lambda)}{n_{a,b}} = \frac{[(1 + \lambda)f_C \log(1 + \lambda) + (1 - (1 + \lambda)f_C) \log \frac{1 - (1 + \lambda)f_C}{1 - f_C}]}{[(1 + \lambda_{avg})f_S \log(1 + \lambda_{avg}) + (1 - (1 + \lambda_{avg})f_S) \log \frac{1 - (1 + \lambda_{avg})f_S}{1 - f_S}]}. \quad (9.2)$$

Whether a gene set increase or decreases power depends on the extent to which it is enriched with genes having large effect sizes.

Similarly, the gain in power due to missense alleles can be obtained by modifying eq. (5.3) accordingly. The study of gene-sets present a tradeoff - including more genes may increase the allele frequency, but may decrease the average effect size. Using gene-set based on prior biological knowledge (e.g. genes in a certain pathway, sharing a same function, or GWAS-hits) may allow increased power.

If genes have different selection coefficients, effect sizes, and gene lengths, the situation becomes more complicated. For example, it will no longer be optimal to filter alleles in different genes by a single threshold. In this case, it is still possible to use gene-specific thresholds, and combine the alleles obtained from different genes.

## 10 RVAS Strategy 6: *De novo* Mutations

Another strategy is to study only *de novo* disruptive mutations. At a first glance, using *de novo* alleles might seem counter productive, because their frequency in the population is so low. However, this strategy may make sense in certain cases - namely when searching for genes with huge effect sizes.

One advantage of *de novo* alleles is that we do not need to estimate the allele frequency,  $f_C$ , from population surveys: the frequency of *de novo* alleles depends only on is determined by the mutation rate (and not the selection coefficient), which can be reliably estimated from genomic parameters, as discussed above.

Consider a gene with disruptive mutation rate  $\mu_D$ , and effect size  $\lambda$ . The sample size needed to detect *de novo* alleles is obtained simply by replacing  $f$  with  $\mu_D$  in eq. (3.7), giving,

$$n_{a,b}(de\ novo) \approx \frac{\nu_{a,b}}{4\mu_D g(\lambda)}. \quad (10.1)$$

The average mutation rate of disruptive alleles in our typical gene is  $\mu_D \approx 1.7 \times 10^{-6}$ , although there is considerable variation in rates between genes. Longer genes with higher overall mutation rates will tend to have more *de novo* alleles, and will be slightly easier to detect.

In Figure S23, we plot the sample size needed to detect burden of *de novo* mutations, for a typical gene. The sample size is huge unless the effect size is also huge. For our typical gene, more than 100,000 cases must be studied for *de novo* mutations to detect a gene in which disruptive alleles increase risk by 20-fold. In the case cited (autism with several mental disabilities), the effect size is 300-fold.

One benefit of using *de novo* alleles is that the proportion of null alleles will be higher (compared to taking all missense alleles), and is insensitive to the selection coefficient - thus using *de novo* alleles may be particularly attractive for genes under strong selection.



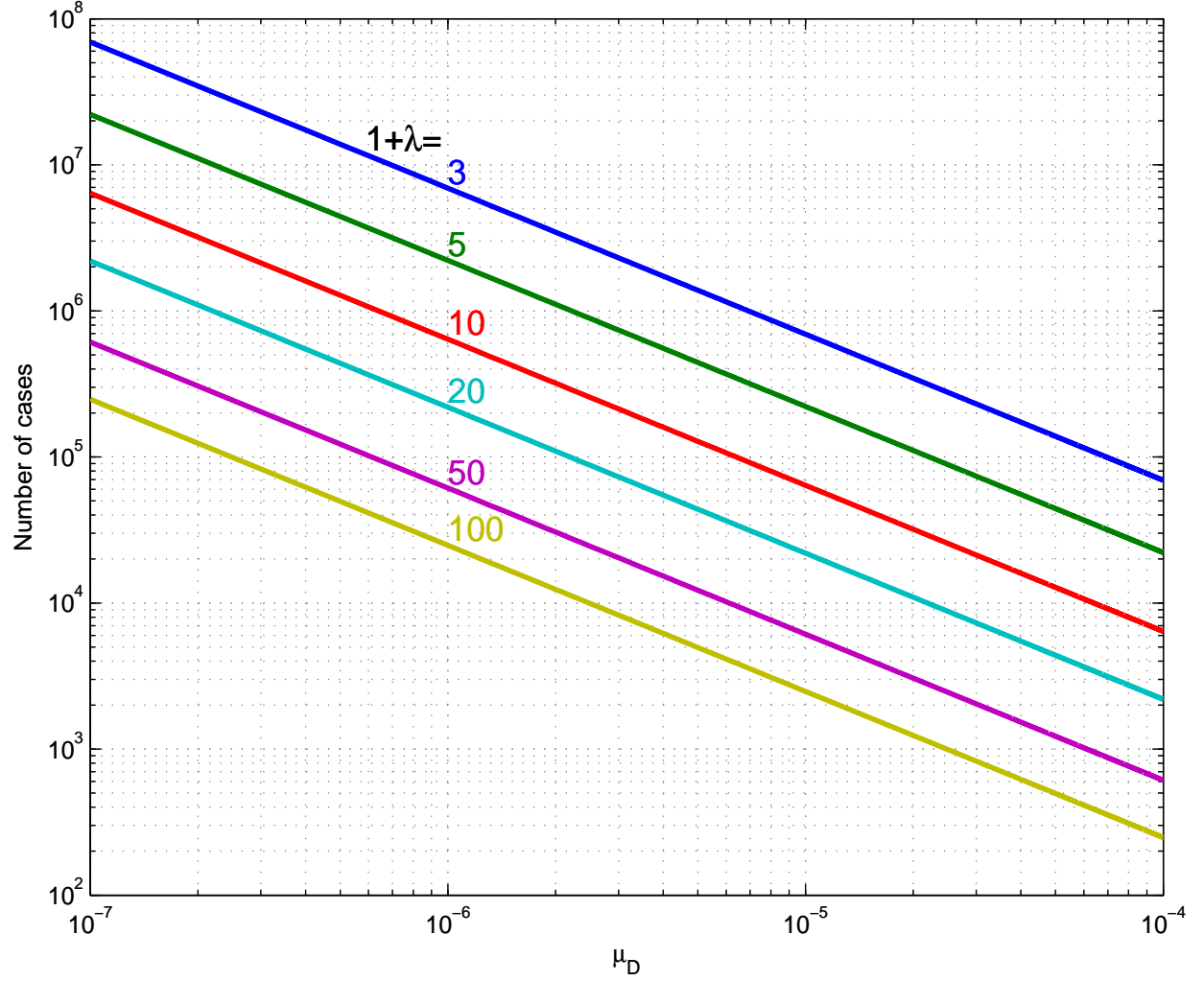


Figure 23: The number of samples (cases) required to detect *de novo* alleles as function of effect size  $1 + \lambda$  (shown as different colored curves), and the overall genic mutation rate  $\mu_D$  (x-axis). We require 90% power and 0.05/20,000 p-value cutoff. Power increases with both effect size and mutation rate. Overall, the sample size is huge, unless effect size is strong and mutation rate is high. For example, for an average gene ( $\mu_D = 1.7 \times 10^{-6}$ ), and with  $1 + \lambda = 20$ , the sample size is over 100,000 cases.

## 11 Prospects for RVAS in Non-coding Regions

It is natural to want to extend RVAS to non-coding regions, especially in light of the observation that the majority of known CVAS hits are non-coding. However, non-coding regions provide a major challenge for RVAS. The main issue is which alleles to aggregate. The density of functional alleles in non-coding regions is expected to be lower than in coding regions, and the effect size of functional alleles is also expected to be lower.

If we let  $\alpha_{NC}$  be the fraction of bases encoding functional DNA elements in a non-coding region that is aggregated for RVAS, the effect size of these functional alleles will be diluted by a factor of  $\alpha_{NC}$ . We can use the same formulations from the two-class model describing missense alleles to study non-coding alleles as well, including power calculations. If we take all alleles below a threshold  $T^*$  we get, similarly to eq. (5.3),

$$\frac{E[\mathcal{L}\mathcal{L}\mathcal{R}_{non-coding}(T^*)]}{E[\mathcal{L}\mathcal{L}\mathcal{R}_{non-coding-functional}]} \sim \frac{\alpha_{NC}\Psi_s(T^*)[(1 + \rho_s(T^*)\lambda)\log(1 + \rho_s(T^*)\lambda) - \rho_s(T^*)\lambda]}{\rho_s(T^*)[(1 + \lambda)\log(1 + \lambda) - \lambda]} \quad (11.1)$$

where  $E[\mathcal{L}\mathcal{L}\mathcal{R}_{non-coding-functional}]$  would be the aggregate effect size in an hypothetical case where we know precisely the functional non-coding variants, and  $E[\mathcal{L}\mathcal{L}\mathcal{R}_{non-coding}(T^*)]$  would be the aggregate effect size we use in practice, where we take all alleles with frequency below  $T^*$  in an entire non-coding region. The resulting inflation in sample size will be between  $\frac{1}{\alpha_{NC}}$  and  $\frac{1}{\alpha_{NC}^2}$ , depending on the effect size  $\lambda$ .

### 11.1 Multiple Hypothesis Burden for Genome-Wide Testing

When performing association tests across the entire genome, the burden of multiple hypothesis testing is also increased relative to the situation of testing only genes. Suppose that we wish to achieve an overall type-1 error of  $a = 0.05$ . When testing for association across 20,000 individual genes, one can simply apply a Bonferroni correction to set the required nominal significance level at  $a/20,000 = 2.5 \times 10^{-6}$ .

When testing for association in overlapping windows across the entire genome, a different approach is needed to calculate the required nominal significance level. Suppose that we study overlapping windows  $W_i$ , each of length  $w$  base-pairs, and calculate for each window a test statistic  $X_i$  with a Normal distribution under the null hypothesis of no association, and we are interested in one-sided tests, i.e. detecting  $X_i$ 's values which are unusually large (Such a statistic arises naturally when testing for excess of rare alleles observed in cases relative to the expected number based on a large set of controls). To achieve genome-wide significance, we need to consider the distribution of  $X = \max_i X_i$  under the null, where the maximum is taken across the entire human genome. The total number of different tests is thus  $\sim 3 \times 10^9$  (equal to the number of positions in the human genome, because a window can start at each nucleotide). Tests corresponding to non-overlapping windows

can be considered independent (because of linkage disequilibrium among *rare* variants), while tests corresponding to overlapping windows are clearly correlated, with the correlation proportional to the extent of overlap. The effective number of independent tests is thus somewhere between  $\frac{3 \times 10^9}{w}$  and  $3 \times 10^9$ .

Considering the situation of family-based linkage analysis, Lander and Botstein [49] showed that the nominal significance level corresponding to a desired genome-wide significance level can be calculated in terms of the largest deviation of an Orenstein-Uhlenbeck diffusion process [50]. Briefly, an Orenstein-Uhlenbeck process describes a stationary random process  $Y(t)$  for  $t \in [0, T]$  such that (i)  $Y(t)$  is a standard normal random variable for all  $t$  and (ii) the local correlation of  $Y(t)$  and  $Y(t+x)$  is  $r(x) = e^{-|x|}$ . According to [51] (Theorem 12.2.9., page 232), the distribution of  $M(T) = \max_{t \in [0, T]} Y(t)$ , the maximum value of the process across an interval of length  $T$ , is asymptotically

$$P[M(T) > u] \sim Tu\phi(u) \sim Tu^2[1 - \Phi(u)] \quad (11.2)$$

where  $\phi(u)$  is the standard Gaussian probability density function, and  $\Phi(u)$  is the standard Gaussian cumulative distribution function.

In the case of RVAS, the statistics  $X_i$  together approximately follow an Orenstein-Uhlenbeck distribution (after rescaling the x-axis by a factor of  $\frac{1}{w}$  and ignoring the division of the genome into 23 chromosomes). The local correlation function  $r(x) = \max\left(0, 1 - \frac{|x|}{w}\right)$  is triangular rather than exponential, but can be reasonably approximated by the exponential  $e^{-|x|/w}$ . (One can also directly study the triangular covariance function; see for example [52].)

With this approximation, the large deviation theory for the Orenstein-Uhlenbeck process implies that the cumulative distribution of  $X$  is given by

$$P(X > x) \approx \frac{3 \times 10^9}{w} x^2 (1 - \Phi(x)). \quad (11.3)$$

(This formula follows from eq. (11.2) above. It is equivalent to Proposition 2 in [49], where the formula is expressed in terms of chi-square, rather than Gaussian, test statistics; the two formulations are equivalent by a simple square transformation).

With  $w = 4$  kilobases and  $a = 0.05$ , we have following equation,

$$0.05 = 750,000 x^2 (1 - \Phi(x)). \quad (11.4)$$

The solution (obtained numerically) is  $x \sim 5.9$ . This corresponds to a genome-wide significance level of  $(1 - \Phi(x)) \approx 1.9 \times 10^{-9}$ , which is much more stringent than the value  $2.5 \times 10^{-6}$  required to control for testing 20,000 genes.

The sample size when testing using a Gaussian test-statistic (Z-score) is proportional to  $\left(\Phi^{-1}(a) + \Phi^{-1}(b)\right)^2$ , where  $a$  is the desired type-1 error,  $b$  is the desired type-2 error, and  $\Phi^{-1}$  is the inverse of the standard Gaussian cumulative distribution function (Z-value). For the case of 50% power ( $b = 0.5$  and  $\Phi^{-1}(b) = 0$ ) and family-wise error rate of 0.05, we have  $\left(\Phi^{-1}(a) + \Phi^{-1}(b)\right)^2 \approx (-4.6 + 0)^2 = 20.8$  when testing 20,000 genes and  $\left(\Phi^{-1}(a) + \Phi^{-1}(b)\right)^2 \approx (-5.9 + 0)^2 = 34.7$  when scanning the entire genome. Thus, 1.66-fold more samples are required when scanning the genome in windows of 4 kb than when testing 20,000 genes. The corresponding numbers for 90% power ( $b = 0.1$  and  $\Phi^{-1}(b) = -1.3$ ) are 34.2 and 51.4, corresponding to a 1.5-fold increase in sample size.

## 12 Estimating the Parameters $s$ and $\alpha$ in the Two-class Model

In our analyses, we have assumed that we know the (gene-specific) parameters  $s$  and  $\alpha$  in our two-class model. In practice, these parameters are unknown and must be estimated. We provide estimators for  $s$  and  $\alpha$ , and discuss their shortcomings - which are especially serious in the case of  $\alpha$ .

### 12.1 Estimating $s$

We can estimate  $s$  from the frequency  $f_D$  of disruptive alleles. For strong selection, we can use equation (1.14) to obtain:

$$\hat{s} = \frac{\mu_D}{f_D} \quad (12.1)$$

To know if the estimator is useful, we need to understand its variance. There are two sources of variation:

1. Sampling noise in our estimation of the true value of  $f_D$  in the population. This variation can be made arbitrarily small by increasing the sample size.
2. Stochastic noise in the realized value of  $f_D$  around its expected value (given  $s$ ), resulting from random events during population history (e.g., two genes with the same  $s$  might reach different allele frequencies due to stochastic variation in the random births of new alleles). This variation cannot be reduced by increasing the sample size, but rather is determined by population history.

Suppose that we use equation (12.1) to infer the selection coefficient  $s$ , based on the observed frequency  $f_D$  of disruptive alleles. Let  $s(x, y)$  be the value of  $s$ , such that  $Prob(\hat{s} \geq x) = y$ . We can define a 95% confidence interval for  $s$  around  $\hat{s}$  to be  $[s(\hat{s}, 0.025), s(\hat{s}, 0.975)]$  and a "median" value to be  $s(\hat{s}, 0.50)$ .

Figure S24 shows that confidence interval and median value for various values of  $\hat{s}$  for the European population. For  $\hat{s} > 7 \times 10^{-3}$ , the confidence interval is acceptably tight for our purposes - a factor of  $\sim 9$ -fold between the upper and lower bound. By contrast, it is hard to obtain good estimates when selection is weak: the size of the confidence interval (relative to the median) blows up. Fortunately, we care primarily about the case of strong selection.

One way to improve the estimator would be to combine estimates from multiple unrelated populations.

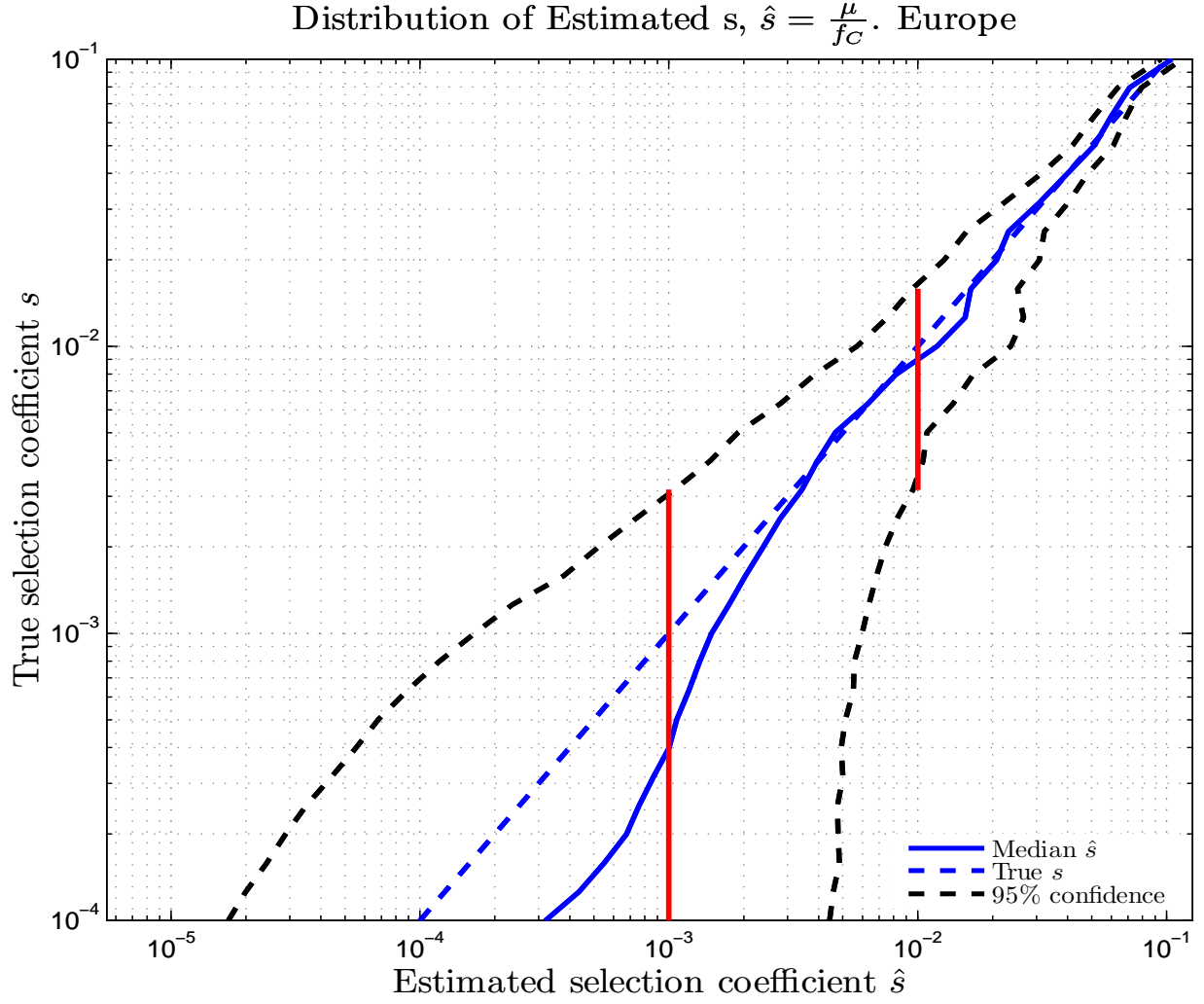


Figure 24: Confidence intervals around estimated value of  $s$ . The y-axis shows true values of  $s$ , while the x-axis shows values of  $\hat{s}$ . Given an estimate  $\hat{s}$ , the curves show the upper confidence limit  $s(\hat{s}, 0.975)$ , the lower confidence limit  $s(\hat{s}, 0.025)$ , and the median  $s(\hat{s}, 0.50)$ . Values obtained from 8,000 simulations for the European population model, assuming  $\mu_G = 1.7 \times 10^{-6}$ . Note: The estimator  $\hat{s} = \frac{\mu_D}{f_D}$  is biased upwards. Although  $E[f_D] = \frac{\mu_D}{s}$ , we have  $s < E[\frac{\mu_D}{f_D}]$  by Jensen's inequality applied to the function  $\frac{1}{x}$ , giving  $E[\frac{1}{x}] > \frac{1}{E[x]}$ .

## 12.2 Estimating $\alpha$

One approach is to estimate  $\alpha$  based on population data by comparing  $f_M$ , the observed CAF for missense alleles ( $f_M$ ), to  $f_{M^*}$ , the CAF that would be expected if all missense alleles were neutral.

We have:

$$f_M = f_{M,neutral} + f_{M,null} \quad (12.2)$$

For a population at equilibrium and strong selection, we can write (by Proposition 2):

$$\begin{aligned} E[f_M] &\approx (1 - \alpha)f_{M^*} + \alpha \frac{\mu_M}{s} \\ &\approx (1 - \alpha)4N_{eq}\mu_M + \alpha \frac{\mu_M}{s} \end{aligned} \quad (12.3)$$

where  $N_{eq}$  is the equilibrium population size for the ancestral human population.

Moreover, this approximation also holds, in expectation, for modern populations (because, as shown above and in the main text, the CAF is essentially unchanged by recent human demography).

We can neglect the term  $f_{M,null} \approx \alpha \frac{\mu_M}{s}$  in eq. (12.3) because

$$\frac{(1 - \alpha)4N_{eq}\mu_M}{\alpha(\mu_M/s)} = \frac{1 - \alpha}{\alpha}4N_{eq}s \gg 1 \quad (12.4)$$

provided that selection is strong. (For very weak selection, one could include the term.)

We can thus solve eq. (12.3) for  $\alpha$  to obtain

$$\alpha \approx 1 - \frac{E[f_M]}{4N_{eq}\mu_M}. \quad (12.5)$$

This provides an estimator  $\hat{\alpha}$ :

$$\hat{\alpha} = 1 - \frac{f_M}{4N_{eq}\mu_M}. \quad (12.6)$$

The variation in the estimator  $\hat{\alpha}$  depends on the variation in the CAF for neutral missense alleles.

As for  $s$  above, there are two sources of variation: (i) sampling noise, which can be decreased by increasing sample size and (ii) stochastic variation in population history, which cannot be reduced by increasing sample size.

As shown in Tables S13-S24, the coefficient of variation in the CAF under neutrality is large: the standard deviation is roughly equal to the mean. This inherently limits the precision in estimates of  $\alpha$ .

Another approach is to estimate  $\alpha$  based on evolutionary comparison, using the estimator:

$$\hat{\alpha}_{evo.} = \frac{dN}{dS} \quad (12.7)$$

where  $dN$  denotes the number of non-synonymous (missense) substitutions per non-synonymous site, and  $dS$  denotes the number of synonymous (silent) substitutions per synonymous site.

If our two-class model is strictly true, this estimator should perform well - because evolution will largely reject null alleles and allow neutral alleles. Thus, the "proportional deficit" in missense alleles (relative to silent alleles) will be an accurate reflection of  $\alpha$ .

A problem arises, however, if there are also hypomorphic alleles (between null and neutral). Evolution will reject hypomorphic alleles when  $s \gg \frac{1}{N_{eff}}$ , where  $N_{eff}$  is the effective population size of the species. For species with large population sizes, evolution will tend to reject alleles under weak selection. For example, evolution will tend to reject alleles with  $s = 10^{-4}$  in a population with  $10^5$  individuals.

In this case, the estimator based on evolution may overestimate the true proportion  $\alpha$  of newborn mutations that are truly null. Still, it is still useful to have an upper bound on  $\alpha$ .

Improved methods for estimating  $s$  and  $\alpha$  would be useful.



## 13 Estimating Variance Explained by Rare Variants

A major open question is the extent to which rare variants contribute to the heritability of complex diseases. To answer this question, we must be able to estimate the heritability explained by rare variants found in RVAS. Here, we provide the simple formula for variance explained for dichotomous trait. We then apply this to two studies of rare variants in two diseases, and calculate the variance explained by different classes of alleles.

### 13.1 Calculating Variance Explained

For a disease with prevalence  $\pi$  and an individual allele with frequency  $f_i$  and effect size  $\lambda_i$ , the contribution to heritability for a disease trait is,

$$V_i = \frac{2f_i}{1 - 2f_i} \frac{\pi}{1 - \pi} \lambda_i^2. \quad (13.1)$$

Therefore, for a class of null alleles with CAF  $f_{null}$  and effect size  $\lambda$ , the total variance explained by the class when  $f_{null}$  is small is,

$$V \approx 2f_{null} \frac{\pi}{1 - \pi} \lambda^2. \quad (13.2)$$

### 13.2 Sample Size Required to Detect Loci Explaining a Given Proportion of the Phenotypic Variance

We can calculate the number of samples needed to detect genes that explain a given proportion of the phenotypic variance of a dichotomous trait. The power to detect an association of a class of alleles is directly related to the total phenotypic variance explained by these alleles. Consider a gene with classes of disruptive ( $D$ ) and (all) *null* alleles, with combined frequencies  $f_D$  and  $f_{null}$ , respectively, and effect size  $\lambda$ .

By taking eq. (13.2) for the variance explained by all null alleles, and eq. (3.7) for the sample size required when testing for disruptive alleles we get,

$$n_{a,b} \approx \left[ NCP^*(a, b) \frac{f_{null}}{f_D} \frac{\pi}{1 - \pi} \right] \frac{\lambda^2}{g(\lambda)} \frac{1}{V}. \quad (13.3)$$

Therefore, for a set of alleles with combined variance explained  $V$ , the sample size is proportional to  $\frac{\lambda^2}{g(\lambda)}$ . The function  $\frac{\lambda^2}{g(\lambda)}$  is monotonically increasing with  $\lambda$ . If the effect size  $\lambda$  is small,  $\frac{\lambda^2}{g(\lambda)} \approx 2$  and the sample size is not sensitive to the effect size. For large values of  $\lambda$ , the sample size increases as we increase  $\lambda$  and keep the variance explained fixed (by decreasing the allele frequencies). The maximum possible sample size occurs for the largest possible effect size, which corresponds alleles

causing full penetrance, i.e.  $\pi(1+\lambda) = 1$  or  $\lambda = \frac{1-\pi}{\pi}$ . In this case we get  $g(\lambda) = g(\frac{1-\pi}{\pi}) = \frac{\pi-1-\log(\pi)}{\pi}$  and

$$n_{a,b}^{(MAX)}(V) \approx NCP^*(a,b) \frac{\pi-1}{\log(\pi)+1-\pi} \left[1 + \alpha \frac{\mu_M}{\mu_D}\right] \frac{1}{V} \quad (13.4)$$

where we recall that a fraction  $\alpha$  of missense alleles at birth is null, hence  $\frac{f_{null}}{f_D} = 1 + \alpha \frac{\mu_M}{\mu_D}$ . For example, suppose that we want to identify genes explaining at least 1% of the phenotypic variance (with significance thresholds of  $a = 0.05/20,000$  and  $b = 0.1$ , and taking  $\alpha = 0.25$  and  $\frac{\mu_M}{\mu_D} = 7.3$ ). We have  $\frac{\pi-1}{\log(\pi)+1-\pi} = 0.27, 0.46$  and  $0.64$  for  $\pi = 0.01, 0.05, 0.10$ . These correspond to sample sizes of 2775, 4707, and 6503 cases, respectively. Once we attain these sample sizes, we are thus reasonably confident that we will have identified all genes explaining at least 1% of the phenotypic variance.

### 13.3 Estimating heritability explained by rare variants for two traits

For two recent RVAS studies that detected association with candidate genes, we calculate the proportion of phenotypic variance explained by rare variants in the genes. In each study, the authors designated the class of alleles that they believe to be deleterious - based on frequency and either (i) genetic and evolutionary data (in the first case) or (ii) biochemical data (in the second case). In calculating the proportion of the phenotypic variance explained, we use this class as the class of null alleles.

#### 13.3.1 Blood Pressure [Ji et al 2008]

Ji et al. [45] studied association between blood pressure and rare variants in three genes (*SCL12A3*, *SCL12A1*, and *KCNJ1*) in which strong mutations cause Bartter's or Gittleman's syndrome, rare recessive diseases in which patients have extremely low blood pressure.

The authors defined (i) rare variants as being those with population frequency  $\leq 1\%$  and (ii) deleterious rare variants as being the subset of rare variants occurring at sites that are evolutionarily conserved and/or are known to cause Bartter's or Gittleman's syndrome. For deleterious rare variants, the total counts are 27, 11 and 12 and the allele frequency is 0.43%, 0.17% and 0.19% for *SLC12A3*, *SLC12A1* and *KCNJ1*, respectively.

The authors studied 3126 individuals from the general population with respect to blood pressure and rare variants in the three genes.

We converted blood pressure into a set of dichotomous traits, by considering individuals with blood pressure in the top 10%, 20%, 30%, 40% and 50% of the sample as well as the bottom 10%, 20%, 30%, 40% and 50% of the sample (based on Table 3 from their paper). Our results are shown in Table S25.

Rare variants in the three gene together explain  $\approx 0.1\% - 0.5\%$  of the phenotypic variance in the dichotomous traits, depending on the percentile chosen. The average proportion explained by each gene is thus  $0.04\% - 0.17\%$ . The proportion of the phenotypic variance explained is similar if blood pressure is treated as a quantitative trait.

Gene	Cases	Unaffecteds	$1 + \lambda$	V
n	313 (top 10%)	2813 (bottom 90%)		
<i>SLC12A3</i> (CAF=0.43%)	1	26	1.08	0.051%
<i>SLC12A1</i> (CAF=0.17%)	0	11	1.13	0.056%
<i>KCNJ1</i> (CAF=0.19%)	0	12	1.15	0.074%
All 3 Genes (CAF=0.79%)	1	49	1.11	0.17%
n	626 (top 20%)	2500 (bottom 80%)		
<i>SLC12A3</i>	3	24	1.12	0.052%
<i>SLC12A1</i>	1	10	1.16	0.035%
<i>KCNJ1</i>	1	11	1.18	0.051%
All 3 Genes	5	45	1.15	0.13%
n	939 (top 30%)	2187 (bottom 70%)		
<i>SLC12A3</i>	3	24	1.28	0.16%
<i>SLC12A1</i>	1	10	1.33	0.085%
<i>KCNJ1</i>	1	11	1.35	0.11%
All 3 Genes	5	45	1.31	0.35%
n	1252 (top 40%)	1874 (bottom 60%)		
<i>SLC12A3</i>	5	22	1.37	0.18%
<i>SLC12A1</i>	1	10	1.55	0.15%
<i>KCNJ1</i>	1	11	1.58	0.19%
All 3 Genes	7	43	1.46	0.5%
n	1453 (top 50%)	1673 (bottom 50%)		
<i>SLC12A3</i>	7	20	1.4	0.14%
<i>SLC12A1</i>	2	9	1.56	0.11%
<i>KCNJ1</i>	1	11	1.77	0.22%
All 3 Genes	10	40	1.52	0.43%

Table 25: Phenotypic variance explained by rare variants in the *SCL12A3*, *SCL12A1*, and *KCNJ1* genes for various dichotomous traits defined by blood pressure. The table shows the number of deleterious rare variants in 'cases', relative risk and proportion of variance explained. This page shows 'cases' at the top percentiles of blood pressure levels (hypertension). The next page shows 'cases' at the bottom percentiles of blood pressure levels (hypotension).

Gene	Cases	Unaffecteds	$1 + \lambda$	V
n	313 (bottom 10%)	2813 (top 90%)		
<i>SLC12A3</i> (CAF=0.43%)	3	24	1.12	0.0014%
<i>SLC12A1</i> (CAF=0.17%)	2	9	1.85	0.028%
<i>KCNJ1</i> (CAF=0.19%)	4	8	3.44	0.25%
All 3 Genes (CAF=0.79%)	9	41	1.83	0.12%
n	626 (bottom 20%)	2500 (top 80%)		
<i>SLC12A3</i>	6	21	1.12	0.0031%
<i>SLC12A1</i>	2	9	0.926	0.00047%
<i>KCNJ1</i>	5	7	2.15	0.12%
All 3 Genes	13	37	1.32	0.041%
n	939 (bottom 30%)	2187 (top 70%)		
<i>SLC12A3</i>	10	17	1.25	0.022%
<i>SLC12A1</i>	3	8	0.926	0.0008%
<i>KCNJ1</i>	6	6	1.72	0.083%
All 3 Genes	19	31	1.29	0.056%
n	1252 (bottom 40%)	1874 (top 60%)		
<i>SLC12A3</i>	13	14	1.21	0.026%
<i>SLC12A1</i>	5	6	1.16	0.0057%
<i>KCNJ1</i>	9	3	1.94	0.22%
All 3 Genes	27	23	1.37	0.15%
n	1673 (bottom 50%)	1453 (top 50%)		
<i>SLC12A3</i>	20	7	1.4	0.14%
<i>SLC12A1</i>	9	2	1.56	0.11%
<i>KCNJ1</i>	11	1	1.77	0.22%
All 3 Genes	40	10	1.52	0.43%

Table 19: Phenotypic variance explained by rare variants for various dichotomous traits defined by blood pressure. (cont.)

### 13.3.2 Type 2 Diabetes [Bonnenfond et al. 2012]

Bonnefond et al. [41] studied association between Type 2 Diabetes and rare variants in *MTNR1B*. By sequencing the genes in 2186 cases and 4804 controls, they found 40 non-synonymous variants associated with the disease. They performed biochemical assays to study the biochemical consequences of each variant on protein function.

Their strongest signal came from a class of 12 variants that they classified as "Loss of Function variants with  $MAF < 0.1\%$ ". They observed 15 counts in cases and 13 counts in controls.

This corresponds to a frequency  $f_{null} = 0.4\%$  and a relative risk of  $1 + \lambda = 2.5$ . The proportion of variance explained is  $0.2\%$ .

[Note: The authors reported a somewhat higher relative risk, based on using the KBAC method [30]. The KBAC method gives more weight to lower frequency alleles, based on the notion that they are more likely to be deleterious. The effect of applying the KBAC method to these data is to down-weight the influence of one specific missense allele (*L60R*, which appears in 5 cases and 6 controls). However, the KBAC does not seem appropriate in this case because the authors used biochemical assays to determine which alleles are non-functional: it is problematic to exclude alleles determined biochemically to be non-functional simply because they have higher frequency.]

## 14 Consequences and Limitations of our Framework

Our simple framework was chosen to maximize insight and intuition. However, it is important to address the limitations of the framework:

### 1. Two-class model

We assumed above that missense mutations are either null or neutral. We ignored hypomorphic missense alleles, treating them as neutral for the purposes of our analysis. Hypomorphic missense alleles would be expected to contribute only modestly to the power of RVAS because (i) population genetic analyses indicate that the selection coefficients for typical hypomorphic alleles are in the range  $10^{-3} - 10^{-4}$  [15, 53, 54], which corresponds primarily to common rather than rare variants, and (ii) the effect sizes for hypomorphic alleles are likely to be smaller, giving rise to smaller enrichment in cases. We tested this expectation by studying a three-class model involving null, hypomorphic and neutral alleles and confirmed that the contribution of hypomorphic alleles is indeed small (see Section 5.1). While likely to contribute little power, hypomorphic missense alleles may seriously skew estimates of effect size based on missense alleles. This consideration strengthens the case for basing estimates of effect size on disruptive alleles.

We have also ignored the potential role of countervailing missense alleles, which act in the opposite direction as null alleles (for example, protective missense alleles in the case that null alleles are deleterious). While countervailing alleles are known to occur and may be highly informative, we expect that the most missense alleles will act in the same direction as null alleles. If desired, our framework could be extended to allow for a proportion of alleles to have countervailing effects. Countervailing alleles would tend to decrease the power of burden tests, because they decrease the imbalance of missense alleles between cases and controls. "Dispersion tests" have been proposed as a way to simultaneously detect both risk-increasing and risk-decreasing alleles [27, 40]. While our simple two-class model may be appropriate for the purpose of discovering gene association, once a gene has been implicated by RVAS it will be important to consider carefully the possibility of hypomorphic and countervailing alleles.

### 2. Constancy of selection

We assumed that the selection coefficient  $s$  has not changed over time. However, changes associated with civilization (such as abundant food, population density and differences in exposure to microorganisms) may have increased the prevalence of certain diseases (such as diabetes, hypertension and autoimmune diseases). Alleles that were once neutral or advantageous may thus have become deleterious in the past several thousand years. In such cases, the allele frequency distributions will still largely reflect the ancestral selection regime - unless the modern selection is extremely strong. For the median allele in a neutral distribution (minor allele frequency  $\sim 25\%$ ) to become rare ( $< 0.5\%$ ) requires nearly 4,000 generations ( $\sim 100,000$  years) if  $s = 10^{-3}$  and nearly 400 generations ( $\sim 10,000$  years) if  $s = 10^{-2}$ , but

only 40 generations ( $\sim 1,000$  years) if  $s = 10^{-1}$ .

### 3. Fixed frequency threshold

We considered burden tests that count alleles with frequency below a pre-specified (although gene-specific) threshold. Various authors have discussed ways to use frequency-based weights, to optimize the allele frequency threshold based on data, or to use variable thresholds [28–35].

### 4. Unrelated individuals

We assumed that cases are unrelated. It may be possible to increase power by studying affected relatives from families with unusually high disease prevalence, because such families may harbor alleles with especially high penetrance, corresponding to high values of  $\lambda$  and greater power. There are two issues with this approach. First, the increase in power from larger must be balanced against the considerable challenge of ascertaining relatives from a very large collection of enriched families. Second, familial enrichment may reflect shared environment rather than shared genetics.

### 5. Discrete traits

We considered only discrete traits - such as having a disease or being in the top 5% of the tail of the distribution for a quantitative trait. Most RVAS studies have been of this type. Various authors have considered the analysis of purely quantitative traits (e.g. [42, 45]).

### 6. Role of environment

We ignore the role of environment, including genotype x environment interaction. Environmental factors cannot be readily studied in case-control studies. They are best explored in large prospective cohorts, with extensive information about exposure.



## References

1. R.A. Fisher. *The genetical theory of natural selection*. Oxford University Press, 1930.
2. S. Wright. Evolution in mendelian populations. *Genetics*, 16(2):97, 1931.
3. W.J. Ewens. *Mathematical population genetics: I. Theoretical introduction*, volume 27. Springer, 2004.
4. M. Kimura. Stochastic processes and distribution of gene frequencies under natural selection. In *Cold Spring Harbor Symposia on Quantitative Biology*, volume 20, pages 33–53. Cold Spring Harbor Laboratory Press, 1955.
5. M. Kimura. Diffusion models in population genetics. *Journal of Applied Probability*, 1(2):177–232, 1964.
6. M. Kimura and J.F. Crow. The number of alleles that can be maintained in a finite population. *Genetics*, 49(4):725, 1964.
7. S.N. Evans, Y. Shvets, and M. Slatkin. Non-equilibrium theory of the allele frequency spectrum. *Theoretical Population Biology*, 71(1):109–119, 2007.
8. D. Živković and W. Stephan. Analytical results on the neutral non-equilibrium allele frequency spectrum based on diffusion theory. *Theoretical Population Biology*, 79(4):184–191, 2011.
9. R.C. Griffiths. The frequency spectrum of a mutation, and its age, in a general diffusion model. *Theoretical Population Biology*, 64(2):241–251, 2003.
10. J.B.S. Haldane. A mathematical theory of natural and artificial selection. In *Mathematical Proceedings of the Cambridge Philosophical Society*, volume 23, pages 607–615. Cambridge Univ Press, 1927.
11. A. Keinan and A.G. Clark. Recent explosive human population growth has resulted in an excess of rare genetic variants. *Science*, 336(6082):740–743, 2012.
12. H. Li and R. Durbin. Inference of human population history from individual whole-genome sequences. *Nature*, 475(7357):493–496, 2011.
13. A. Helgason, S. Siguróardóttir, J.R. Gulcher, R. Ward, and K. Stefánsson. mtDNA and the origin of the icelanders: deciphering signals of recent population history. *The American Journal of Human Genetics*, 66(3):999–1016, 2000.
14. E. Jakkula, K. Rehnström, T. Varilo, O.P.H. Pietiläinen, T. Paunio, N.L. Pedersen, U. deFaire, M.R. Järvelin, J. Saharinen, N. Freimer, et al. The genome-wide patterns of variation expose significant substructure in a founder population. *The American Journal of Human Genetics*, 83(6):787–794, 2008.
15. A.R. Boyko, S.H. Williamson, A.R. Indap, J.D. Degenhardt, R.D. Hernandez, K.E. Lohmueller,

- M.D. Adams, S. Schmidt, J.J. Sninsky, S.R. Sunyaev, et al. Assessing the evolutionary impact of amino acid mutations in the human genome. *PLoS Genetics*, 4(5):e1000083, 2008.
16. Y.B. Simons, M.C. Turchin, J.K. Pritchard, and G. Sella. The deleterious mutation load is insensitive to recent population history. *Nature Genetics*, *in press*.
  17. J.R. Lupski, J.W. Belmont, E. Boerwinkle, and R.A. Gibbs. Clan genomics and the complex architecture of human disease. *Cell*, 147(1):32–43, 2011.
  18. A. Siepel and D. Haussler. Phylogenetic estimation of context-dependent substitution rates by maximum likelihood. *Molecular Biology and Evolution*, 21(3):468–488, 2004.
  19. D.G. Hwang and P. Green. Bayesian markov chain monte carlo sequence analysis reveals varying neutral substitution patterns in mammalian evolution. *Proceedings of the National Academy of Sciences*, 101(39):13994–14001, 2004.
  20. P.F. Arndt and T. Hwa. Identification and measurement of neighbor-dependent nucleotide substitution processes. *Bioinformatics*, 21(10):2322–2328, 2005.
  21. S. Asthana, M. Roytberg, J. Stamatoyannopoulos, and S. Sunyaev. Analysis of sequence conservation at nucleotide resolution. *PLoS Computational Biology*, 3(12):e254, 2007.
  22. A.S. Kondrashov. Direct estimates of human per nucleotide mutation rates at 20 loci causing mendelian diseases. *Human Mutation*, 21(1):12–27, 2003.
  23. A. Kong, M.L. Frigge, G. Masson, S. Besenbacher, P. Sulem, G. Magnusson, S.A. Gudjonsson, A. Sigurdsson, A. Jonasdottir, A. Jonasdottir, et al. Rate of de novo mutations and the importance of father’s age to disease risk. *Nature*, 488(7412):471–475, 2012.
  24. B.M. Neale, Y. Kou, L. Liu, A. Maayan, K.E. Samocha, A. Sabo, C-F. Lin, C. Stevens, L-S. Wang, V. Makarov, et al. Patterns and rates of exonic de novo mutations in autism spectrum disorders. *Nature*, 485(7397):242–245, 2012.
  25. J.C. Cohen, A. Pertsemlidis, I.K. Kotowski, R. Graham, C.K. Garcia, and H.H. Hobbs. Low LDL cholesterol in individuals of african descent resulting from frequent nonsense mutations in *PCSK9*. *Nature Genetics*, 37(2):161–165, 2005.
  26. J.C. Cohen, E. Boerwinkle, T.H. Mosley Jr, and H.H. Hobbs. Sequence variations in *PCSK9*, low LDL, and protection against coronary heart disease. *New England Journal of Medicine*, 354(12):1264–1272, 2006.
  27. B. Li and S.M. Leal. Methods for detecting associations with rare variants for common diseases: application to analysis of sequence data. *The American Journal of Human Genetics*, 83(3):311–321, 2008.
  28. B.E. Madsen and S.R. Browning. A groupwise association test for rare mutations using a weighted sum statistic. *PLoS Genetics*, 5(2):e1000384, 2009.

29. C.R. King, P.J. Rathouz, and D.L. Nicolae. An evolutionary framework for association testing in resequencing studies. *PLoS Genetics*, 6(11):e1001202, 2010.
30. D.J. Liu and S.M. Leal. A novel adaptive method for the analysis of next-generation sequencing data to detect complex trait associations with rare variants due to gene main effects and interactions. *PLoS Genetics*, 6(10):e1001156, 2010.
31. A.L. Price, G.V. Kryukov, P.I.W. de Bakker, S.M. Purcell, J. Staples, L-J. Wei, and S.R. Sunyaev. Pooled association tests for rare variants in exon-resequencing studies. *The American Journal of Human Genetics*, 86(6):832–838, 2010.
32. I. Ionita-Laza, J.D. Buxbaum, N.M. Laird, and C. Lange. A new testing strategy to identify rare variants with either risk or protective effect on disease. *PLoS Genetics*, 7(2):e1001289, 2011.
33. B.M. Neale, M.A. Rivas, B.F. Voight, D. Altshuler, B. Devlin, M. Orho-Melander, S. Kathiresan, S.M. Purcell, K. Roeder, and M.J. Daly. Testing for an unusual distribution of rare variants. *PLoS Genetics*, 7(3):e1001322, 2011.
34. J.H. Sul, B. Han, D. He, and E. Eskin. An optimal weighted aggregated association test for identification of rare variants involved in common diseases. *Genetics*, 188(1):181–188, 2011.
35. M.C. Wu, S. Lee, T. Cai, Y. Li, M. Boehnke, and X. Lin. Rare-variant association testing for sequencing data with the sequence kernel association test. *The American Journal of Human Genetics*, 89(1):82–93, 2011.
36. S. Basu and W. Pan. Comparison of statistical tests for disease association with rare variants. *Genetic Epidemiology*, 35(7):606–619, 2011.
37. N.O. Stitzel, A. Kiezun, S. Sunyaev, et al. Computational and statistical approaches to analyzing variants identified by exome sequencing. *Genome Biology*, 12(9):227, 2011.
38. M. Ladouceur, Z. Dastani, Y.S. Aulchenko, C.M.T. Greenwood, and J. B. Richards. The empirical power of rare variant association methods: Results from sanger sequencing in 1,998 individuals. *PLoS Genetics*, 8(2):e1002496, 2012.
39. C.T. Johansen, J. Wang, M.B. Lanktree, H. Cao, A.D. McIntyre, M.R. Ban, R.A. Martins, B.A. Kennedy, R.G. Hassell, M.E. Visser, et al. Excess of rare variants in genes identified by genome-wide association study of hypertriglyceridemia. *Nature Genetics*, 42(8):684–687, 2010.
40. M.A. Rivas, M. Beaudoin, A. Gardet, C. Stevens, Y. Sharma, C.K. Zhang, G. Boucher, S. Ripke, D. Ellinghaus, N. Burt, et al. Deep resequencing of gwas loci identifies independent rare variants associated with inflammatory bowel disease. *Nature Genetics*, 43(11):1066–1073, 2011.
41. A. Bonnefond, N. Clément, K. Fawcett, L. Yengo, E. Vaillant, J.L. Guillaume, A. Dechaume, F. Payne, R. Roussel, S. Czernichow, et al. Rare *MTNR1B* variants impairing melatonin receptor 1b function contribute to type 2 diabetes. *Nature Genetics*, 44(3):297–301, 2012.

42. J.C. Cohen, R.S. Kiss, A. Pertsemlidis, Y.L. Marcel, R. McPherson, and H.H. Hobbs. Multiple rare alleles contribute to low plasma levels of HDL cholesterol. *Science*, 305(5685):869–872, 2004.
43. S. Romeo, W. Yin, J. Kozlitina, L.A. Pennacchio, E. Boerwinkle, H.H. Hobbs, and J.C. Cohen. Rare loss-of-function mutations in ANGPTL family members contribute to plasma triglyceride levels in humans. *The Journal of Clinical Investigation*, 119(1):70–79, 2009.
44. D. Diogo, F. Kurreeman, E.A. Stahl, K.P. Liao, N. Gupta, J.D. Greenberg, M.A. Rivas, B. Hickey, J. Flannick, B. Thomson, et al. Rare, low-frequency, and common variants in the protein-coding sequence of biological candidate genes from gwas contribute to risk of rheumatoid arthritis. *The American Journal of Human Genetics*, 92(1):15–27, 2013.
45. W. Ji, J.N. Foo, B.J. O’Roak, H. Zhao, M.G. Larson, D.B. Simon, C. Newton-Cheh, et al. Rare independent mutations in renal salt handling genes contribute to blood pressure variation. *Nature Genetics*, 40(5):592–599, 2008.
46. I.A. Adzhubei, S. Schmidt, L. Peshkin, V.E. Ramensky, A. Gerasimova, P. Bork, A.S. Kondrashov, and S.R. Sunyaev. A method and server for predicting damaging missense mutations. *Nature Methods*, 7(4):248–249, 2010.
47. P.C. Ng and S. Henikoff. Sift: Predicting amino acid changes that affect protein function. *Nucleic Acids Research*, 31(13):3812–3814, 2003.
48. J.M. Schwarz, C. Rödelberger, M. Schuelke, and D. Seelow. Mutationtaster evaluates disease-causing potential of sequence alterations. *Nature Methods*, 7(8):575–576, 2010.
49. E.S. Lander and D. Botstein. Mapping mendelian factors underlying quantitative traits using rflp linkage maps. *Genetics*, 121(1):185–199, 1989.
50. G.E. Uhlenbeck and L.S. Ornstein. On the theory of the brownian motion. *Physical Review*, 36(5):823–841, 1930.
51. M.R. Leadbetter, G. Lindgren, and H. Rootzén. *Extremes and related properties of random sequences and processes*. Springer Berlin Heidelberg New York, 1982.
52. D. Slepian. First passage time for a particular gaussian process. *The Annals of Mathematical Statistics*, 32(2):610–612, 1961.
53. G.V. Kryukov, L.A. Pennacchio, and S.R. Sunyaev. Most rare missense alleles are deleterious in humans: implications for complex disease and association studies. *The American Journal of Human Genetics*, 80(4):727–739, 2007.
54. G.V. Kryukov, A. Shpunt, J.A. Stamatoyannopoulos, and S.R. Sunyaev. Power of deep, all-exon resequencing for discovery of human trait genes. *Proceedings of the National Academy of Sciences*, 106(10):3871–3876, 2009.